UNIVERSITY OF LIVERPOOL

Numerical Simulations of THz Photoconductive Antenna

by

Aznida Abu Bakar Sajak

thesis submitted in accordance with
the requirement of the University of Liverpool
for the degree of Doctor of Philosophy

Department of Electrical Engineering and Electronics
The University of Liverpool
December 2018

Abstract

Terahertz (THz) (0.1 – 10 THz) region of the electromagnetic spectrum spans the frequency range between the mid-infrared and the millimetre range. THz technology has generated a lot of interest recently due to its potential applications as a tomographic imaging and material spectroscopic characterization technique in a wide range of industry sectors including aerospace industry, wood products industry, the pharmaceutical industry, art conservation and semiconductor industry. There have been significant advances in the development of THz sources and detectors. The radiated THz power from these devices, however, is very low, and they are very inefficient. Hence, there are still a lot of continued interests in developing more powerful and compact THz sources as this will enable new applications of this electromagnetic spectrum.

In this thesis, a novel photoconductive antenna with an embedded electrode structure had been proposed. Formulated equations had been used with COMSOL Multiphysics software package for the proposed THz photoconductive antenna analysis. Simulation results indicate that the proposed THz antenna can store two times more effective electric energy than the conventional photoconductive antenna. These results suggest higher THz power could potentially be obtained using the proposed structure. The proposed model also exhibits almost double the value of current when the substrate material mobility is doubled.

Based on the appraised parameters of the proposed model, the best dimension of a THz photoconductive antenna had been recommended to be constructed.

Acknowledgements

First and foremost, I would like to thank my supervisor Professor Yaochun Shen, for his invaluable guidance and patience in numerous and lengthy discussions throughout the period of my PhD studies. I am forever grateful for his advice, continuous and generous support and trust in my capabilities. I would also like to thank Professor Yi Huang who has endorsed this life changing opportunity for me.

At the Wireless Engineering group, I would also like to express my gratitude to the past and present members; to Dr. Samuel Lawman for all fruitful discussions, to Dr, Rula Alrawashdeh and Umniyyah Ulfa Hussine for all good time we had in our office, to Dr. Neda Khiabani for her inspiring suggestions and time for me. I am delighted that I have found many good friends during my PhD studies.

Thanks to all my friends, from high-school, college and Malaysian Society who had been with me in the very crucial moments of my studies and for boosting my morale. I am very grateful for all their support and effort to cheer me up. In the department, it is a great pleasure to thank the postgraduate staff, Allison and Hannah for their full support especially in the very challenging moment of my studies.

I would like to offer my personal and special thanks to my parents and my siblings who have encouraged me over the years. Primarily this must be my father and mother, who believed in me and surrounded me with their love and blessing. I must also mention my sister, Azliana for proof readings my work. I am very thankful for their patience on all my stresses during this journey.

Finally, I should thank the Islamic Development Bank, Saudi Arabia and Universiti Kuala Lumpur Malaysia for sponsoring my PhD studies. Also the Government of Malaysia for taking care of me while I am abroad.

List of Publications

1. A. Abu Bakar Sajak, Y. Shen and Y. Huang "Analysis of a Photoconductive Antenna using COMSOL", *10th UK-Europe-China Workshop on Milimetre Waves and Terahertz Technologies (UCMMT)*, Liverpool, UK, September, 2017.

2. Z. Zhang, L. Liu, **A. Abu Bakar Sajak**, L. Gan, Y. Huang and Y. Shen, "Spinning disk as a spatial light modulator for rapid infrared imaging", *IET Microwaves, Antennas & Propagation*, Volume 11, Issue 3, February 2017, p. 317 – 323.

3. R. Alrawashdeh, Y. Huang, M.Kod and **A. Abu Bakar Sajak, "**A Broadband Flexible Implantable Loop Antenna With Complementary Split Ring Resonators", *IEEE Antennas and Wireless Propagation Letters*, Volume 14, February 2015, p.1506-1509.

4. **A. Abu Bakar Sajak**, Y. Shen, Y. Huang, and R. Alrawashdeh, "A Comparison of the Effect of Substrate on the Performance of THz Antenna", *Proceeding of the ICE2T*, Malaysia, August, 2014.

5. Q. Xu, Y. Huang, X. Lei and **A. Abu Bakar Sajak**, "Statistical Electromagnetic Analysis of PEC Sphere Scattering", *Proceeding of the ICE2T*, Malaysia, August, 2014.

6. R. Alrawashdeh, Y. Huang, and **A. Abu Bakar Sajak**, "Orientation Effect of Flexible Implantable Antennas on Performance," *2014 IEEE International Symposium on Antennas and Propagation and USNC-URSI National Radio Science Meeting* , Memphis, Tennessee, USA, July, 2014.

7. **A. Abu Bakar Sajak**, Y. Shen, Y. Huang, and R. Alrawashdeh, "The Effect of Substrate on the Performance of THz Antenna", *IET Colloquium on Millimetre-wave and Terahertz Engineering & Technology*, Liverpool, UK, 2014.

8. **A. Abu Bakar Sajak**, Y. Shen, Y. Huang, and R. Alrawashdeh, "An Investigation on THz Antennas Using Graphene as a Substrate", *The 8th European Conference on Antennas and Propagation*, The Hague, The Netherlands, April, 2014.

9. R. Alrawashdeh, Y. Huang, and **A. Abu Bakar Sajak**, "A Flexible Loop Antenna for Biomedical Bone Implants", *The 8th European Conference on Antennas and Propagation*, The Hague, The Netherlands, April 2014.

10. N. Khiabani, Y. Huang, Y. Shen, and **A. Abu Bakar Sajak**, "Photoconductive THz Antennas *Loughborough Antennas & Propagation Conference*, Loughborough, UK, November 2013.

Table of Contents

List of Tables

List of Figures

List of abbreviation

AlGaAs	Aluminium Gallium Arsenide
AR	Anti-Reflection
BW	Bandwidth
BWO	Backward Wave Oscillator
CAD	Computer Aided Design
CW	Continuous Wave
CPW	Coplanar Waveguide
DFG	Difference Frequency Generation
EM	ElectroMagnetic
EO	Electro-Optic
ErAs	Erbium Arsenide
FDTD	Finite Difference Time Domain
FWHM	Full Width at Half Maximum
GaAs	Gallium Arsenide
HEB	Hot Electron Bolometer
IMPATT	IMPact Avalanche and Transit Time
ITO	Indium Tin Oxides
LEC	Liquid Encapsulated Czochralski
LT-GaAs	Low Temperature-GaAs
MBE	Molecular Beam Epitaxy
MEMS	MicroElectroMechanical System
MMIC	Monolithic Microwave Integrated Circuits
MW	Microwave

QCL	Quantum-Cascade lasers
QTDS	Quasi Time Domain Spectroscopy
RF	Radio Frequency
RTD	Resonant Tunnelling Diodes
RX	Receiver
SEM	Scanning Electron Microscopy
Si	Silicon
SI-GaAs	Semi-Insulating GaAs
SI-InP	Semi-Insulating Indium phosphide
SIS	Superconductor–Insulator– Superconductor
SNR	Signal-to-Noise Ratio
TEM	Transverse ElectroMagnetic
THz	Terahertz
THz-TDI	THz Time Domain Imaging
THz-TDS	THz Time Domain Spectroscopy
Ti	Titanium
TWT	Travelling Wave Tube
TX	Transmitter
ZnTe	Zinc Telluride

Chapter 1 Introduction

1.1 The Terahertz Spectrum

The region of the electromagnetic spectrum in the range of 100 GHz (3 mm) to 10 THz (30 μm) which is between the millimetre and infrared frequencies is used to describe the THz radiation typically [2, 3]. THz band has variously been named such as sub-millimetre, far infrared and near millimetre wave. At 1 THz, the radiated signal has a wavelength of 300 μm in free space, a period of 1 ps, 4.14 meV photon energy and hf / k_B = 48 K temperature; where h is Planck's constant, f is frequency and k_B is Boltzmann's constant. The THz band in the electromagnetic spectrum is shown in Fig. 1.1

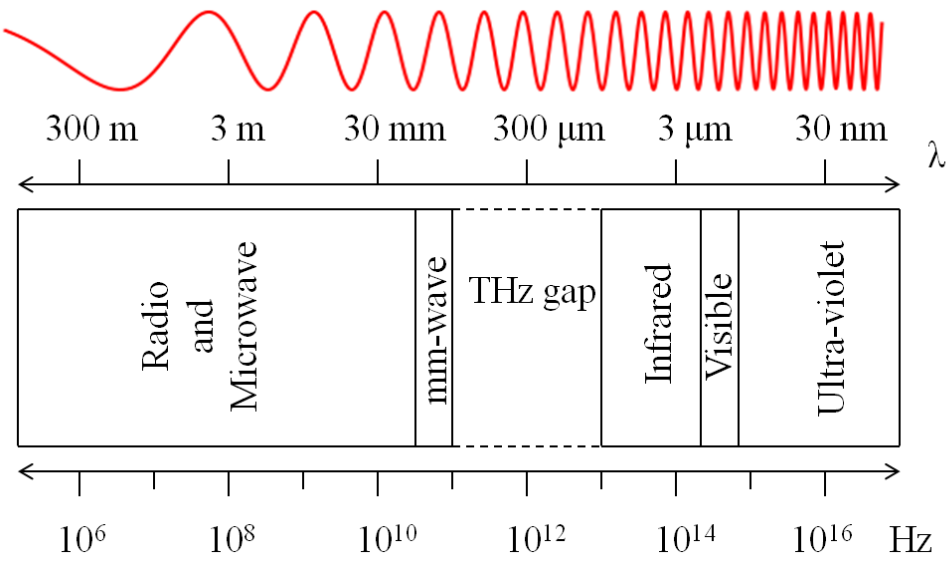

Fig. 1.1 Schematic diagram showing the location of THz band in the electromagnetic spectrum [1-2]

Due to the absence of efficient, coherent, and compact THz sources and detectors, this segment of the electromagnetic spectrum is the least explored region [3, 4]. Common microwave-frequency sources such as transistors or RF/MW antennas and devices working in the visible and infrared range, for example, semiconductor laser diodes exhibit these characteristics [5]. Due to the significant reduction in power and efficiency, it is not possible to adopt these technologies for operation in the THz region. Solid-state electronic devices, such as diodes generated power that has roll-offs of $1/f^2$ [6] due to reactive-resistive effects and long transit times at the lower extreme of THz frequency range [6]. Furthermore, lack of materials with adequately small bandgap energies [5] making optical devices, such as diode lasers, perform poorly at THz range limit. Therefore, the term "THz gap" is invented to explain the lack of maturity of this band compared to fully developed adjacent spectral regions. Various types of research on new emitters and detectors based on semiconductor technology are emerging to address these issues [4, 7-9].

In this chapter, the THz radiation is explained. Its properties and application are discussed. Then, different THz sources and detectors are reviewed and evaluated. Based on the built foundation, the research motivations and objectives of this thesis are outlined.

1.2 The THz Wave Properties and Applications

Interest in THz region dates back to 1920s [30], though only within the past three decades extensive research has been dedicated to this spectrum. Endless applications possibility in the THz frequency range and remarkable wave properties is the reason for the sudden interest in the region. Since THz region is contained between microwave-millimetre and infrared areas it has mid-characteristics borrowed from the two bands. These properties can be summarised as follows [1-2]:

1. *Penetration:* The wavelength of THz radiation is longer than the infrared wavelength; hence, THz waves have less scattering and better penetration depths (~ cm) compared to infrared ones (~ μm). Therefore, dry and non-metallic materials are transparent in this range but are opaque in the visible spectrum.

2. *Safety:* In contrary to X-rays, the photon energies in the THz band are much lower. Therefore, THz radiation is non-ionising.
3. *Spectral fingerprint:* Inter- and intra-vibrational modes of many molecules lie in THz range.
4. *Resolution:* THz waves have shorter wavelengths in comparison to the microwave ones, this gives a better spatial imaging resolution.

1.2.1 Atmospheric Characteristics of THz Waves

Compared to the microwave and infrared waves THz radiation has distinct atmospheric characteristics. THz waves have extremely high absorption in the atmospheric situation and the moist environment. Fig. 1.2 shows the atmospheric attenuation across the electromagnetic spectrum. Signal degradation in this range- with the main peak attenuation between 1 to 10 THz- is considerably more than the microwave and infrared bands. THz signal absorbs water significantly. Thus, for long range (> few hundred meters) applications, the required power for signal transmission is high and impractical [6]. However, the application of THz waves in the two following cases is different.

1. Signal absorption and attenuation due to water drops are not problems in space since the ambient is near-vacuum. Moreover, black body temperatures of THz signals lie in the range of 4.8-480 K which means the majority of ambient radiation is THz waves. Considering spectral signature of interstellar dust which is located in THz region and advantage above of THz signals in space, THz technology is a very interesting and widely used technique in radio astronomy and space science [10]. European Space Agency launched the largest infrared space telescope known as Herschel Space Observatory in 2009 [11].
2. Atmospheric attenuation does not have any significant impact for short range applications, typically less than 100 m is not a big issue. Hence, THz technology has substantial potential for fundamental investigations in various disciplines such as chemistry and physic.

Despite adverse effect of water vapour lines on THz signals, these lines are narrow enough, and their positions have been known; thus, this allows removal or recognition of the water vapour lines effect in THz applications such as spectroscopy [12].

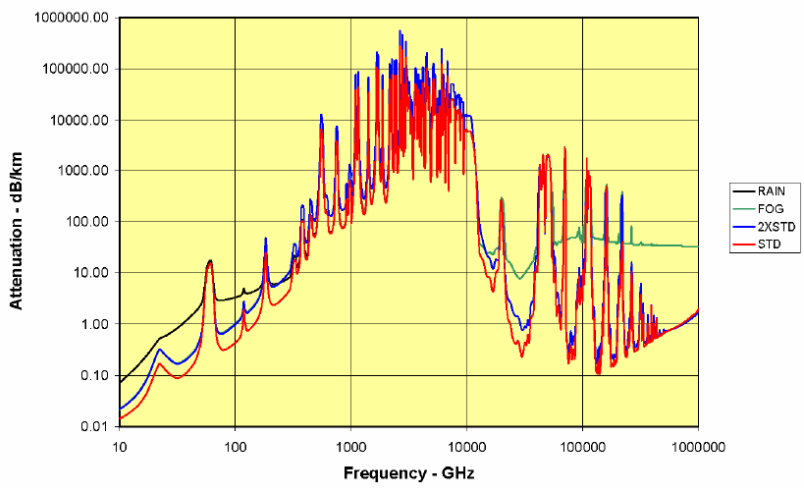

Fig. 1.2 Attenuation at sea level for different atmospheric situations, Rain = 4 mm/h, Fog = 100 m visibility, STD = 7.5 gm/m^3 water vapour, and 2×STD = 15 gm/m^3 water vapour [13]

1.2.2 Applications of THz Radiation

THz radiation can be applied in many possible applications including imaging, spectroscopy and wireless communication based on THz wave properties [11, 14-15]. Even though THz applications have widely been explored, only in the recent decade, companies such as TeraView Ltd [16], Terametrix (formerly known as Picometrix) [17] and Toptica [18] had manufactured several commercial THz imaging and spectroscopy systems. In early 2011, the first THz camera that can see and record in real-time at room temperature was introduced by Traycer [19].

1.2.2.1 THz Pulsed System Applications

Pioneer work in THz pulsed imaging in [20] and THz CW imaging [21] spur many research areas on applications based on THz imaging areas [22]. One of the main subcategories in this field is medical imaging. Since THz waves can penetrate up to a few hundred micrometres (μm) in human tissues, therefore, making it a potential method for body surfaces such as skin, breast and mouth cancer detection [23-24] and dental imaging [25]. Early detection of cancerous tissues and tooth decay or minimisation of the damage to the surrounding

healthy skin in a biopsy are the benefit from this technology. THz medical imaging, however, has two major drawbacks where the equipment is expensive and data acquisition time is long. Arrays of antennas and micro lenses are employed in [22] to address the long data acquisition time.

Since the first introduction of THz pulsed spectroscopy in [27], a fascinating application for commercialising THz technology in diverse areas [26] can be observed. THz spectroscopy is a compelling technique to characterise material properties and understand their signature which lies in the THz band. This is because many molecules have rotational and vibrational transition lines in this range of frequency. Among interesting THz spectroscopy application is in biochemical science such as analysis of DNA signatures and protein structures [28].

Investigating material integrity and inspecting multi-layered materials such as wood, composites, and cloths can also be done using THz radiation. All of these materials are transparent in THz frequencies. THz pulsed imaging and spectroscopy have been adopted for non-destructive testing; for example, on imaging antiquities [29, 30] to reveal the thickness of the different layers of the artwork and to show the types of their materials [31]. This technique can be used for in-line control of polymeric compounding processes as well [32]. THz pulsed imaging and spectroscopy are also two robust quantitative and qualitative non-invasive methods for examining pharmaceutical solid dosage forms [33, 34].

Security applications using THz systems is also a huge possibility [22] because of the possibility of using these systems in personnel screening [16], solid explosive material detection [35, 36], and mail screening [37]. However, metals are not transparent to THz signals; therefore, they are not suitable for imaging inside the metallic suitcases. This system can perhaps be treated as a backup for the well-established monitoring techniques like X-ray [22].

One of the major drawbacks of the THz technology is its high water absorption. However, this drawback can be manipulated positively to distinguish the hydrated substances from dried ones. For instance, in the paper industry, THz spectroscopy has been used for monitoring the thickness and moisture content of papers by manufacturers [38-39].

Finally, a very convenient method to take 3D images from the inside of an integrated circuit device can be done using THz pulsed imaging. This is better compared to the 2D images provided by the X-ray method [22].

In a nutshell, a schematic overview of various THz applications based upon optoelectronic systems is depicted in Fig. 1.3 [1,2].

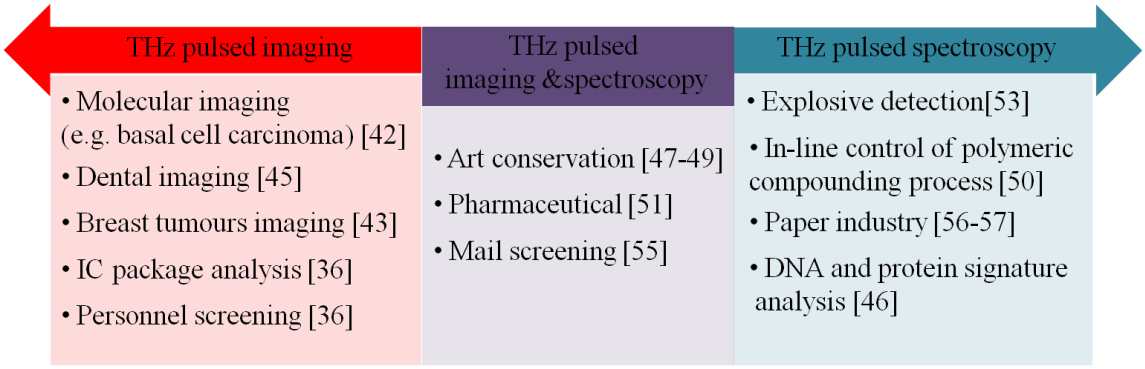

Fig. 1.3 Schematic overview illustrating some commercial and laboratory applications of THz pulsed imaging and spectroscopy across the various sciences [1]

THz application in wireless communication, one interesting THz application which cannot be categorised in either THz pulsed imaging or spectroscopy. To provide sufficient transmission capacity for future high data rate demands, higher carrier frequencies need to be utilized, and THz frequencies had the potential to satisfy these needs. However, THz communication links have two main limitations where THz communication systems are only suitable for line of sight cases, and THz signals can only propagate over a short path length due to severe atmospheric attenuation. Considering these restrictions, THz communication systems can be a suitable option for indoor short distances which is limited to several tens of meters such as multipoint to point/multipoint basis at frequencies between about 0.2 to 0.3 THz [40]. From another point of view, these restrictions are beneficial for secure THz communication since the beam can be highly directional and it attenuates severely over the distance; unwanted signal detection is difficult. THz data communications for short ranges less than < 1m is based upon THz time domain systems and have been tested at 0.3 THz in recent years [41]. In [42] external semiconductor THz modulator is used with data transmission of 6 kHz while in [43] audio signals through the voltage of the transmitter THz antenna modulates

the THz frequency, and the reported data transmission was 5 kb/s. Block diagrams of these two approaches are demonstrated in Fig. 1.4.

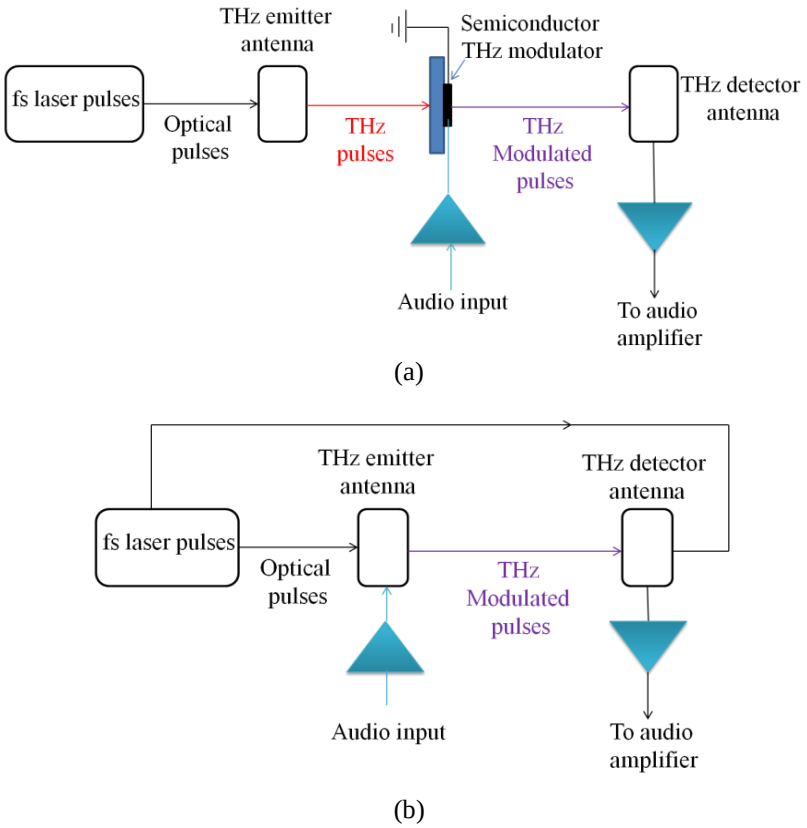

Fig. 1.4 Schematic diagram of THz communication links for (a) system of [42] with external modulator (b) system of [43] where voltage modulation of the THz antenna is used

1.2.2.2 THz CW applications

Narrowband high resolution systems are required for some applications such as gas-phase spectroscopy, high frequency dielectric measurements of electronic, metamaterials and nano-materials, and signature analysing in microliter DNA [22,44-46]. This opportunity can be realised via THz CW imaging and spectroscopy systems [47-48]. For some applications like imaging of aircraft glass-fibre composites or determining the thickness of a sample however both pulsed and CW imaging methods can be used [41, 49].

1.3 THz Sources

Among all the elements in THz technology, the THz source has been considered as the most challenging component to accomplish [26]. Numerous research and effort have been done to extend RF/MW and optical technologies to THz band. Combining both of the technologies

to realise THz sources with better performance had also been considered [50]. Due to this effort, THz emitters are divided into three main groups: THz sources developed from RF/MW side, THz sources extended from optical side, and THz sources combining RF/MW and optical techniques.

1.3.1 THz Sources from RF/MW Side

In this category, diodes and THz vacuum tube sources are explained.

1.3.1.1 Diodes and Frequency Multipliers

On the lower end of the THz spectrum, diodes can transfer the functionality of lower frequency electronics into the THz band. There are several types of diodes, such as Gunn diodes, IMPATT diodes and resonant tunnelling diodes (RTD). The principle of power generation from these diodes is based upon their negative differential resistance [51] although the operation bases of these diodes are different. Each of these diodes has their own advantages and disadvantages [51-56]. Still, in these components, dramatic reduction in powers can be observed with increasing frequency [53].

Another method to reach THz band is the use of frequency multipliers which outperform other solid-state electronic sources. This is because the diode multipliers are physically and operationally simple [52]. Since higher order multipliers are incredibly inefficient, series arrangements of doublers and triplers have mostly been implemented [26]. In this method, chains of microwave sources, such as GaAs Schottky diodes, at lower GHz bands (20 – 40 GHz) can be used in series to drive multiplication at THz ranges [52]. However, the output power from multipliers decreases at higher frequencies [57], like the diodes mentioned above. The bandwidth of these sources is also limited [57].

1.3.1.2 THz Vacuum Tube Sources

Free electrons emission from microwave tubes is one of the traditional THz generation methods. THz tubes such as travelling wave tube (TWT), backward wave oscillator (BWO), klystron and gyratron can produce strong power levels at the lower end of THz band. In [58] a

power level of 52 mW at about 0.6 THz from a BWO has been reported. One of the main operational similarities in all of these tubes is the interaction of an electron beam with an electromagnetic wave to produce THz energy. Although THz tubes can produce much stronger power levels at the lower end of THz band compared to previously explained solid-state components [51], they are very bulky. They also need large magnetic biases and high voltage power supplies. This restricts the use of these sources in wide operational settings, making it inflexible.

1.3.2 THz Sources from Optical Side

THz sources from optical side are mainly divided into lasers with different generation techniques and nonlinear crystals [2].

1.3.2.1 Molecular Lasers

THz signals with a power level of few ten milliwatts can be produced by injecting grating tuned CO_2 lasers into low-pressure flowing gas cavities [2,26]. The frequency of this THz power depends on the spectral line of the gas; for example, a rotational transition of methanol occurs at 2.522 THz.

1.3.2.2 THz Semiconductor Lasers

Semiconductor diode lasers are very successful and prevalent in the near-infrared and visible frequency ranges. In THz bands, natural materials with suitable band gaps are not available, artificially engineered materials are considered [5, 59]. Therefore, the concept of THz Quantum-Cascade lasers (QCL) which are intra-band lasers and require the creation of quantised sub-bands was introduced [4]. For this purpose, several few-nm-thick GaAs layers separated by AlGaAs barriers need to be fabricated. Therefore, proper engineering of the thickness of the semiconductor layers (or quantum wells) and also a choice of the appropriate bias voltage is required to achieve population inversion. Because the energy of the system is inversely proportional to the square of the layers thicknesses, by narrowing or widening the

quantum wells, series of multi layers of energy can be created. Thus, the electron motion from one miniband to the next results in an emission of a THz photon at each transition.

QCL can operate in both pulsed and continuous-wave (CW) modes. QCL operating frequency is controlled by quantum well design (band gap engineering), and different wavelengths can be achieved in the same material [2]. QCLs have been one of the most intensive research topics in THz area during the past decade and the survey on different THz QCLs show that the frequency ranges of these devices span from 0.84 THz to 5 THz at various cryogenic working temperatures [60-63] with the best peak optical power of 200 mW at about 4.5 THz [5] . The best peak operating temperature of 200 K at about 3.2 THz reported in [64]. In room temperature situation, a THz QCL with a power of 8.5 μW at 4 THz has been demonstrated [65].

As a conclusion, QCLs have larger output power at higher THz frequencies and as frequency decreases the power reduces considerably [2]. One of the main limitations of THz QCLs is that for THz operation they need cryogenic cooling and this restricts the operation of QCLs to only laboratory environments making it unattractive.

1.3.2.3 Optical Down Converters

One of the common methods for THz generation is the use of nonlinear crystals with large second order susceptibility, χ, for down conversion of power from optical regime [2]. Several nonlinear materials for this purpose can be employed [11]. THz parametric processes such as parametric oscillator or difference frequency generation (DFG) are techniques for production of monochromatic highly tunable THz wave sources with a high spectral resolution [66-68]. Another optical down conversion method is the optical rectification in which all possible difference frequencies of spectrally broad optical pulses are generated.

The drawbacks of this method are that the phase matching between the optical fields and induced THz field is needed. This requires thorough design on the thickness of the nonlinear material. The THz output power in this method is low, and to generate significant THz power, high power optical sources are needed.

1.3.3 THz Sources Combining RF/MW and Optical Techniques

THz antennas which are based upon photoconduction which is the basis of this thesis can be assigned to this category of THz sources. As shown in Fig.1.5, a Photoconductive THz antenna consists of a voltage-biased antenna mounted on a photoconductive substrate where GaAs is commonly used. Optical laser sources as the excitation sources of THz antennas are used to produce THz waves by inducing rapid changes in the current/carrier density in the photoconductive substrate. Depending on the type of optical excitation, there are two alternatives for THz antennas based upon photoconduction technique:

1) THz photoconductive antennas in pulsed systems

2) THz photomixer antennas in CW systems

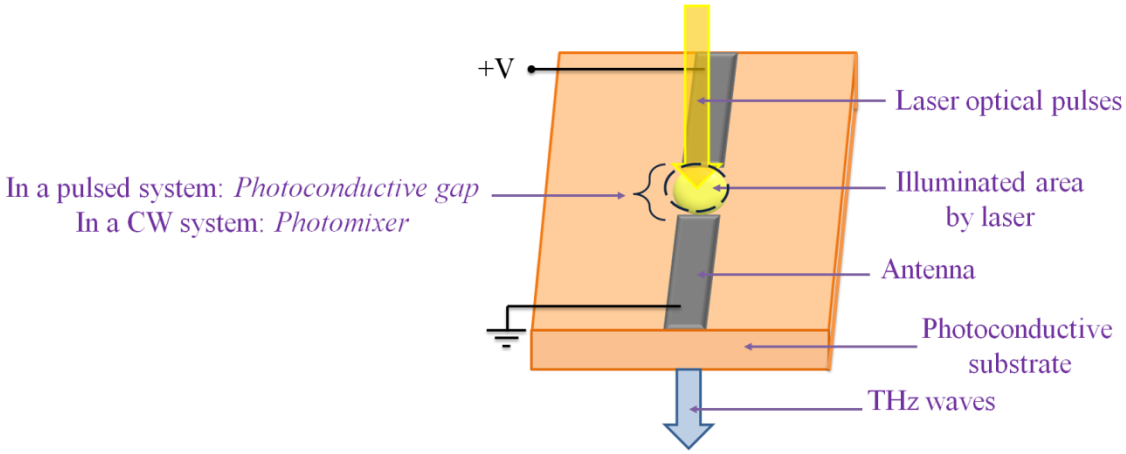

Fig. 1.5 Schematic diagram of a THz antenna as an emitter for both pulsed and CW THz systems

Although it is possible to use the same antenna in both systems, different excitation methods dictate different requirements for each antenna type and result in different THz waves and applications. In THz pulsed systems, because of the external bias field, the optically induced photo-carriers in the photoconductive gap give rise to rapid changes in the current density. These currents induce a THz electromagnetic field in the connected antenna, and as a consequence, ultrafast electrical pulses are produced and radiated into free space. In CW systems the process is same; however, usually two monochromatic lasers with slightly different optical frequencies (the difference is in THz) are used for THz emission from the antenna. This inherent excitation difference in THz pulsed and CW systems leads to the generation of ultra wideband and narrowband THz waves respectively. In a CW system, the term “photomixer”

refers to the antenna gap (which can have various designs) in an analogy of “photoconductive gap” in a THz pulsed system. The focus of this thesis will be on these types of sources. Detailed and comprehensive study and investigation on THz antennas will be presented in next chapters.

1.4 THz Detectors

Compared to emitters/sources, development in THz detectors has been more aggressive [26]. One of the main issues in the detection of THz waves is that the photon energy in this frequency band is in the range of 0.41 to 41 meV which is comparable to the background thermal noise energy. Therefore, to overcome this problem mainly two methods have been adopted: cryogenic cooling and signal integration for long enough periods [26].

THz detection can be categories into coherent and incoherent techniques. The main difference between them is that in coherent technique both the amplitude and phase of the received signal are determined. Meanwhile, an incoherent technique only the intensity of the signal is measured [2].

Important, coherent technique in detecting weak and narrowband signals is heterodyne detection. In this method, a mixer, a nonlinear device, as a local oscillator is used for frequency down conversion. Fig. 1.6 demonstrates the process of electronic heterodyne detection. The amplitude of the detected signal is proportional to the amplitude of the THz signal [2]. There are various types of mixers in the THz range. A Schottky diode is a common and basic mixer type for room temperature detectors where a modest sensitivity is required. However, for high sensitivity applications, superconducting heterodyne detectors are employed which operate in cryogenic temperatures. SIS tunnel junction mixers and HEB mixers are two examples of mixers in this category.

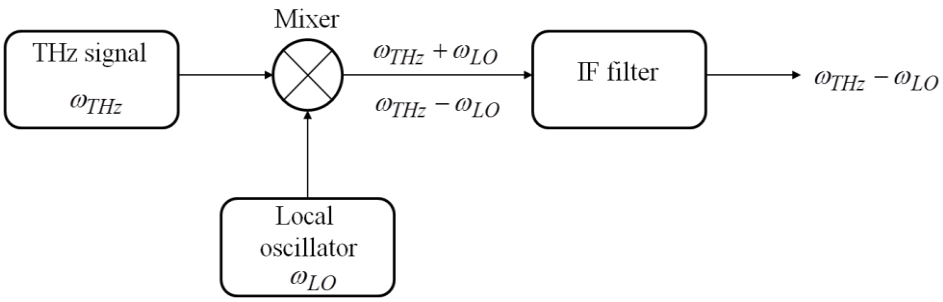

Fig. 1.6 Block diagram of a THz heterodyne detector [2]

Electro-Optic (EO) and photoconduction samplings are also coherent methods. In the former, the amplitude and phase of the THz signal are measured by using a nonlinear crystal. In the photoconduction samplings as shown in Fig. 1.7, the THz signal induces a voltage across the antenna which leads to a generation of THz current due to the existence of free electron-hole pairs in the antenna gap. The phase of the THz signal in these methods can be measured by varying the optical path length of the optical probe pulse.

Other incoherent detectors are direct detectors such as Golay cells and bolometers. These detectors in room temperature are appropriate for applications where high spectral resolution and rapid response time in the order of seconds are not required [26]. For a better sensitivity and dynamic range, cryogenic cooled direct detectors such as cryogenically cooled bolometers which have a response time in the order of microseconds can be used [26].

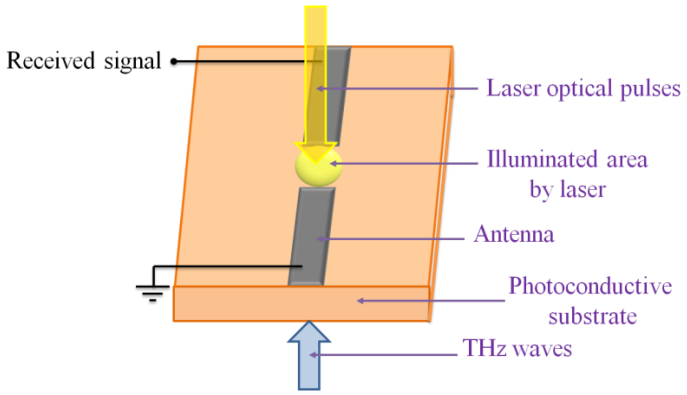

Fig. 1.7 Schematic diagram of a THz antenna as a THz detector for both pulsed and CW THz systems [2]

1.5 Research Motivations and Objectives

The primary motivation for this research is triggered by the limitation in the development of high output power and efficient sources in the fast growing THz technology.

Though light and radio waves belong to the same electromagnetic spectrum, their behaviour is different. THz region is the intermediate part of the spectrum which has a mixture of both characteristics. Despite the fascinating and unique properties, THz technology has been largely avoided by the late of the twentieth century due to the lack of robust, coherent, efficient and cost effective THz sources and detectors [1-2]. However, the advent of femtosecond lasers in the 1980s and later photoconductive antennas in 1984 [68], developed accessibility to THz gap. Since then and over the last three decades, due to interests in new THz applications in different fields as discussed previously, THz technology has undergone extraordinary progress. Commercial THz imaging and spectroscopy systems have started to be introduced to the market. Still, there are various issues, such as the low output power and working temperature of THz sources, which need to be tackled for this technology to be as mature as radio and optical technologies.

THz photoconductive antennas are one of the keys and common components in many THz systems. The popularity of these THz antennas is because of the several advantages that these types of THz sources are offered as compared to other THz sources discussed earlier. For instance, they work in a room-temperature environment, they are compact, and they can operate both in the emitter and detector sides [1-2].

Although these types of components have been widely employed in established THz systems, the radiated power from them is very low, which is about few microwatts, and they are inefficient [69]. For this purpose, it is crucial to establish the effect of various parameters of optical sources, photoconductive materials and antennas on the performance of the THz antennas. Thus, having a model which links these parameters can be very useful for both, designing a THz antenna and tuning a THz system to achieve the optimum power conversion efficiency and THz radiated power. Therefore, as fundamental research work on the THz

photoconductive antennas, a numerical model is developed in this study considering the interaction between laser beams, photoconductive materials and antennas in a typical THz scheme.

Utilising a package of commercial simulation tool is an essential part of radio frequency (RF) antenna analysis. This step is crucial to determine the necessary parameters before preceding to any experimental procedure. However, the major difference in analysing THz antennas as compared to RF antennas is the optoelectronic characteristics of THz antennas which are the result of the optical excitation and photoconductive material response. Some commercial semiconductor solvers such as TCAD Sentaurus [70] and COMSOL [71] perform advanced simulations on characterising semiconductor devices considering their complex physical phenomena, and various information for instance on electric field distribution and charge concentration can be provided by them. Sentaurus is a suite of TCAD tools which simulates the fabrication, operation and reliability of semiconductor devices, but COMSOL COMSOL Multiphysics is a cross-platform finite element analysis, solver and multiphysics simulation software. One software product with a lot of different modules. COMSOL offers a single and comprehensive software set. One advantage provided through COMSOL is the ease of setting up a multi-physics simulation. With one pre-processor, solver and post-processor, simulation analysts don't have to use a wide range of tools to get one job done. COMSOL is a consolidated environment hence simulation analysts don't have to worry about mapping the results of one simulation onto another simulation. For THz antenna analysis, the THz current source is the main input that needs to be fed to full-wavelength simulation tools. This combination of semiconductor solvers with full-wave electromagnetic solvers can provide a possibility of simulation of THz antennas, and this method can predict the outcome of any experimental procedure hence saving cost on unsuccessful experimental procedure.

As a summary, the main objectives of this research are as follows:

- To develop a novel model which perform better than conventional THz photoconductive antenna that will produce higher radiated THz power by identifying the related parameters that can be improved
- To formulate an equation that will be used with a new simulation method for THz photoconductive analysis
- To appraise the parameters of the proposed model and recommend the best dimension to be constructed

1.6 Thesis Overview

The thesis is organised as follows. To focus on the scope of the research to THz Photoconductive antennas, Chapter 2 starts with providing comparisons of THz antennas with conventional RF/MW (microwave) antennas from various aspects. To build the foundation for the contributions of this thesis, the necessity of new look and approach on analysis of THz antennas as compared to RF/MW antennas are highlighted. In the second part, the problems and reasons for THz antennas having low efficiency are elaborated, and some of the previous work on the previous photoconductive antenna is reviewed.

In Chapter 3, the impact of substrate dimensions and substrate material on the performance of THz photoconductive antenna were investigated. The investigations were done using commercial software, CST (Computer Simulation Technology). The radiated power and the efficiencies of a THz photoconductive antenna with various substrate dimensions were simulated. Both parameters were also simulated for THz photoconductive antenna with different substrate materials.

Electrodes are main components which are responsible for the generation of THz current. Geometrical modification and optimisation of electrodes can lead to a generation of more THz current which couples to the antenna. A study on the electrode structure's effect and electrode material's effect using CST (Computer Simulation Technology) are studied in this

chapter. However, the results from this commercial software are found insufficient. Hence, the investigation of the electrode structure effect is done thoroughly in Chapter 5 using COMSOL.

A novel design of a Photoconductive Antenna with an embedded electrode is proposed in Chapter 5. A novel concept to enhance the generated THz photocurrent in the Photoconductive Antenna is elaborated. Then, the proposed antenna is compared to the conventional antenna and proven to perform better using a simulation tool COMSOL where the combination of semiconductor solvers with full-wave electromagnetic solvers is used. Also, a novel analytical method is introduced in this chapter. The antenna operation principle, design procedure and simulated results are systematically described in Chapter 5.

Finally, Chapter 6 the concludes the research. The main objectives are reviewed, and the achievements are highlighted. Furthermore, the challenges and suggestions worthwhile to investigate as future further works are also discussed.

References

[1] N. Khiabani, "*Modelling, design and characterisation of Terahertz photoconductive antenna*". PhD thesis, Department of Electrical and Electronics Engineering, University of Liverpool, 2013.

[2] Y. Lee, *Principles of terahertz science and technology*, 1st ed. New York, NY: Springer, 2008.

[3] B. Ferguson and X. Zhang, "Materials for terahertz science and technology," *Nat Mater,* vol. 1, pp. 26-33, 2002.

[4] R. Kohler, A. Tredicucci, F. Beltram, H. E. Beere, E. H. Linfield, A. G. Davies, D. A. Ritchie, R. C. Iotti, and F. Rossi, "Terahertz semiconductor-heterostructure laser," *Nature,* vol. 417, pp. 156-159, 2002.

[5] B. S. Williams, "Terahertz quantum-cascade lasers," *Nat Photon,* vol. 1, pp. 517-525, 2007.

[6] C. M. Armstrong, "The truth about terahertz," *IEEE Spectrum,* vol. 49, pp. 36-41, 2012.

[7] P. R. Smith, D. H. Auston, and M. C. Nuss, "Subpicosecond photoconducting dipole antennas," *IEEE Journal of Quantum Electronics,* vol. 24, pp. 255-260, 1988.

[8] E. R. Brown, F. W. Smith, and K. A. McIntosh, "Coherent millimetre-wave generation by heterodyne conversion in low-temperature-grown GaAs photoconductors," *Journal of Applied Physics,* vol. 73, pp. 1480-1484, 1993.

[9] J. Faist, F. Capasso, D. L. Sivco, C. Sirtori, A. L. Hutchinson, and A. Y. Cho, "Quantum Cascade Laser," *Science,* vol. 264, pp. 553-556, 1994.

[10] E. Nichols and J. Tear, " Joining the infra-red and electric wave spectra," *Astrophysical Journal,* vol. 61, pp. 17-37, 1925.

[11] T. de Graauw, et al., "The Herschel-Heterodyne Instrument for the Far-Infrared (HIFI)," *A&A,* vol. 518, p. L6, 2010.

[12] R. Appleby and H. B. Wallace, "Standoff Detection of Weapons and Contraband in the 100 GHz to 1 THz Region," *IEEE Transactions on Antennas and Propagation,* vol. 55, pp. 2944-2956, 2007.

[13] M. C. Kemp, "Millimetre wave and terahertz technology for the detection of concealed threats: a review," pp. 64020D1-19, 2006.

[14] P. U. Jepsen, D. G. Cooke, and M. Koch, "Terahertz spectroscopy and imaging – Modern techniques and applications," *Laser & Photonics Reviews,* vol. 5, pp. 124-166, 2011.

[15] D. L. Woolard, R. Brown, M. Pepper, and M. Kemp, "Terahertz Frequency Sensing and Imaging: A Time of Reckoning Future Applications?," *Proceedings of the IEEE,* vol. 93, pp. 1722-1743, 2005.

[16] http://www.teraview.com/.

[17] http://www.macom.com/hsor/.

[18] http://www.toptica.com/.

[19] http://www.traycer.com/.

[20] B. B. Hu and M. C. Nuss, "Imaging with terahertz waves," *Opt. Lett.,* vol. 20, pp. 1716-1718, 1995.

[21] T. Kleine-Ostmann, P. Knobloch, M. Koch, S. Hoffmann, M. Breede, M. Hofmann, G. Hein, K. Pierz, M. Sperling, and K. Donhuijsen, "Continuous-wave THz imaging," *Electronics Letters,* vol. 37, pp. 1461-1463, 2001.

[22] P. U. Jepsen, D. G. Cooke, and M. Koch, "Terahertz spectroscopy and imaging – Modern techniques and applications," *Laser & Photonics Reviews,* vol. 5, pp. 124-166, 2011.

[23] V. P. Wallace, A. J. Fitzgerald, S. Shankar, N. Flanagan, R. Pye, J. Cluff, and D. D. Arnone, "Terahertz pulsed imaging of basal cell carcinoma ex vivo and in vivo," *British Journal of Dermatology,* vol. 151, pp. 424-432, 2004.

[24] A. J. Fitzgerald, V. P. Wallace, M. Jimenez-Linan, L. Bobrow, R. J. Pye, A. D. Purushotham, and D. D. Arnone, "Terahertz Pulsed Imaging of Human Breast Tumors," *Radiology,* vol. 239, pp. 533-540, 2006.

[25] D. Crawley, C. Longbottom, V. P. Wallace, B. Cole, D. Arnone, and M. Pepper, "Three-dimensional terahertz pulse imaging of dental tissue," *Journal of Biomedical Optics,* vol. 8, pp. 303-307, 2003.

[26] P. H. Siegel, "Terahertz technology," *IEEE Transactions on Microwave Theory and Techniques,* vol. 50, pp. 910-928, 2002.

[27] M. V. Exter, C. Fattinger, and D. Grischkowsky, "Terahertz time-domain spectroscopy of water vapour," *Opt. Lett.,* vol. 14, pp. 1128-1130, 1989.

[28] D. F. Plusquellic, K. Siegrist, E. J. Heilweil, and O. Esenturk, "Applications of terahertz spectroscopy in biosystems," *Chemphyschem,* vol. 8, pp. 2412-31, 2007.

[29] K. Fukunaga, Y. Ogawa, S. i. Hayashi, and I. Hosako, "Terahertz spectroscopy for art conservation," *IEICE Electronics Express,* vol. 4, pp. 258-263, 2007.

[30] J. B. Jackson, M. Mourou, J. F. Whitaker, I. N. Duling Iii, S. L. Williamson, M. Menu, and G. A. Mourou, "Terahertz imaging for non-destructive evaluation of mural paintings," *Optics Communications,* vol. 281, pp. 527-532, 2008.

[31] A. J. L. Adam, P. C. M. Planken, S. Meloni, and J. Dik, "TeraHertz imaging of hidden paintlayers on canvas," *Opt. Express,* vol. 17, pp. 3407-3416, 2009.

[32] N. Krumbholz, T. Hochrein, N. Vieweg, T. Hasek, K. Kretschmer, M. Bastian, M. Mikulics, and M. Koch, "Monitoring polymeric compounding processes inline with THz time-domain spectroscopy," *Polymer Testing,* vol. 28, pp. 30-35, 2009.

[33] Y. C. Shen, "Terahertz pulsed spectroscopy and imaging for pharmaceutical applications: a review," *Int J Pharm,* vol. 417, pp. 48-60, 2011.

[34] J. A. Zeitler and Y. Shen, *Terahertz Spectroscopy and Imaging*. Berlin Heidelberg: Springer 2013.

[35] Y. C. Shen, T. Lo, P. F. Taday, B. E. Cole, W. R. Tribe, and M. C. Kemp, "Detection and identification of explosives using terahertz pulsed spectroscopic imaging," *Applied Physics Letters,* vol. 86, p. 241116, 2005.

[36] Y. Shen, P. F. Taday, and M. C. Kemp, "Terahertz spectroscopy of explosive materials," *Proceedings of SPIE,* vol. 5619, pp. 82-89, 2004.

[37] K. Kawase, Y. Ogawa, Y. Watanabe, and H. Inoue, "Non-destructive terahertz imaging of illicit drugs using spectral fingerprints," *Opt. Express,* vol. 11, pp. 2549-2554, 2003.

[38] P. Mousavi, F. Haran, D. Jez, F. Santosa, and J. S. Dodge, "Simultaneous composition and thickness measurement of paper using terahertz time-domain spectroscopy," *Appl. Opt.,* vol. 48, pp. 6541-6546, 2009.

[39] D. Banerjee, W. von Spiegel, M. D. Thomson, S. Schabel, and H. G. Roskos, "Diagnosing water content in paper by terahertz radiation," *Opt. Express,* vol. 16, pp. 9060-9066, 2008.

[40] J. Federici and L. Moeller, "Review of terahertz and subterahertz wireless communications," *Journal of Applied Physics,* vol. 107, p. 111101, 2010.

[41] D. Saeedkia, *Handbook of terahertz technology for imaging, sensing and communications*. Cambridge, UK: Woodhead, 2013.

[42] T. Kleine-Ostmann, K. Pierz, G. Hein, P. Dawson, and M. Koch, "Audio signal transmission over THz communication channel using semiconductor modulator," *Electronics Letters,* vol. 40, pp. 124-126, 2004.

[43] T. Liu, G. Lin, Y. Chang, and C. Pan, "Wireless audio and burst communication link with directly modulated THz photoconductive antenna," *Opt. Express,* vol. 13, pp. 10416-10423, 2005.

[44] T. M. Korter and D. F. Plusquellic, "Continuous-wave terahertz spectroscopy of biotin: vibrational anharmonicity in the far-infrared," *Chemical Physics Letters,* vol. 385, pp. 45-51, 2004.

[45] W. Zhang, E. R. Brown, M. Rahman, and M. L. Norton, "Observation of terahertz absorption signatures in microliter DNA solutions," *Applied Physics Letters*, vol. 102, p. 023701, 2013.

[46] F. Hindle, A. Cuisset, R. Bocquet, and G. Mouret, "Continuous-wave terahertz by photomixing: applications to gas phase pollutant detection and quantification," *Comptes Rendus Physique*, vol. 9, pp. 262-275, 2008.

[47] I. S. Gregory, W. R. Tribe, C. Baker, B. E. Cole, M. J. Evans, L. Spencer, M. Pepper, and M. Missous, "Continuous-wave terahertz system with a 60 dB dynamic range," *Applied Physics Letters*, vol. 86, p. 204104, 2005.

[48] J. Karsten, H. Quast, R. Leonhardt, T. Loffler, M. Thomson, T. Bauer, H. G. Roskos, and S. Czasch, "Continuous-wave all-optoelectronic terahertz imaging," *Applied Physics Letters*, vol. 80, pp. 3003-3005, 2002.

[49] R. Wilk, F. Breitfeld, M. Mikulics, and M. Koch, "Continuous wave terahertz spectrometer as a noncontact thickness measuring device," *Appl. Opt.*, vol. 47, pp. 3023-3026, 2008.

[50] M. Tonouchi, "Cutting-edge terahertz technology," *Nat Photon*, vol. 1, pp. 97-105, 2007.

[51] D. M. Pozar, *Microwave engineering*, 4th ed. Hoboken, NJ: Wiley, 2012.

[52] T. W. Crowe, W. L. Bishop, D. W. Porterfield, J. L. Hesler, and R. M. Weikle, II, "Opening the terahertz window with integrated diode circuits," *IEEE Journal of Solid-State Circuits*, vol. 40, pp. 2104-2110, 2005.

[53] R. J. Trew, "High-frequency solid-state electronic devices," *IEEE Transactions on Electron Devices*, vol. 52, pp. 638-649, 2005.

[54] H. Eisele, "InP Gunn devices for 400-425 GHz," *Electronics Letters*, vol. 42, pp. 358-359, 2006.

[55] H. Eisele and R. Kamoua, "Submillimeter-wave InP Gunn devices," *IEEE Transactions on Microwave Theory and Techniques*, vol. 52, pp. 2371-2378, 2004.

[56] N. Orihashi, S. Suzuki, and M. Asada, "One THz harmonic oscillation of resonant tunnelling diodes," *Applied Physics Letters*, vol. 87, p. 233501, 2005.

[57] A. Maestrini, J. Bruston, D. Pukala, S. Martin, and I. Mehdi, "Performance of a 1.2 THz frequency tripler using a GaAs frameless membrane monolithic circuit," in *2001 IEEE MTT-S International Microwave Symposium Digest*, 2001, pp. 1657-1660 vol.3.

[58] J. Tucek, D. Gallagher, K. Kreischer, and R. Mihailovich, "A compact, high power, 0.65 THz source," in *IEEE International Vacuum Electronics Conference, 2008. IVEC 2008.* , pp. 16-17.

[59] A. G. Davies, E. H. Linfield, and M. B. Johnston, "The development of terahertz sources and their applications," *Physics in Medicine and Biology*, vol. 47, p. 3679, 2002.

[60] B. S. Williams, S. Kumar, H. Qing, and J. L. Reno, "High-power terahertz quantum cascade lasers," in *Conference on Lasers and Electro-Optics and Quantum Electronics and Laser Science Conference. CLEO/QELS 2006.* , 2006, pp. 1-2.

[61] S. Kumar, B. S. Williams, S. Kohen, Q. Hu, and J. L. Reno, "Continuous-wave operation of terahertz quantum-cascade lasers above liquid-nitrogen temperature," *Applied Physics Letters*, vol. 84, pp. 2494-2496, 2004.

[62] C. Worrall, J. Alton, M. Houghton, S. Barbieri, H. E. Beere, D. Ritchie, and C. Sirtori, "Continuous wave operation of a superlattice quantum cascade laser emitting at 2 THz," *Opt. Express*, vol. 14, pp. 171-181, 2006.

[63] C. Walther, M. Fischer, G. Scalari, R. Terazzi, N. Hoyler, and J. Faist, "Quantum cascade lasers operating from 1.2 to 1.6 THz," *Applied Physics Letters*, vol. 91, p. 131122, 2007.

[64] S. Fathololoumi, E. Dupont, C. W. I. Chan, Z. R. Wasilewski, S. R. Laframboise, D. Ban, A. Mátyás, C. Jirauschek, Q. Hu, and H. C. Liu, "Terahertz quantum cascade lasers operating up to about 200 K with optimised oscillator strength and improved injection tunnelling," *Opt. Express*, vol. 20, pp. 3866-3876, 2012.

[65] Q. Y. Lu, N. Bandyopadhyay, S. Slivken, Y. Bai, and M. Razeghi, "Room temperature single-mode terahertz sources based on intracavity difference-frequency generation in quantum cascade lasers," *Applied Physics Letters*, vol. 99, p. 131106, 2011.

[66] W. Shi, Y. J. Ding, and P. G. Schunemann, "Coherent terahertz waves based on difference-frequency generation in an annealed zinc–germanium phosphide crystal: improvements on tuning ranges and peak powers," *Optics Communications*, vol. 233, pp. 183-189, 2004.

[67] K. Suizu and K. Kawase, "Monochromatic-Tunable Terahertz-Wave Sources Based on Nonlinear Frequency Conversion Using Lithium Niobate Crystal," *IEEE Journal of Selected Topics in Quantum Electronics*, vol. 14, pp. 295-306, 2008.

[68] W. Shi, Y. J. Ding, N. Fernelius, and K. Vodopyanov, "Efficient, tunable, and coherent 0.18-5.27-THz source based on GaSe crystal," *Opt. Lett.*, vol. 27, pp. 1454-1456, 2002.

[69] M. Tani, S. Matsuura, K. Sakai, and S.-i. Nakashima, "Emission characteristics of photoconductive antennas based on low-temperature-grown GaAs and semi-insulating GaAs," *Appl. Opt.*, vol. 36, pp. 7853-78.

[70] https://www.synopsys.com/

[71] https://www.comsol.com/

Chapter 2 THz Photoconductive Antennas

2.1 Introduction

This chapter focussed on the THz Photoconductive antenna. As emitters, it converts optical waves to THz waves. As detectors side, it transforms THz energy to electric energy detectable by a lock-in amplifier. However, special excitation method of this antenna imposes new and different approaches for antenna analysis, simulation, fabrication and measurement as compared to a common RF/MW antenna. Thus, in this chapter after highlighting the necessity of having an antenna, THz antennas are compared with RF/MW antennas. This comparison is significant because it highlights research options in THz antennas and it builds the base for contributions of this thesis.

2.2 The Importance of Having a THz Antenna in a THz System

Semiconductor materials like LT-GaAs and InP can generate THz waves [1, 2]. Under the illumination of femtosecond optical pulses, electron-hole pairs on the surface of a semiconductor substrate are separated. Then, due to the acceleration of the carriers in the electric field originating in the surface depletion layer of this semiconductor, THz wave is radiated [3]. Carrier mobility and the intensity of the static internal field affect the amplitude and phase of the radiated THz field [1]. THz emission can be enhanced by applying an external magnetic field from semiconductor surfaces, and this is due to the reorientation of the created dipole in semiconductor towards the surface [4]. Nevertheless, the emitted power based on this method is small. Therefore, this can be improved by employing antenna electrodes on the semiconductors and applying an external bias field across the antenna which surpasses the

surface depletion field [5]. Companies such as Thorlabs [6], Toptica [7], Tetechs [8] and Menlosystem [9], had manufactured commercially THz antennas. Hence, THz antenna plays a vital role in stronger THz generation and detection.

2.3 The THz Photoconductive Antenna

THz photoconductive antennas, consisting of two metal usually gold electrodes on a photoconductive substrate. When used as an emitter these electrodes act mainly as a means for biasing the device and also as an antenna. The distance between the electrodes is referred to as the photoconductive gap. This gap is where the laser pulses illuminate. This gap is also where the electron-hole pairs are produced [10].

Through the differences in the photoconductive gap sizes, THz photoconductive antennas can be categorised into three types, firstly, small gap antennas with a gap size of about 5 to 50 μm. Secondly, large-aperture antennas where the gap dimension is much greater than the centre wavelength of the emitted THz radiation where the gap sizes are usually larger than few hundred micrometres [11] and lastly, semi-large gap antennas which the gap size is between the two previous types [12]. With small gap antennas, larger spectral ranges can be achieved [12, 14]. Meanwhile, large-aperture and semi-large antennas are better heating handling capability due to larger deposited electrode areas on the substrate and the ease of fabrication [13]. Electrodes of a THz antenna made a bigger impact on the THz power and bandwidth of small gap antennas rather than large-aperture antennas [12]. More detailed performance comparison of the small gap and large-aperture antennas are provided in the next section.

As shown in Fig. 2.1, an antenna electrode can have various shapes and geometries. Commonly used in THz pulsed systems due to their frequency independent characteristics are the bowtie antennas. Furthermore, the sharp ends of the antenna lead to singular electric fields hence enhancing the THz radiation from the device [15]. Besides bowtie antennas, a large gap coplanar strip line is also favoured because it does not need micro-fabrication techniques like small gap antennas. Also, for a precise laser focus alignment, a large gap coplanar strip line is not as sensitive as small gap antennas.

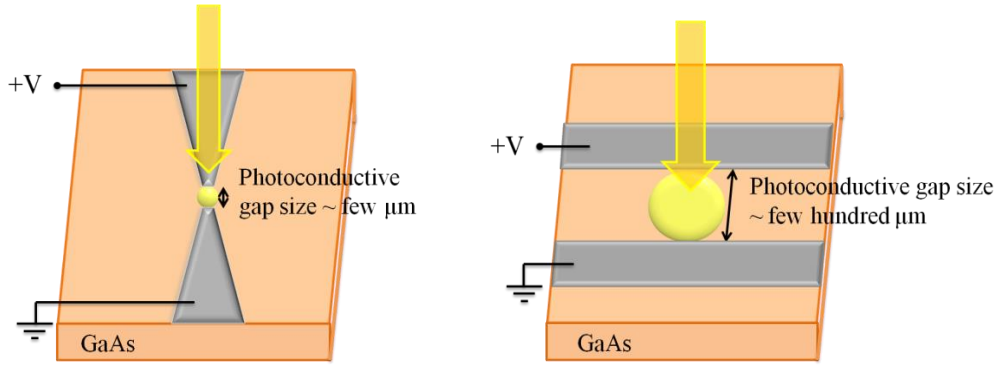

(a) (b)

Fig. 2.1 Sketch of THz photoconductive antennas (a) small gap bowtie antenna (b) large-aperture coplanar strip line [10]

2.3.1 Theoretical Principle of THz Photoconductive Antenna as an Emitter

Electron-hole pairs are created when the THz photoconductive antenna as an emitter is excited by ultra-short laser pulses. These ultra-short laser pulse's photon energy is higher than the bandgap energy of semiconductor material. Due to the bias voltage across the electrodes of the antenna, transient photocurrents are produced, because of the acceleration and deceleration of the photo-generated carriers. As a result, the THz wave is radiated into free space by the antenna. The theory of generation of THz photocurrent may differ [11] from each other due to the differences in the antenna gap size. In the following section, this is discussed in detail.

2.3.1.1 Large-Aperture Antennas

The emission of THz radiation from the large-aperture antenna is in line with the theory of dipole antenna. The generated photocurrent can be assumed as surface current confined to a thin layer in the photoconductive gap [11, 16-17] under the laser illumination. Hence, the on–axis radiated THz field in the temporal format can be written as [17]:

$$\vec{E}_{THz}(r,t) = -\frac{\mu}{4\pi}\int \frac{\partial \vec{J}_s(t)}{\partial t}\frac{dS}{r} = -\frac{\mu S}{4\pi z}\frac{d\vec{J}_s(t)}{dt} \tag{2.1}$$

where $\vec{J}_s(t)$ is the surface current density, μ is the permeability, S is the photo-excited area in the antenna gap and z is the on-axis distance from the antenna gap.

According to the detailed explanations in Appendix A, the surface current density in a large-aperture antenna is:

$$\vec{J}_s(t) = \frac{\sigma_s(t)\vec{E}_{bias}(t)}{\frac{\sigma_s(t)\eta_0}{1+\sqrt{\varepsilon_r}}+1} \tag{2.2}$$

where $\sigma_s(t) = e \cdot \mu_e \cdot n(t)$ is the surface conductivity of the photoconductive substrate, m^* is the effective mass and μ_e is the electron mobility and related to photoconductive material characteristics as $\mu_e = e\tau_s / m^*$.

Through equations 2.1 and 2.2, the radiated THz field can be obtained as:

$$\vec{E}_{THz}(z,t) = -\frac{\mu S}{4\pi z}\frac{\frac{d\sigma_s(t)}{dt}}{(\frac{\sigma_s(t)\eta_0}{1+\sqrt{\varepsilon_r}}+1)^2}\vec{E}_{bias} = -\frac{\mu S}{4\pi z}\frac{e\mu_e\frac{dn(t)}{dt}}{(\frac{e\mu_e n(t)\eta_0}{1+\sqrt{\varepsilon_r}}+1)^2}\vec{E}_{bias} \tag{2.3}$$

Hence, it can be interpreted that large aperture antennas relied on surface current density and applied bias to antenna electrodes.

2.3.1.2 Small Gap Antennas

While the emission of THz radiation from a large-aperture antenna is in line with the theory of dipole antenna, the emission of THz radiation from a small gap antenna is in line with the theory of Hertzian dipole. The radiated electric field is proportional to the time derivative of the current, I_{pc}, (or equivalently it is proportional to the current density, J_{pc}) as [18, 19]:

$$E_{THz}(t) \propto \frac{\partial I_{pc}(t)}{\partial t} \propto \frac{\partial J_{pc}(t)}{\partial t} \tag{2.4}$$

The movement of electrons from the valence band to the conduction band under the laser illumination generated the photocurrent. Since the electron (free carrier) density in the conduction band is *n(t)*, and the velocity of carriers is *v(t)*, the current density, J_{pc} *(t)* is given by [20]:

$$J_{pc}(t) = -e \cdot n(t) \cdot v(t) \tag{2.5}$$

Where *e* is the electron charge. This current relation applies to the hole, but with a positive sign. Hole contribution to THz current and radiation is much smaller [21] due to the effective mass of a hole is much larger than that of the electron; hence it is often be neglected.

A simple one-dimensional Drude-Lorentz model has been developed in [14] in order to explain the main features of this photocurrent density and carrier dynamics. This model consists of three interlinked differential equations describing the relation of free carrier density, the velocity of carriers, and the polarisation caused by separated carriers under the bias field, P_{sc}. These equations are as follows:

$$\frac{dn(t)}{dt} = -\frac{n(t)}{\tau_c} + G(t) \tag{2.6}$$

$$\frac{dv(t)}{dt} = -\frac{v(t)}{\tau_s} + \frac{e}{m^*} E_{local} \tag{2.7}$$

$$E_{local} = E_{bias} - \frac{P_{sc}}{\zeta \varepsilon} \tag{2.8}$$

$$\frac{dP_{sc}}{dt} = -\frac{P_{sc}}{\tau_r} + J_{pc}(t) \tag{2.9}$$

Where τ_c is the carrier lifetime where it is the average time span that excess free electrons survive before recombining [20], τ_s is the momentum relaxation time or carrier scattering time where it is the average time between two collisions of each electron in the conduction band, and it is in the order of a tenth of ps [20], τ_r is the carrier recombination lifetime [22], $G(t)$ is the generation rate of carriers by laser pulses, m^* is the effective mass, E_{local} is the electric field in the photoconductive gap, E_{bias} is the applied bias to antenna electrodes, and ζ is the geometrical factor [14]. $J_{pc}(t)$ and $E_{THz}(t)$ can be found through numerical calculations of equations (2.6) -(2.9)

Radiated THz field can be related to carrier dynamics and calculated as:

$$E_{THz}(t) \propto \frac{\partial J_{pc}(t)}{\partial t} = e \cdot \frac{dn(t)}{dt} \cdot v(t) + e \cdot n(t) \cdot \frac{dv(t)}{dt} \tag{2.10}$$

by considering both equations (2.4) and (2.5)

Hence, it can be interpreted that for small gap antennas, THz radiation relies on the results of ultrafast variation in carrier density and acceleration of photo-carriers. This THz radiation can be increased by applying a large bias field and large optical power.

By comparing equations (2.3) for large-aperture antennas and (2.10) for small gap antennas, it can be interpreted that different antenna gap sizes impose different analysis criteria and different equations for the radiated THz field. The focus of this thesis is on small gap antennas which are used in the proposed model in Chapter 5.

2.3.2 Theoretical Principle of a THz Photoconductive Antenna as a Detector

THz detection by photoconductive antennas is the opposite of the emitting process. No bias voltage is applied across the electrodes in detection. The incident THz radiation induces a voltage across the antenna which accelerates photo-carriers generated by the gating laser pulse from the optical source. The arrival time of the gating pulse can be adjusted using a variable time delay gating pulse thus the temporal behaviour of the photocurrent due to THz radiation can be measured. The photocurrent can be measured by a current meter or lock-in amplifier [10].

Based upon the Ohm's law, the detected photocurrent at a time delay of *t* can be explained as shown in the equation below as:

$$J_{\det}(t) = E_{THz}(t) * \sigma_{\det}(t) = \int_{-\infty}^{\infty} E_{THz}(t') \cdot e \cdot \mu_e \cdot n_r(t'-t)dt' \tag{2.11}$$

Where $E_{THz}(t)$ is the received THz signal, $\sigma_{det}(t)$ is the time-varying conductivity of the detector, and $n_r(t)$ is the generated photo-carrier density by the gating pulse [19]. For photoconductive materials with ultra-short carrier lifetime $n_r(t) = \delta(t)$, then the detected current from equation (2.11) will be proportional to the original income THz signal where $J_{\det}(f) \propto E_{THz}(f)$. For materials with extremely long carrier lifetime like SI-GaAs, it is presumed that $n_r(t)$ has behaviour like a step function then $J_{\det}(f) \propto E_{THz}(f)/f$. This proves that the bandwidth of the detected signal of affected by the characteristics of the photo-carrier density in the detector antenna and its decay behaviour. The in-between case is the realistic situation where the distortion effect of the detector on the incident THz field is considered by convolving the detector response with THz field in time domain [21]. Thus, the detected photocurrent for the

in-between situation can be explained considering the spectral behaviour of laser pulses, $I_l(f)$, and carrier dynamics in the photoconductive antenna, $B(f)$ as equation (2.12) [18, 23].

$$J_{\det}(f) \propto I_l(f) B(f) E_{THz}(t) \tag{2.12}$$

The amount of detected signal at high frequencies is determined by the response time of the detector [10]. Other factors that determine the amount of detected signal are finite carrier recombination lifetime of semiconductor, τ_r, and the RC time constant related to the device capacitance [24]. Hence, THz photoconductive antenna in detector side can be construed as a low pass filter dominated by carrier lifetime and carrier recombination time of photoconductive material. Small gap photoconductive antennas are commonly employed as detectors. The sensitivity of a detector reduces once the antenna gap size is increasing as the optical intensity on the gap reduces [14]. The maximum response of detector shifts to lower frequencies also is the outcome of a bigger antenna gap size [14].

2.4 Comparison of THz Antennas with RF/MW Antennas

Fig. 2.2a and Fig. 2.2b show common RF/MW and THz antenna measurement setups respectively [25, 26]. It is apparent that THz antennas differ significantly from the conventional RF/MW antennas from the measurement facility, feeding method and antenna structure points of views. These differences are elaborated and summarised in this section.

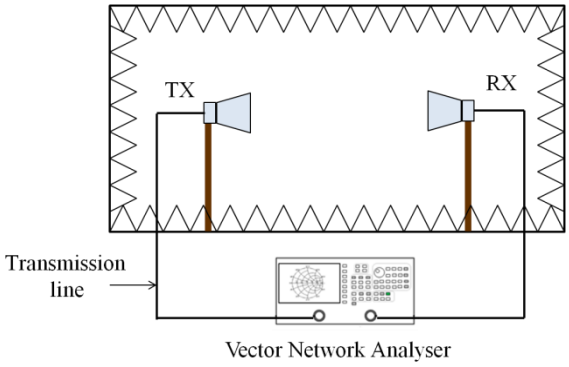

(a)

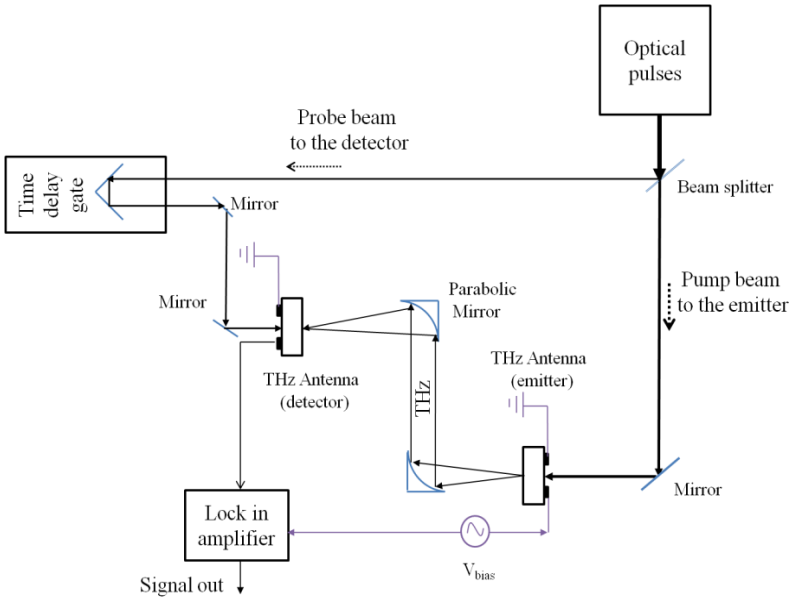

(b)

Fig. 2.2 Common (a) RF/MW antenna (b) THz antenna measurement setup (both the emitter and detector are antennas) [10]

2.4.1 Fabrication and Measurement

Fabrication of RF/MW antennas is common. Manufacturing a THz antenna is rather complicated and expensive. Manufacturing of a THz antenna consists of the fabrication and preparation of the photoconductive substrate and also patterning the antenna on the substrate. Photolithography and electron beam lithography is used for patterning the antenna on the substrate. The latter method which is more expensive than the former one is employed for sub-micron dimensions that fall below the resolution of the photolithography method [10].

These two types of antennas are also very different from measurement setups and measurement techniques points of views. In RF/MW antennas as illustrated in Fig. 2.2a, both transmitter (TX) and receiver (RX) antennas are connected to a vector network analyser, and

the various parameters of the antenna under tests such as radiation pattern, gain, efficiency, impedance/VSWR, bandwidth, and polarisation can be determined. The alignment of TX and RX antennas is relatively easy. Measurement facilities for RF/MW antennas are known as anechoic chambers and reverberation chambers. Antenna measurements can take on many forms, including near-field and far-field measurements. A basic test system requires at least a source antenna with a transmitter and the antenna under test with a receiver. The main idea in this testing is to use the source antenna and a transmitter with suitable bandwidth and polarisation to illuminate the antenna under test with plane waves, which can then be measured by the receiver being fed by the antenna under test. One variation on this system involves a switchable reference antenna for feeding the test receiver with known performance characteristics. Another involves some kind of a positioning system to rotate the antenna under test relative to the source antenna, thus measuring the radiation pattern as a function of angle.

In the THz measurement setup as shown in Fig. b, there is no physical connection between the optical source and the emitter and/or detector antenna. Various optical components such as parabolic mirrors are allocated between the emitter and detector antennas to direct the electromagnetic wave which may attenuate and broaden the THz signal. From the shown setup in Fig. 2.2b, the amplitude and phase of the THz signal can be detected. However, for pattern measurement of the antenna, another setup using fibre coupled detectors is needed [27, 28] as the antenna under test in the THz system cannot be rotated in contrast to RF/MW antennas as the rotation will cause the loss of laser illumination on the THz antenna gap. Moreover, the alignment of the THz system is a very sensitive task, and the detected THz signal is crucially affected by it. Finally, as THz signals are sensitive to water vapours, it is better for THz measurement bench to be in an enclosed environment and to be purged with dry nitrogen.

2.4.2 Feeding, Excitation Source and Biasing

Coplanar Waveguide (CPW), coaxial cable, and microstrip are among various feed lines available for conventional antennas but, for a THz antenna, there is none. There are two ways to couple the optical pulses to a THz antenna firstly through the air and secondly through

a fibre. Typically, optical waves are coupled to the antenna through the air. However, for some industrial applications where flexible and movable emitters and detectors are essential, optical fibres are employed. Recently some fibre-coupled THz systems have been presented for 800 nm laser pulses [29] and 1550 nm which are telecommunication wavelength pulses [30, 31]. The feed line for THz antennas is actually a laser; therefore, the source impedance of the antenna is variable, and this is different to commonly used 50 Ohms feed lines of RF/MW antennas.

Another difference between RF/MW and THz antennas are from bias voltage point of view. RF/MW antennas do not need any biasing. However, as shown in Fig 2.2b, THz antennas as emitters require voltage biasing as it is the fundamental procedure of THz generation. When employed as a detector, THz antennas do not need bias voltage.

2.4.3 Electrode Material

Highly conductive metals such as copper and silver usually made RF/MW antennas. In THz antennas, an AuGe alloy and a layer of Ti/Au (Titanium/Gold) are employed as the electrode material. These are suitable metallization types on LT-GaAs substrates and can provide ohmic contacts [32]. AuGe alloys such as AuGe/Ni/Au have been used in THz antennas [33, 34]. However, Ti/Au (or Ti/Pd/Au) layer stack is more extensively employed [5,36-38] where a thin layer of Ti is initially deposited to improve adhesion of the Au to the substrate [39]. The advantage of the Ti/Au contact over the AuGe alloy is that for its deposition no annealing is required and it is more thermally stable under laser illumination [32]. The electrical conductivity, σ, of Au is 45.2×10^6 S/m [16]. Most of the current flow occurs in a very thin region near the surface of the conductor since the skin depth or characteristic depth of penetration, $\delta = \sqrt{1/\pi f \mu \sigma}$ for Au at 1 THz is 74.9 nm. The surface resistance, in this case, is 0.29 Ω. In practice for THz antennas, usually 10-20 nm thick Ti followed by Au with a thickness of ≥ 100 nm is deposited on the photoconductive substrate.

Graphene is another type of material which very recently has been theoretically studied as an antenna electrode material [40-41]. It is a one-atom-thick 2D carbon crystal which has

extraordinary mechanical, electronic and optical properties [42] and has a Young modulus of 1.5 TPa, the carrier mobility of 200 000 $cm^2.V^{-1}.s^{-1}$ [43], and an absorption coefficient of 24×10^4 cm^{-1} [44]. Various parameters such as temperature and chemical potential determine the surface conductivity of graphene. The chemical potential of graphene is one of the parameters which can be tuned to achieve antennas with different radiation characteristics thus realising reconfigurable antennas [45].

2.4.4 Substrate Material

A low-loss dielectric material is desirable in planar RF/MW antennas. One of the most common dielectric materials for this type of antennas is FR4 which consists of fibreglass reinforced epoxy laminate sheet. Special MW antenna category, for example, monolithic microwave integrated circuit (MMIC), however, needs GaAs as the main substrate material due to its high carrier mobility and homogeneous nature [39, 46].

For THz antennas, the substrate material used is a photoconductive material which is basically a semiconductor, such as Si, InP, GaAs, and InGaAs. LT-GaAs is the most popular material due to its desirable characteristics, namely ultra-short carrier lifetime in order to obtain fast current pulses or CW current variation, relatively high electron mobility in order to obtain strong THz signals, high intrinsic resistivity and high breakdown voltage in order to support applying high bias voltages [47-48]. Since photoconductive materials play a crucial role in THz wave generation and detection, characteristics and effective parameters of them with the main focus on LT-GaAs is described in the next sub-section.

One of the intensely studied topics in the THz field is the THz photoconductive material. No natural material exists to allow an efficient and powerful THz emission, hence spurred the interest [49]. The intrinsic carrier lifetime of materials is not fast enough to reach very high frequency ranges of the THz spectrum. Thus, to reduce the carrier lifetime, material studies for THz are very crucial and the research and improvement of material characteristics for optoelectronic applications still ongoing [50, 51].

The first THz antenna developed in [52] used silicon as the photoconductive substrate material. The bandgap of the silicon is 1.12 eV at 300 K, with corresponding intrinsic resistivity of 2.3×10^5 Ω.cm. However, the bandgap of silicon is indirect which means that the minimum of conduction-band is misaligned compared to the maximum of valence-band [53]. This results in a relatively slow optical recombination process.

GaAs, on the other hand, has a direct bandgap, and photon emission is possible without phonon exchange with the lattice. The intrinsic resistivity of GaAs is 10^8 Ω.cm. As GaAs an III-V compound, it is possible to modify its composition of alloys by adding defects to tune the electrical and optical behaviours. Many development and improvement in characteristics of GaAs is one of the main reason progress in THz antennas is possible [54]. GaAs crystal can be grown in semi-insulating (SI) form by liquid encapsulated Czochralski (LEC) method. In this process, all dependencies of GaAs on quartz and carbon components are eliminated [55]. This forms a substrate where it is possible to grow another epitaxial layer.

The carrier lifetime of SI-GaAs is in the range of hundreds of picoseconds. This satisfies the needs to have THz antennas with large bandwidth and good SNR. This may be achieved by incorporating additional energy levels in the bandgap through various native point defect types [47]. Therefore, another recombination path can be provided by trapping electrons in intermediate states. For this purpose, point defects should be introduced into the crystal. Adding defects can reduce carrier lifetime of the material which is desirable. On the other hand, it reduces thermal conductivity and the carrier mobility because the mean free paths are decreased as a result of new scattering centres introduced by trapping levels [20,56]. These consequences are unfavourable. Hence, it can be concluded that the primary challenge in the development of ultrafast photoconductive materials is to have material with a sub-picoseconds carrier lifetime, high mobility and a high dark resistivity.

Low temperature growth technique in molecular beam epitaxy Molecular beam epitaxy (MBE) is one of the conventional technique to introduce defects into the material. This method produces LT-GaAs. Typically, at a low growth temperature between 200 to 250°C, GaAs is deposited in excess of As which leads to the formation of a relatively high density of point

defects. Under an As overpressured at high annealing temperature typically between 500 and 600°C, it is annealed [48,57] to increase the resistivity. A 1 to 2 μm-thick LT-GaAs layer as the active layer is usually grown on SI-GaAs [47].

LT-GaAs was first used in 1988 [58], and since then continuous research on the effect of various growth and annealing factors on properties of LT-GaAs has been performed [57, 59-61]. However, still in literature when a THz antenna on LT-GaAs is used, the full parameters related to the production of the LT-GaAs wafer especially on its growth and its annealing temperatures wafer and the derived carrier lifetime are discussed. Each MBE chamber is unique, and even in the same chamber, it is challenging to replicate the same wafer's characteristics. This fabrication process is sensitive to the ambient condition, and the exact growth temperature is difficult to control. Another parameter of the photoconductive material influenced by the fabrication procedure is the material resistivity. The resistivity decreases with the growth of the temperature [62]. Annealing process helps to increase this resistivity that was effected before.

Other methods to modify the characteristics of GaAs have been practised like ion-implantation [63] and use of self-assembled ErAs islands in GaAs [54, 64-65]. The objective of these techniques is to create a similar material with a carrier lifetime mirroring LT-GaAs. The results are ErAs: GaAs which has high resistivity but with low mobility and Ion-implanted GaAs which has high mobility but with very low intrinsic resistivity. Hence, LT-GaAs is still the best material for THz antennas [49].

Indium based is another category of photoconductive materials for THz applications is from III-V compounds. These materials have narrower bandgap energy. The bandgap of InGaAs is 0.75 eV compared to 1.43 eV of LT-GaAs. Thus, Indium based III-V compounds are suitable materials at higher optical wavelengths. Ultra-short carrier lifetime and high resistivity of LT-InGaAs had been reported in [51]. Most application for LT-InGaAs is in the telecommunication wavelength of 1.55 um. Fibre amplifiers with high power, narrow line-width and tunable wavelength in this frequency are also available [69]. Compatibility with 1.55 μm has been achieved with Fe-implanted InGaAs [70-71], ErAs: InGaAs [72], heavy-ion

irradiated InGaAs [73], embedded InGaAs layers between InAlAs trapping layers [30], and low-temperature-grown Be doped InGaAs [74].

Table 2.1 summarised the properties of different main THz photoconductive materials for optical sources of 800 nm and 1.55 μm

Table 2.1 Properties of various photoconductive materials in THz antennas [10,16]

Material	Carrier lifetime (ps)	Mobility ($cm^2.V^{-1}.s^{-1}$)	Resistivity (Ω.cm)	Breakdown voltage ($V.cm^{-1}$)
SI-GaAs	Several hundred	8500	~ 10^7	4×10^5
LT-GaAs	< 1	200	>10^7	5×10^5
LT-InGaAs	Larger than LT-GaAs	26	760	~ 6×10^4

The carrier lifetime, resistivity, and breakdown voltage of LT-GaAs at 1550 nm are very low. However, the most significant advantage of this material is that it can be used with well-established communication optical sources. This feature is attractive as this can reduce the cost of a THz system. Most THz antennas use LT-GaAs as the photoconductive material because of its excellent characteristics.

SI-GaAs has high mobility but lower breakdown voltage compared to LT-GaAs. Hence, the amount of dc bias field for any THz antennas using SI-GaAs as a substrate is limited. SI-GaAs also has lower resistivity that results in a generation of larger dark current even when there is no laser illumination as a feed in comparison to LT-GaAs. This will lead to heating of the THz antenna and quicker breakdown. Finally, SI-GaAs has large carrier lifetime which limits the achievable spectral range, and it leads to more noise.

2.4.5 Type of Current

Conduction current due to the motion of conduction electrons is the current type in RF/MW. In THz antennas however the generation of current in the photoconductive material is attributed to two phenomena which are the generation of electron-hole pairs under electric bias field known as drift current and displacement current which is due to second order nonlinear optical characteristics of the photoconductive substrate. However, the effect of the displacement current is only considered at low bias fields. At high bias fields (more than 10^5 $V.cm^{-1}$) drift current is dominant [14, 75]. More details on the current type are discussed in Chapter 4.

2.4.6 Computer Aided Design

There is no available and complete design tool available for THz antenna designs though Computer Aided Design (CAD) is now a common practice for conventional antenna designs. Generation of THz waves from the antennas consists of two processes which are optoelectronic and electromagnetic (EM) parts. Most available commercial tools can only simulate the first or second part of the process. No readymade commercial software is dedicated to the THz antenna. Therefore, the development of a new method that can facilitate analysis of THz antennas by combining numerical and CAD method is required. This is the main contributions of this thesis that will be explained in Chapter 5.

To sum up, the significant differences between these two types of antennas are reviewed in Table 2.2. The dissimilarities highlight the necessity of having a different analysis approach for THz antennas.

Table 2.2 Comparison of THz antennas with common RF/MW antennas [10,25]

Parameter	THz antenna	RF/MW antenna
Excitation source/feeding	Laser pulses	Transmission line
Bias voltage	Emitter: biased	Emitter: unbiased
	Receiver: unbiased	Receiver: unbiased
Substrate material	High resistive semiconductor	Low loss dielectric
Antenna electrode material	AuGe and Ti/Au	Highly conductive metals
Type of current	Drift current and displacement current	Conduction current
Fabrication	Complex and expensive	Relatively easy and cheap
Computer aided design	Not available in one package	Available

2.5 Problems of THz Photoconductive Antennas

Although other THz sources may have better THz radiation performance in certain circumstances, THz antennas had useful characteristics compared to the other source. Unlike QCLs THz Photoconductive Antennas can operate in room temperature. Also, unlike diodes they can operate over a broader range of THz frequencies and unlike BWOs, they are compact. Nevertheless, the radiated THz power and the optical-to-THz conversion efficiency from THz Photoconductive Antenna is still deficient (<2%) [76].

Generation of THz wave through the photoconduction process has shown promising performance [54, 77-80]. Under a laser illumination, for each absorbed photon by the photoconductive material, one electron-hole pair is generated, and when this pair reaches the antenna, several THz photons can be emitted which is the considerable advantage of using THz Photoconductive antennas [81]. Thus, the optical-to-THz conversion efficiency of a THz antenna can theoretically reach 100 % which is much larger than the Manley–Rowe limit [82]. However, in reality, the radiated THz power is in the range of few μW and the optical-to-THz conversion efficiency of THz antennas is very low (< 2%).

The entire wave generation process from a THz antenna needs to be considered in order to have a better view and to understand the reason for having a low power level and efficiency. For this purpose, the adopted method here is to divide the process into three parts [16, 25]:

1) Generation of THz photocurrent from optical power in the photoconductive material. The related efficiency; *i.e.* optical-to-electrical efficiency, η_1, can be defined as the ratio of the generated THz power in the photoconductive gap to the optical power

2) The amount of coupled THz power from the photoconductive gap to the antenna electrodes; *i.e.* matching efficiency, η_2

3) The amount of coupled THz wave from the antenna to the free space; *i.e.* radiation efficiency, η_3.

The first two parts are different for THz antennas in a pulsed and a CW system due to the excitation type, and they are separately described in the next sections. However, the latter part; *i.e.* radiation efficiency, for both systems is the same, and it depends on the antenna radiation characteristics- mainly the electrical thickness of the substrate and the relative permittivity of photoconductive material. Since the photoconductive substrate has high permittivity (ε_r = 12.9 for GaAs), as substrate thickness increases, the radiation efficiency decreases sharply depending on substrate thickness. This is due to the generation of surface waves.

2.5.1 Problems Related to THz Photoconductive Antennas

In order to find out how part one and two of the THz generation process contribute to the optical-to-THz efficiency, a preliminary and straightforward calculation with approximate assumptions is performed for a THz photoconductive antenna in a pulsed system [85].

1. The average photocurrent [86], I_{avp}, and approximate photoconductive resistance [87], R_{app}, are considered as equations (2.13) and (2.14) respectively:

$$I_{avp} = \frac{e\mu_e \tau_c V_{bias} P_{av}}{hfL^2} \tag{2.11}$$

$$R_{app} = \frac{3hfL^2}{2e\mu_e P_{av} t_{rep}} \tag{2.12}$$

where V_{bias} is the bias voltage, L is the antenna gap length, and P_{av} is the average optical power. Then, the optical-to-electrical efficiency can be estimated as:

$$\eta_{1p} = \frac{R_{app} I_{avp}^2}{P_{av}} = \frac{3e\mu_e \tau_c^2 V_{bias}^2}{2t_{rep} hfL^2} \tag{2.13}$$

The index of "*p*" is added to represent THz photoconductive antenna in a pulsed system. Considering some typical values as μ_e = 1000 $cm^2.V^{-1}.s^{-1}$, τ_c = 0.5 ps, V_{bias} = 30 V, P_{av} = 50 mW, L = 5 μm, t_{rep} = 1/80 μs, and f = 375 THz and plugging in these values in equation (2.13), $\eta_{1p} = 7.2 \times 10^{-5}$.

2. The matching efficiency can be calculated according to equation (2.14) for a half-wavelength dipole antenna on a substrate with ε_r = 12.9. Assuming the antenna resistance in free space, Z_{free}, is 73 Ω and by using the above values in equation (2.12) R_{app} is 0.89 Ω, then the matching efficiency will be η_{2p} = 0.16.

$$\eta_{2p} = 1 - \left| \frac{Z_{free}/\sqrt{\varepsilon_r} - R_{app}}{Z_{free}/\sqrt{\varepsilon_r} + R_{app}} \right|^2 \tag{2.14}$$

The total antenna efficiency for this sample, which is a multiplication of efficiencies from described processes, is calculated as 5.7×10^{-6} [88]. Although this value is comparable with what most people obtained in practice, it is smaller than some reported best efficiencies. This could be due to better parameters realised in the best cases [88]. The details calculations can be found in Appendix B.

2.6 Previous work on THz Photoconductive Antennas

Some previous research published had been focused on specific criteria to make improvement in the radiated THz antenna performance and also efficiency. This section will discuss the notable contribution done by the researchers.

2.6.1 Varying Antenna Gap Area Geometry

Commonly used THz antennas are bowtie, dipole and coplanar strip line. Antenna gap area is essential as it is where the electron-hole pairs are generated and coupled to the antenna electrodes. Demonstrated in [12, 15, 33] antennas with sharp tip ends can produce larger THz power compared to the antennas with rectangular edges in the gap. Sharper antenna tips, will results in enhanced THz emission even with less optical power due to the overlapping of the laser spot and the electric field area in the antenna gap. Though the fabrication of tiny sharp tips for small gap antennas is difficult in reality, the importance of the geometry of the electrode should not be undermined.

2.6.2 Improving Optical Power Coupling

Higher photo-carrier density and transient photocurrent can be achieved by increasing the absorption of infrared laser power to the antenna. In order to increase the absorption, anti-reflection (AR) coating Si_3N_4 is used on the antenna electrode. The coating is essentially an optically transparent layer [128]. The reflection of optical waves from the surface of the device will be suppressed with the existing of the additional layer. An AR with a refractive index of $\sqrt{n_{GaAs}}$, where n_{GaAs} is the refractive index of the photoconductive material is usually used. Another approach is to use AlAs: GaAs or AlAs: AlGaAs Bragg reflectors [54,89]. This material acts as a mirror for optical waves, and it is transparent to THz waves. It is located beneath the active layer of a substrate. Fig. 2.3 shows the schematic view of an antenna with both an AR coating and Bragg reflectors.

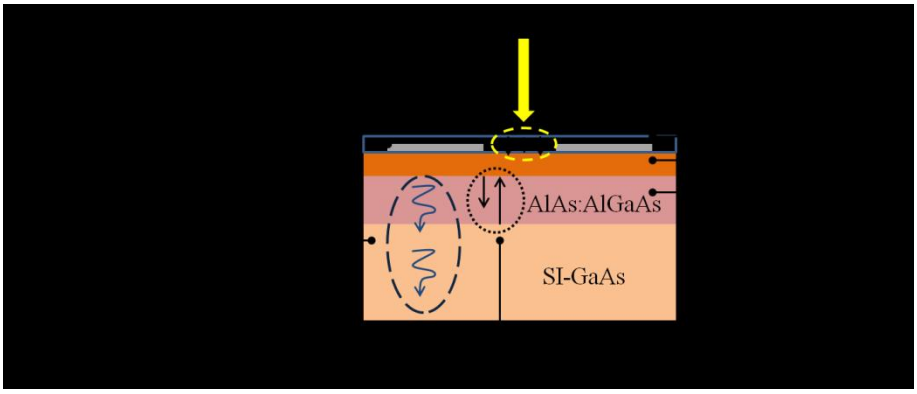

Fig. 2.3 Schematic view of the material structure of a THz antenna with AR coating on top of the antenna electrodes and Bragg reflectors beneath the photoconductive layer [89]

As shown in [90-91] another method to enhance the generation of photo-carriers in the antenna gap [90-91] is the usage of nanoantennas in the photoconductive gap. A locally enhanced electric field can be obtained as this optical nanoantennas can strongly concentrate the emitted laser waves. Increased THz power emission can be achieved using this method since more optical power can be confined to the substrate active layer. This is due to the fact that these nano antennas are deposited on the substrate. Fig. 2.4 shows two types of nanoantennas in the form of nanorods and nanoislands in the photoconductive gap. The width of nanorods or thickness of nanoislands may be varied in order to tune resonance frequencies of these antennas. The fabrication cost of these devices is high, and due to its miniature size, it is important to avoid an electric short circuit.

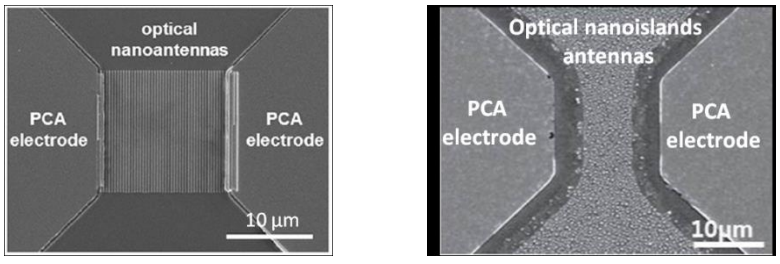

(a) (b)

Fig. 2.4 SEM image of the THz photoconductive antenna with (a) nanorods [90] (b) nanoislands [91] in the photoconductive gap

In [92], nano-structuring of metals or nanoplasmonic electrodes is another cutting edge technology introduced in order to improve the coupling of optical power to the antenna and the THz radiated power. The main goal is to reduce the photo-carrier transport time, and this can be done by employing arrays of sub-micron electrodes. Due to the coupling of light with the surface plasmon of the sub-wavelength arrays, the interaction and concentration of the emitted wave on noble metals for example gold are increased [93]. Here, surface plasmon is introduced as collective oscillation of free electrons at the boundary between a conductor and a dielectric material.

Also using this concept, an array of dipole antennas with plasmonic contacts has been reported by [69] as shown in Fig. 2.5.Ultra-short THz pulses with superior responsivity have been achieved from this device as an emitter, even though the antenna was mounted on large electron mobility and large carrier lifetime material. This is due to the short carrier transport time provided by electrodes and increased transmission of laser power to the sub-wavelength gaps of electrodes because of surface plasmon waves.

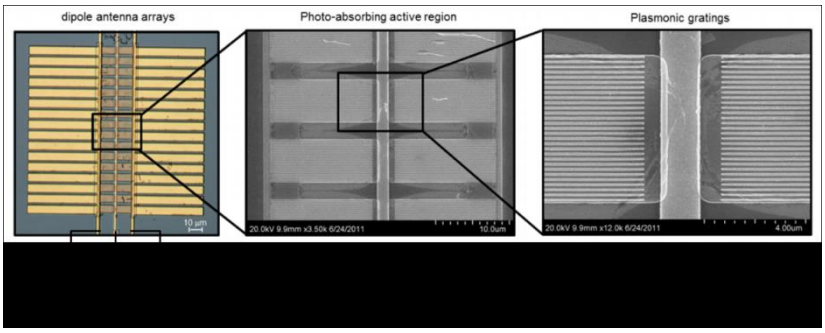

Fig. 2.5 SEM image of plasmonic THz dipole arrays, a middle ground electrode is added to collect the remaining electron-holes in the antenna gap quicker to prevent the screening effect [69]

A small gap dipole antenna with nanoplasmonic interdigitated fingers on SI-GaAs as shown in Fig. 2.6 [94] were also introduced. Nano distance gaps (100 nm) allows coupling of generated photo-carriers to the antenna more efficiently due to reducing transport distance. This geometry, however, is prone to break down at high optical powers due to narrow distance between the fingers.

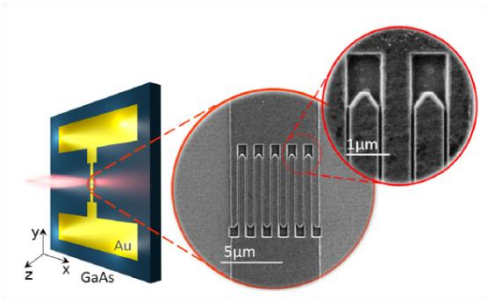

Fig. 2.6 SEM image of the nanoplasmonic interdigitated antenna [94]

Another example is, a bowtie antenna with plasmonic contact electrode gratings [82] as shown in Fig. 2.7. Due to the very short carrier transport path lengths as an effect of plasmonic contacts (~100 nm), a high number of generated photo-carriers can be coupled to the antenna before recombination. It was found that the optical-to-terahertz conversion efficiency of the photoconductive THz antenna emitter could be 50 times higher than that of a conventional emitter [95]. Plasmonic contact electrodes used were nanoscale gold gratings designed to allow excitation of surface plasmon waves along the nanoscale gratings in response to the incident optical pump. Yang et al. reported that an optical-to-terahertz power conversion efficiency of 7.5% could be achieved by using these plasmonic contact electrodes [96]

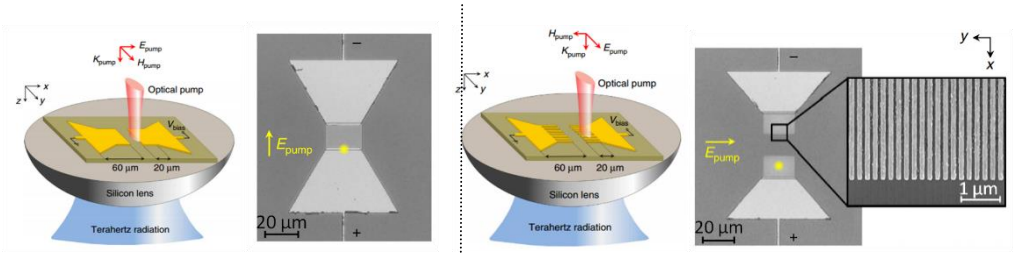

(a) (b)

Fig. 2.7 Schematic and SEM image of the (a) conventional bowtie antenna (b) nanoplasmonic bowtie antenna [95]

Tip-to-tip rectangular nano gap meander antenna had been introduced in Fig.2.8 [97]. This geometry reduces the photo-carrier transit time between the electrodes and provides a strongly enhanced electric field in the gap.

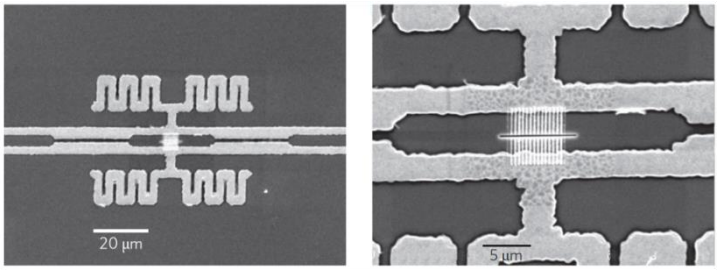

Fig. 2.8 SEM image of the tip-to-tip rectangular nano gap meander antenna [97]

Finally, the work done by [16] with a new geometry is shown in Fig. 2.9. A top hat loaded antenna with trapezoidal tip-to-tip fingers in the photomixer part integrated with a conical horn was proposed. Simulation results demonstrated a reduction in capacitance value and improvement in E-field intensity for the trapezoidal tip-to-tip configuration. This should lead to a larger THz current generated in the antenna gap. For the 6-finger trapezoidal electrodes, the normalised E-field to the electrode area in the gap is increased four times as compared to rectangular electrodes.

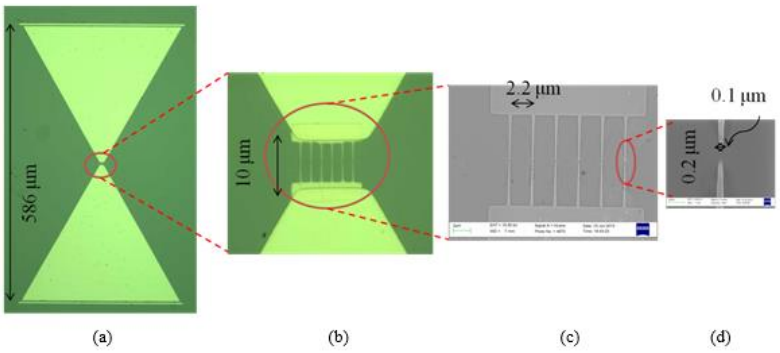

Fig. 2.9 Microscopic images of the THz bowtie antenna with trapezoidal tip-to-tip fingers (a) overall antenna view (b) zoom-in of the photomixer section (c) SEM zoom-in of the trapezoidal tip-to-tip finger (d) SEM zoom-in of a nanogap trapezoidal finger [16]

2.7 Summary

The necessity of having a THz antenna and the theoretical principle of THz photoconductive antenna as an emitter and as a detector was elaborated in this chapter. Its differences from conventional RF/MW antennas in various aspects were also discussed in this chapter. These differences highlight the requirement of different methods in THz antenna analysis, simulation, fabrication, and measurement. Problems related to THz photoconductive antenna is also addressed. Published work on THz antenna was discussed on the end of the chapter in order to introduce the design concept by various researchers of THz antenna design.

References

[1] X. C. Zhang, B. B. Hu, J. T. Darrow, and D. H. Auston, "Generation of femtosecond electromagnetic pulses from semiconductor surfaces," *Applied Physics Letters,* vol. 56, pp. 1011-1013, 1990.

[2] M. Johnston, D. Whittaker, A. Corchia, A. Davies, and E. Linfield, "Simulation of terahertz generation at semiconductor surfaces," *Physical Review B,* vol. 65, 2002.

[3] C. Weiss, R. Wallenstein, and R. Beigang, "Magnetic-field-enhanced generation of terahertz radiation in semiconductor surfaces," *Applied Physics Letters,* vol. 77, pp. 4160-4162, 2000.

[4] M. B. Johnston, D. M. Whittaker, A. Corchia, A. G. Davies, and E. H. Linfield, "Theory of magnetic-field enhancement of surface-field terahertz emission," *Journal of Applied Physics,* vol. 91, pp. 2104-2106, 2002.

[5] I. S. Gregory, C. Baker, W. R. Tribe, I. V. Bradley, M. J. Evans, E. H. Linfield, A. G. Davies, and M. Missous, "Optimization of photomixers and antennas for continuous-wave terahertz emission," *IEEE Journal of Quantum Electronics,* vol. 41, pp. 717-728, 2005.

[6] http://www.thorlabs.co.uk/newgrouppage9.cfm?objectgroup_id=4716.

[7] http://www.toptica.com/products/terahertz_generation/fs_packages/photoconductive switches.html

[8] http://www.tetechs.com/.

[9] http://www.menlosystems.com/products/?families=77

[10] Y. Lee, Principles of Terahertz science and technology, 1st ed. New York, NY: Springer, 2008.

[11] J. T. Darrow, Z. Xi-Cheng, D. H. Auston, and J. D. Morse, "Saturation properties of large-aperture photoconducting antennas," *IEEE Journal of Quantum Electronics,* vol. 28, pp. 1607-1616, 1992.

[12] M. R. Stone, M. Naftaly, R. E. Miles, J. R. Fletcher, and D. P. Steenson, "Electrical and radiation characteristics of semilarge photoconductive terahertz emitters," *IEEE Transactions on Microwave Theory and Techniques,* vol. 52, pp. 2420-2429, 2004.

[13] G. Zhao, R. N. Schouten, N. v. d. Valk, W. T. Wenckebach, and P. C. M. Planken, "Design and performance of a THz emission and detection setup based on a semi-insulating GaAs emitter," *Review of Scientific Instruments,* vol. 73, pp. 1715-1719, 2002.

[14] P. U. Jepsen, R. H. Jacobsen, and S. R. Keiding, "Generation and detection of terahertz pulses from biased semiconductor antennas," *J. Opt. Soc. Am. B,* vol. 13, pp. 2424-2436, 1996.

[15] Y. Cai, I. Brener, J. Lopata, J. Wynn, L. Pfeiffer, and J. Federici, "Design and performance of singular electric field terahertz photoconducting antennas," *Applied Physics Letters,* vol. 71, pp. 2076-2078, 1997.

[16] N. Khiabani, "*Modelling, design and characterisation of Terahertz photoconductive antenna*". PhD thesis, Department of Electrical and Electronics Engineering, University of Liverpool, 2013.

[17] P. K. Benicewicz, J. P. Roberts, and A. J. Taylor, "Scaling of terahertz radiation from large-aperture biased photoconductors," *J. Opt. Soc. Am. B,* vol. 11, pp. 2533-2546, 1994.

[18] P. U. Jepsen, D. G. Cooke, and M. Koch, "Terahertz spectroscopy and imaging – Modern techniques and applications," *Laser & Photonics Reviews,* vol. 5, pp. 124-166, 2011.

[19] K. Sakai, *Terahertz optoelectronics*, 1st ed. Berlin: Springer 2005.

[20] J. Colinge and C. A. Colinge, Physics of semiconductor devices. Boston: Kluwer Academic Publishers, 2002.

[21] Z. Piao, M. Tani, and K. Sakai, "Carrier Dynamics and Terahertz Radiation in Photoconductive Antennas," *Jpn. J. Appl. Phys.,* vol. 39, pp. 96-100, 2000.

[22] S. D. Brorson, J. Zhang, and S. R. Keiding, "Ultrafast carrier trapping and slow recombination in ion-bombarded silicon on sapphire measured via THz spectroscopy," *Applied Physics Letters,* vol. 64, pp. 2385-2387, 1994.

[23] L. Duvillaret, F. Garet, J. F. Roux, and J. L. Coutaz, "Analytical modelling and optimisation of terahertz time-domain spectroscopy experiments, using photoswitches as antennas," *IEEE Journal of Selected Topics in Quantum Electronics,* vol. 7, pp. 615-623, 2001.

[24] S. Kono, M. Tani, P. Gu, and K. Sakai, "Detection of up to 20 THz with a low-temperature-grown GaAs photoconductive antenna gated with 15 fs light pulses," *Applied Physics Letters,* vol. 77, pp. 4104-4106, 2000.

[25] Y. Huang, N. Khiabani, S. Shen, and L. Di, "Terahertz photoconductive antenna efficiency," in *2011 International Workshop on Antenna Technology (iWAT),* 2011, pp. 152-156.

[26] N. Khiabani, Y. Huang, Y. Shen, and S. Boyes, "Theoretical Modeling of a Photoconductive Antenna in a Terahertz Pulsed System," *IEEE Transactions on Antennas and Propagation,* vol. PP, pp. 1-1, 2013.

[27] J. Klier, S. Wohnsiedler, W. Zouaghi, E. Peytavit, J. Lampin, J. Jonuscheit, and R. Beigang, "Far-field THz radiation pattern from photoconductive emitters on different substrates," in *36th International Conference on Infrared, Millimeter and Terahertz Waves (IRMMW-THz), 2011* 2011, pp. 1-2.

[28] J. Van Rudd and D. M. Mittleman, "Influence of substrate-lens design in terahertz time-domain spectroscopy," *J. Opt. Soc. Am. B,* vol. 19, pp. 319-329, 2002.

[29] F. Ellrich, T. Weinland, D. Molter, J. Jonuscheit, and R. Beigang, "Compact fibre-coupled terahertz spectroscopy system pumped at 800 nm wavelength," *Review of Scientific Instruments,* vol. 82, p. 053102, 2011.

[30] B. Sartorius, H. Roehle, H. Künzel, J. Böttcher, M. Schlak, D. Stanze, H. Venghaus, and M. Schell, "All-fiber terahertz time-domain spectrometer operating at 1.5 um telecom wavelengths," *Opt. Express,* vol. 16, pp. 9565-9570, 2008.

[31] S. Han, H. Ko, N. Kim, H. Ryu, C. Wook Lee, Y. Ahn Leem, D. Lee, M. Yong Jeon, S. Kyu Noh, H. Sook Chun, and K. Hyun Park, "Optical fibre-coupled InGaAs-based terahertz time-domain spectroscopy system," *Opt. Lett.*, vol. 36, pp. 3094-3096, 2011.

[32] N. Vieweg, M. Mikulics, M. Scheller, K. Ezdi, R. Wilk, H. W. Hübers, and M. Koch, "Impact of the contact metallization on the performance of photoconductive THz antennas," *Opt. Express*, vol. 16, pp. 19695-19705, 2008.

[33] M. Tani, S. Matsuura, K. Sakai, and S.-i. Nakashima, "Emission characteristics of photoconductive antennas based on low-temperature-grown GaAs and semi-insulating GaAs," *Appl. Opt.*, vol. 36, pp. 7853-7859, 1997.

[34] S. Matsuura, M. Tani, and K. Sakai, "Generation of coherent terahertz radiation by photomixing in dipole photoconductive antennas," *Applied Physics Letters*, vol. 70, pp. 559-561, 1997.

[35] Y. C. Shen, P. C. Upadhya, H. E. Beere, E. H. Linfield, A. G. Davies, I. S. Gregory, C. Baker, W. R. Tribe, and M. J. Evans, "Generation and detection of ultrabroadband terahertz radiation using photoconductive emitters and receivers," *Applied Physics Letters*, vol. 85, pp. 164-166, 2004.

[36] Y. Gao, M. Chen, S. Yin, P. Ruffin, C. Brantley, and E. Edwards, "Terahertz enhancement from terahertz-radiation-assisted large aperture photoconductive antenna," *Journal of Applied Physics*, vol. 109, p. 033108, 2011.

[37] S. Verghese, K. A. McIntosh, S. Calawa, W. F. Dinatale, E. K. Duerr, and K. A. Molvar, "Generation and detection of coherent terahertz waves using two photomixers," *Applied Physics Letters*, vol. 73, pp. 3824-3826, 1998.

[38] D. L. Woolard, R. Brown, M. Pepper, and M. Kemp, "Terahertz Frequency Sensing and Imaging: A Time of Reckoning Future Applications?," *Proceedings of the IEEE*, vol. 93, pp. 1722-1743, 2005.

[39] D. M. Pozar, *Microwave engineering*, 4th ed. Hoboken, NJ: Wiley, 2012.

[40] M. Tamagnone, J. S. Gomez-Diaz, J. R. Mosig, and J. Perruisseau-Carrier, "Analysis and design of terahertz antennas based on plasmonic resonant graphene sheets," *Journal of Applied Physics,* vol. 112, p. 114915, 2012.

[41] I. Llatser, C. Kremers, A. Cabellos-Aparicio, J. M. Jornet, E. Alarcón, and D. N. Chigrin, "Graphene-based nano-patch antenna for terahertz radiation," *Photonics and Nanostructures - Fundamentals and Applications,* vol. 10, pp. 353-358, 2012.

[42] A. K. Geim and K. S. Novoselov, "The rise of graphene," *Nat Mater,* vol. 6, pp. 183-191, 2007.

[43] M. Dragoman, A. A. Muller, D. Dragoman, F. Coccetti, and R. Plana, "Terahertz antenna based on graphene," *Journal of Applied Physics,* vol. 107, p. 104313, 2010.

[44] B. Heshmat, H. Pahlevaninezhad, T. E. Darcie, and C. Papadopoulos, "Evaluation of carbon nanotubes for THz photomixing," in *2010 IEEE Radar Conference*, 2010, pp. 1176-1179.

[45] M. Tamagnone, J. S. Gómez-Díaz, J. R. Mosig, and J. Perruisseau-Carrier, "Reconfigurable terahertz plasmonic antenna concept using a graphene stack," *Applied Physics Letters,* vol. 101, p. 214102, 2012.

[46] D. Singh, C. Kalialakis, P. Gardner, and P. S. Hall, "Small H-shaped antennas for MMIC applications," *IEEE Transactions on Antennas and Propagation*, vol. 48, pp. 1134-1141, 2000.

[47] S. Gupta, J. F. Whitaker, and G. A. Mourou, "Ultrafast carrier dynamics in III-V semiconductors grown by molecular-beam epitaxy at very low substrate temperatures," *IEEE Journal of Quantum Electronics,* vol. 28, pp. 2464-2472, 1992.

[48] S. Gupta, M. Y. Frankel, J. A. Valdmanis, J. F. Whitaker, G. A. Mourou, F. W. Smith, and A. R. Calawa, "Subpicosecond carrier lifetime in GaAs grown by molecular beam epitaxy at low temperatures," *Applied Physics Letters,* vol. 59, pp. 3276-3278, 1991.

[49] M. Martin and E. R. Brown, "Critical comparison of GaAs and InGaAs THz photoconductors," pp. 826102-826102, 2012.

[50] I. Kostakis, D. Saeedkia, and M. Missous, "Characterization of low temperature InGaAs-InAlAs semiconductor photo mixers at 1.55 mu wavelength illumination for terahertz generation and detection," *Journal of Applied Physics*, vol. 111, p. 103105, 2012.

[51] C. Baker, I. S. Gregory, W. R. Tribe, I. V. Bradley, M. J. Evans, E. H. Linfield, and M. Missous, "Highly resistive annealed low-temperature-grown InGaAs with sub-500 fs carrier lifetimes," *Applied Physics Letters*, vol. 85, pp. 4965-4967, 2004.

[52] D. H. Auston, K. P. Cheung, and P. R. Smith, "Picosecond photoconducting Hertzian dipoles," *Applied Physics Letters*, vol. 45, pp. 284-286, 1984.

[53] S. M. Sze and K. K. Ng, *Physics of semiconductor devices*, 3rd ed. Hoboken, N.J.: Wiley-Interscience, 2007.

[54] Z. D. Taylor, E. R. Brown, J. E. Bjarnason, M. P. Hanson, and A. C. Gossard, "Resonant-optical-cavity photoconductive switch with 0.5% conversion efficiency and 1.0W peak power," *Opt. Lett.*, vol. 31, pp. 1729-1731, 2006.

[55] L. Hrivank, "Semi-insulating GaAs," *Czech. J. Phys. B*, vol. 34, pp. 436-444, 1984.

[56] A. W. Jackson, J. P. Ibbetson, A. C. Gossard, and U. K. Mishra, "Reduced thermal conductivity in low-temperature-grown GaAs," *Applied Physics Letters*, vol. 74, pp. 2325-2327, 1999.

[57] I. S. Gregory, C. Baker, W. R. Tribe, M. J. Evans, H. E. Beere, E. H. Linfield, A. G. Davies, and M. Missous, "High resistivity annealed low-temperature GaAs with 100 fs lifetimes," *Applied Physics Letters*, vol. 83, pp. 4199-4201, 2003.

[58] F. W. Smith, H. Q. Le, V. Diadiuk, M. A. Hollis, A. R. Calawa, S. Gupta, M. Frankel, D. R. Dykaar, G. A. Mourou, and T. Y. Hsiang, "Picosecond GaAs-based photoconductive optoelectronic detectors," *Applied Physics Letters*, vol. 54, pp. 890-892, 1989.

[59] J. K. Luo, H. Thomas, D. V. Morgan, D. Westwood, and R. H. Williams, "The electrical breakdown properties of GaAs layers grown by molecular beam epitaxy at low temperature," *Semiconductor Science and Technology*, vol. 9, p. 2199, 1994.

[60] R. Yano, Y. Hirayama, S. Miyashita, H. Sasabu, N. Uesugi, and S. Uehara, "Pump–probe spectroscopy of low-temperature grown GaAs for carrier lifetime estimation: arsenic pressure dependence of carrier lifetime during MBE crystal growth," *Physics Letters A*, vol. 289, pp. 93-98, 2001.

[61] M. Missous, "Stoichiometric low temperature (SLT) GaAs and AlGaAs grown by molecular beam epitaxy," *Microelectronics Journal*, vol. 27, pp. 393-409, 1996.

[62] H. Nemec, A. Pashkin, P. Kuzel, M. Khazan, S. Schnull, and I. Wilke, "Carrier dynamics in low-temperature grown GaAs studied by terahertz emission spectroscopy," *Journal of Applied Physics*, vol. 90, pp. 1303-1306, 2001.

[63] T. Liu, M. Tani, M. Nakajima, M. Hangyo, and C. Pan, "Ultrabroadband terahertz field detection by photoconductive antennas based on multi-energy arsenic-ion-implanted GaAs and semi-insulating GaAs," *Applied Physics Letters*, vol. 83, pp. 1322-1324, 2003.

[64] J. E. Bjarnason, T. L. J. Chan, A. W. M. Lee, E. R. Brown, D. C. Driscoll, M. Hanson, A. C. Gossard, and R. E. Muller, "ErA s:GaAs photomixer with two-decade tunability and 12 mu W peak output power," *Applied Physics Letters*, vol. 85, pp. 3983-3985, 2004.

[65] C. Kadowa and e. al, "Self-assembled ErAs islands in GaAs for THz applications," *Physica E* vol. 7, pp. 97-100, 2000.

[66] A. Krotkus, R. Viselga, K. Bertulis, V. Jasutis, S. Marcinkevicius, and U. Olin, "Subpicosecond carrier lifetimes in GaAs grown by molecular beam epitaxy at low substrate temperature," *Applied Physics Letters*, vol. 66, pp. 1939-1941, 1995.

[67] M. Tani and e. al, "Spectroscopicharacterisationn of Low-temperature- Grown GaAs epitaxial films," *Jpn. J. Appl. Phys.*, vol. 33, pp. 4807-4811, 1994.

[68] P. A. Loukakos, C. Kalpouzos, I. E. Perakis, Z. Hatzopoulos, M. Logaki, and C. Fotakis, "Ultrafast electron trapping times in low-temperature-grown gallium

arsenide: The effect of the arsenic precipitate spacing and size," *Applied Physics Letters,* vol. 79, pp. 2883-2885, 2001.

[69] C. Berry and M. Jarrahi, "Terahertz generation using plasmonic photoconductive gratings," *New Journal of Physics,* vol. 14, p. 105029, 2012.

[70] M. Suzuki and M. Tonouchi, "Fe-implanted InGaAs photoconductive terahertz detectors triggered by 1.56 mu m femtosecond optical pulses," *Applied Physics Letters,* vol. 86, p. 163504, 2005.

[71] C. D. Wood, O. Hatem, J. E. Cunningham, E. H. Linfield, A. G. Davies, P. J. Cannard, M. J. Robertson, and D. G. Moodie, "Terahertz emission from metal-organic chemicavapouror deposition grown F e:InGaAs using 830 nm to 1.55 mu m excitation," *Applied Physics Letters,* vol. 96, p. 194104, 2010.

[72] M. Sukhotin, E. R. Brown, D. Driscoll, M. Hanson, and A. C. Gossard, "Picosecond photocarrier-lifetime in ErAs.

[73] J. Mangeney and P. Crozat, "Ion-irradiated In0.53Ga0.47As photoconductive antennas for THz generation and detection at 1.55 μm wavelength," *Comptes Rendus Physique,* vol. 9, pp. 142-152, 2008.

[74] A. Takazato, M. Kamakura, T. Matsui, J. Kitagawa, and Y. Kadoya, "Terahertz wave emission and detection using photoconductive antennas made on low-temperature-grown InGaAs with 1.56 mu m pulse excitation," *Applied Physics Letters,* vol. 91, p. 011102, 2007.

[75] B. B. Hu, A. S. Weling, D. H. Auston, A. V. Kuznetsov, and C. J. Stanton, "dc-electric-field dependence of THz radiation induced by femtosecond optical excitation of bulk GaAs," *Physical Review B,* vol. 49, pp. 2234-2237, 1994.

[76] B. Ferguson and X. Zhang, "Materials for terahertz science and technology," *Nat Mater,* vol. 1, pp. 26-33, 2002.

[77] E. Peytavit, S. Lepilliet, F. Hindle, C. Coinon, T. Akalin, G. Ducournau, G. Mouret, and J.-F. Lampin, "Milliwatt-level output power in the sub-terahertz range generated

by photomixing in a GaAs photoconductor," *Applied Physics Letters,* vol. 99, p. 223508, 2011.

[78] V. Pacebutas, A. Biciunas, S. Balakauskas, A. Krotkus, G. Andriukaitis, D. Lorenc, A. Pugzlys, and A. Baltuska, "Terahertz time-domain-spectroscopy system based on femtosecond Y fibreer laser and GaBiAs photoconducting components," *Applied Physics Letters,* vol. 97, p. 031111, 2010.

[79] G. Matthaus, S. Nolte, R. Hohmuth, M. Voitsch, W. Richter, B. Pradarutti, S. Riehemann, G. Notni, and A. Tunnermann, "Microlens coupled interdigital photoconductive switch," *Applied Physics Letters,* vol. 93, p. 091110, 2008.

[80] H. Roehle, R. J. B. Dietz, H. J. Hensel, J. Böttcher, H. Künzel, D. Stanze, M. Schell, and B. Sartorius, "Next generation 1.5 µm terahertz antennas: mesa-structuring of InGaAs/InAlAs photoconductive layers," *Opt. Express,* vol. 18, pp. 2296-2301, 2010.

[81] S. Preu, G. H. Döhler, S. Malzer, L. J. Wang, and A. C. Gossard, "Tunable, continuous-wave Terahertz photomixer sources and applications," *Journal of Applied Physics,* vol. 109, p. 061301, 2011.

[82] C. W. Berry, N. Wang, M. R. Hashemi, M. Unlu, and M. Jarrahi, "Significant performance enhancement in photoconductive terahertz optoelectronics by incorporating plasmonic contact electrodes," *Nat Commun,* vol. 4, p. 1622, 2013.

[83] M. Beck, H. Schäfer, G. Klatt, J. Demsar, S. Winnerl, M. Helm, and T. Dekorsy, "Impulsive terahertz radiation with high electric fields from an amplifier-driven large-area photoconductive antenna," *Opt. Express,* vol. 18, pp. 9251-9257, 2010.

[84] M. Jarrahi and T. H. Lee, "High-power tunable terahertz generation based on photoconductive antenna arrays," in *IEEE MTT-S International Microwave Symposium Diges* , 2008, pp. 391-394.

[85] S. Fathololoumi, E. Dupont, C. W. I. Chan, Z. R. Wasilewski, S. R. Laframboise, D. Ban, A. Mátyás, C. Jirauschek, Q. Hu, and H. C. Liu, "Terahertz quantum cascade lasers operating up to about 200 K wioptimisedzed oscillator strength and improved injection tunneling," *Opt. Express,* vol. 20, pp. 3866-3876, 2012.

[86] P. R. Smith, D. H. Auston, and M. C. Nuss, "Subpicosecond photoconducting dipole antennas," *IEEE Journal of QuantElectronicsns,*, vol. 24, pp. 255-260, 1988.

[87] K. Ezdi, M. N. Islam, Y. A. N. Reddy, C. Jördens, A. Enders, and M. Koch, "A numerical study of photoconductive dipole antennas: the real emission frequency and an improved antenna design," *Proceeding of SPIE,* vol. 6194, pp. 61940G-61940G, 2006.

[88] C. A. Balanis, *Antentheory:y : analysis and design*, 3rd ed. Hoboken, NJ: John Wiley, 2005.

[89] R. Faulks, M. Evans, H. Page, S. Malik, I. Gregory, I. Farrer, D. Ritchie, and M. Pepper, "Enhanced Terahertz Receiver Using a Distributed Bragg Reflector Coupled to a Photoconductive Antenna," *IEEE Photonics Technology Letter* , vol. 21, pp. 1603-1605, 2009.

[90] S. Park, K. H. Jin, M. Yi, J. C. Ye, J. Ahn, and K. Jeong, "Enhancement of Terahertz Pulse Emission by Optical Nanoantenna," *ACS Nano*, vol. 6, pp. 2026-2031, 2012/03/27 2012.

[91] S. Park, Y. Choi, Y. Oh, and K. Jeong, "Terahertz photoconductive antenna with metal nanoislands," *Opt. Express*, vol. 20, pp. 25530-25535, 2012.

[92] T. W. Ebbesen, H. J. Lezec, H. F. Ghaemi, T. Thio, and P. A. Wolff, "Extraordinary optical transmission through sub-wavelength hole arrays," *Nature*, vol. 391, pp. 667-669, 1998.

[93] W. L. Barnes, A. Dereux, and T. W. Ebbesen, "Surface plasmon subwavelength optics," *Nature*, vol. 424, pp. 824-830, 2003.

[94] B. Heshmat, H. Pahlevaninezhad, Y. Pang, M. Masnadi-Shirazi, R. Burton Lewis, T. Tiedje, R. Gordon, and T. E. Darcie, "Nanoplasmonic Terahertz photoconductive switch on GaAs," *Nano Letters*, vol. 12, pp. 6255-6259, 2012.

[95] J. Faist, F. Capasso, D. L. Sivco, C. Sirtori, A. L. Hutchinson, and A. Y. Cho, "Quantum cascade laser," *Science*, vol. 264, pp. 553-556, 1994.

[96] Y. Shang-Hua; M.R. Hashemi, C.W. Berry, M. Jarrahi, "7.5% Optical-to-Terahertz conversion efficiency offered by photoconductive emitters with three-dimensional plasmonic contact electrodes, "*Terahertz Science and Technology, IEEE Transactions,* vol.4, pp.575-581, 2014.

[97] H. Tanoto, J. H. Teng, Q. Y. Wu, M. Sun, Z. N. Chen, S. A. Maier, WangB, C. C. Chum, G. Y. Si, A. J. Danner, and S. J. Chua, "Greatly enhanced continuous-wave terahertz emission by nano-electrodes in a photoconductive photomixer," *Nat Photon,* vol. 6, pp. 121-126, 2012.

Chapter 3 A Comparison of the Effect of Substrate on the Performance of THz Antenna

3.1 Introduction

Radiation patterns and the radiated power of the photoconductive antenna can be significantly affected by the substrate thickness and size [1]. Hence, the effects of photoconductive material's dimensions on the performance of the THz antennas are investigated in this chapter.

In this chapter also, the effects of photoconductive material parameters on THz antennas are investigated since they play an essential role in THz wave generation and detection. The main reason is that naturally, no material exists to allow an efficient and powerful THz emission. The intrinsic carrier lifetime of materials is not fast enough to reach very high frequency ranges of the THz spectrum. Thus, to reduce the carrier lifetime, materials studies for THz are very crucial. In THz antennas, the substrate is a photoconductive material which is basically a semiconductor [2]. LT-GaAs is the most popular material due to its desirable characteristics, namely ultra-short carrier lifetime, relatively high electron mobility, high intrinsic resistivity and high breakdown voltage. Table 3.1 shows the properties of various photoconductive materials used as a substrate in THz antennas.

Table 3.1 Properties of various photoconductive materials [3, 5-6]

Material	Carrier lifetime (ps)	Mobility ($cm^2.V^{-1}.s^{-1}$)	Resistivity (Ω.cm)	Breakdown voltage ($V.cm^{-1}$)
SI-GaAs	Several hundred	8500	~10^7	4 x 10^5
LT-GaAs	< 1	200	>10^7	5 x 10^5
LT-InGaAs	Larger than LT-GaAs	26	760	~ 6 x 104
Graphene	N/A	15000	10^{-6}	N/A

Nevertheless, graphene in Fig. 3.1, a one-atom-thick layer of carbon atoms arranged in a honeycomb lattice has recently attracted considerable interest as a potential material due to its high electron mobility [5-7].

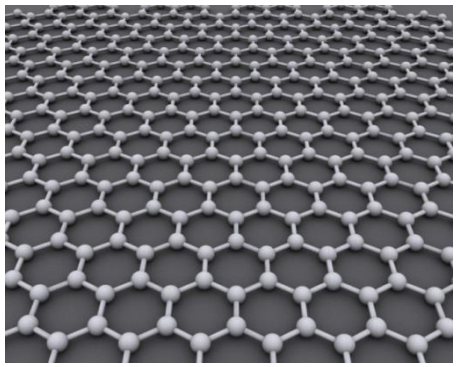

Fig. 3.1 2D of Graphene [2]

In Fig. 3.2, a femtosecond laser pulse with energy more significant than the band gap of substrate material at a room temperature illuminating the antenna gap. The electron-hole pairs are produced in the semiconductor substrate and accelerated by the electric field formed by the DC bias voltage. Thus, the photocurrent is generated. The antenna can radiate an electromagnetic wave in the THz region. Hence, photoconductive material plays a vital role in THz wave generation and detection.

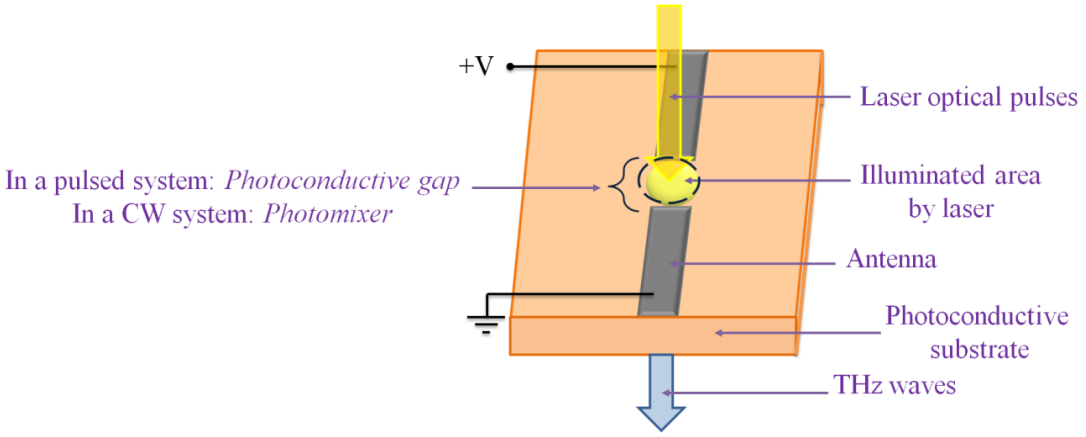

Fig. 3.2 Schematic diagram of a THz antenna as an emitter [18]

3.2 Previous Investigation on the Effects of Substrate on THz Antennas

Various studies had been done to investigate the effects of substrate on the performance of the THz Antennas. Most studies had been focused on the substrate thickness and the dimensions of the substrate [1,8-9]. For antennas working in THz range, the thickness of the substrate is usually comparable with the wavelength and sometimes even higher than the wavelength.

In [1] the effects of the substrate's thickness on the performance of photoconductive antennas had been investigated. LT-GaAs had been chosen as the semiconductor substrate in that study. A dipole antenna with a fixed length of 50 μm had been simulated using Computer Simulation Tool (CST), and the substrate thicknesses had been varied. It was found that the radiation patterns and the radiated power of the photoconductive antenna are significantly affected by the substrate thickness and size.

Meanwhile, in [3] the effects of the substrate's thickness using graphene on the performance of Terahertz antenna had been studied. Graphene nanoantennas with various geometries had been simulated using Method of Moments (MoM-2D) and Comsol. The substrate thicknesses had been varied. It was observed that for smaller sizes, the resonance

frequencies shifted to higher frequencies and the values of absorption cross section are increased. These prove that graphene has the capability to harvest light.

To generate a high frequency THz signal with significant power, the photoconductive material has to show three main properties [4]:

1) A short electron-hole recombination time to obtain fast current pulses or CW current variation in the antenna

2) High carrier mobility to obtain these signals

3) A high dark resistivity to produce THz efficiently and to support a high static bias voltage.

A high dark resistivity permits applying higher bias voltages across the antenna without contributing to a considerable amount of heat which can influence the performance of the device. In [4], photoconductive devices using GaAs and InGaAs had been compared in terms of materials design and solid-state metrics such as electron-hole lifetime, carrier mobility and resistivity. It is found that GaAs still has superior performance due to its high dark resistivity and high mobility as [3].

Fig. 3.3 showed that when a dipole antenna is located in free space, the antenna has an omnidirectional pattern in azimuth. It radiates in all direction along the plane perpendicular to the electric field of the dipole. When the dipole is fabricated on a photoconductive substrate, the radiation pattern becomes asymmetrical. This radiation pattern enhanced towards the substrate [1] as shown in Fig. 3.4.

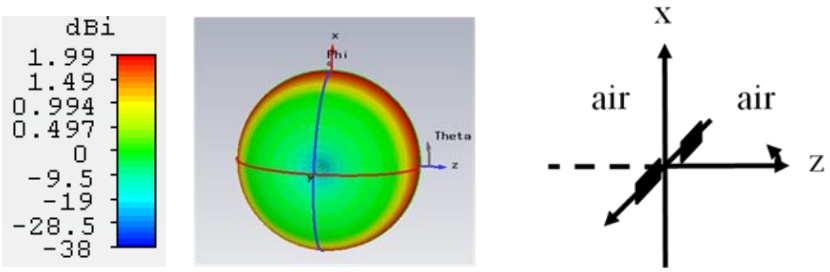

Fig. 3.3 Dipole antenna [8] surrounded by air and its radiation pattern

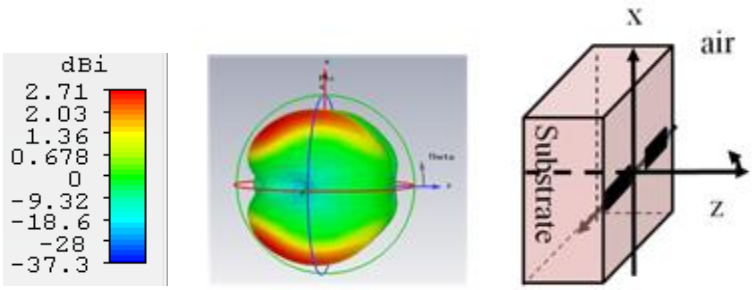

Fig. 3.4 Dipole antenna [8] on a GaAs substrate and its radiation pattern

Since the photoconductive substrate has high permittivity (ε_r = 12.9 for GaAs), most of the power is radiated towards the substrate rather than the free space. Hence, a photoconductive substrate with a low permittivity is also desirable in addition to the material properties mentioned before.

In [4], photoconductive devices using GaAs and InGaAs had been compared in terms of materials design and solid-state metrics such as electron-hole lifetime, carrier mobility and resistivity. It is found that GaAs still has superior performance due to its high dark resistivity and high mobility.

Photoconductive dipole antenna based on semi-insulating GaAs substrate has been used as an emitter in [3]. The surface of the antenna is coated with Si_3N_4 and later sealed with transparent silicon gel. It had been demonstrated that the THz power had been increased by 1 order and the breakdown voltage had been increased by 3 times when the antenna been coated with Si_3N_4. Coated antenna generates stronger THz radiation due to the higher electric field.

Graphene is a one-atom thick sheet of carbon atoms arranged in a honeycomb lattice. It was first discovered in 2004 by exfoliation of graphite. Due to its attractive mechanical, thermal and electrical properties such as high electron mobility, graphene had been seen as a potential research topic by researchers. Possible applications of graphene in solar cells and light- emitting devices, photodetectors, microwave transistors and had been identified and currently being investigated extensively [3,5-7].

Graphene offers a substantial advantage as its properties can be readily tuned by applying a gate voltage. In [10], a dipole antenna made by gold deposition on a graphene layer placed on a grown over a SiO2/Si substrate had been studied. It had been shown that by tuning the gate voltage, the radiation pattern could be exploited. The radiation pattern is switched ON and OFF by the two states of resistivity in graphene. At 1.05THz by using IE3D software, the radiation efficiency is 95.80%, and the antenna efficiency is 89.14%.

In [11], a graphene dipole-like antenna had also been studied. However, graphene is now used as an electrode instead as a substrate. The proposed antenna was simulated using Ansys HFSS. Values of 0-0.2 eV range of chemical potential had been chosen base on experimental activity. The gate voltage used is between 0-3 V. By varying the chemical potential, it had been demonstrated that radiation efficiencies increases.

3.3 Simulation Results

3.3.1 Substrate Thickness

Firstly, the length and the width of the substrate are both fixed to 150 μm, and the frequencies are varied from 0.5 THz to 1 THz. The substrate thickness, however, is varied from 15 μm to 300 μm. Fig. 3.5 shows that at 1 THz the radiated power is higher once the thickness of the substrate is at the minimum size which is at 15 μm. Fig. 3.6 shows that at 1 THz, the efficiency is greater once the thickness of the substrate is at the minimum size which is at 15 μm. The results consist with the findings in [1]. It was found that when increasing the thickness of the substrate, the dipole antennas couple power to higher-order substrate modes. Also, more than 90% of the power can be trapped in the substrate. Therefore, not all the power radiated from the dipole structure can be directly transferred into the air.

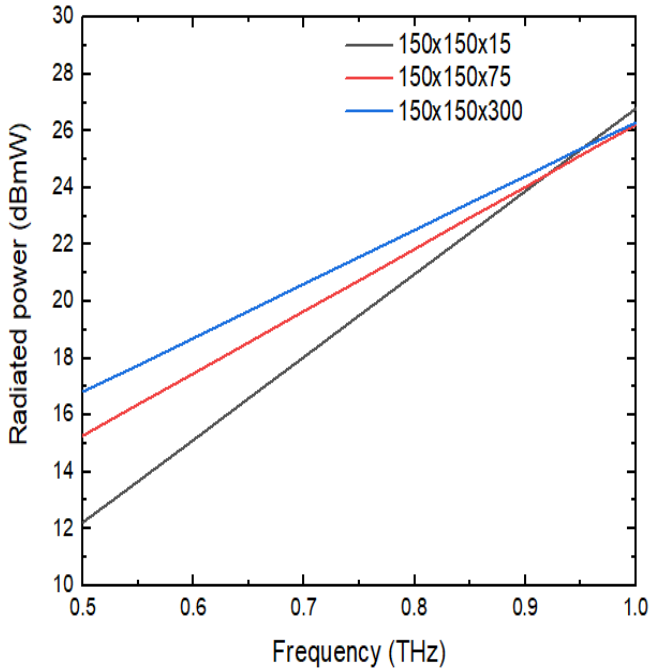

Fig. 3.5 Total radiated power when substrate thickness is varied while length and the width of the substrate are both fixed to 150 µm

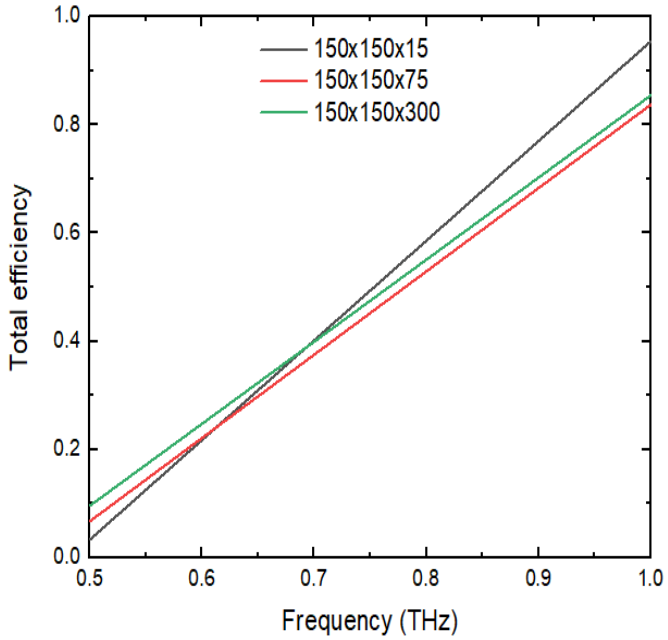

Fig. 3.6 Total efficiency when substrate thickness is varied while length and the width of the substrate are both fixed to 150 µm

Secondly, the substrate thickness is fixed to 15 µm while the length and the width of the substrate are chosen to be 150 µm x 150 µm, 300 µm x 300 um and 600 µm x 600 µm. The frequencies are varied from 0.5 THz to 1 THz. Fig. 3.7 shows that at 1 THz, the radiated power is more significant for the substrate with 150 µm length and 150 µm width compared to the other dimensions. Fig. 3.8 also shows that at 1 THz, the efficiency is greater for the substrate with 150 µm length and 150 µm width. At 1 THz, the efficiency is 0.9543 for a substrate thickness with dimensions of 150 µm x 150 µm x 15 µm. For a substrate thickness with dimensions of 300 µm x 300 µm x 15 µm, the efficiency is 0.9392 and for a substrate thickness with dimensions of 600 µm x 600 µm x 15 µm, the efficiency is 0.8782. Hence, the dimensions of 150 µm x 150 µm x 15 µm should be used for as the substrate dimensions for any further study on the substrate material.

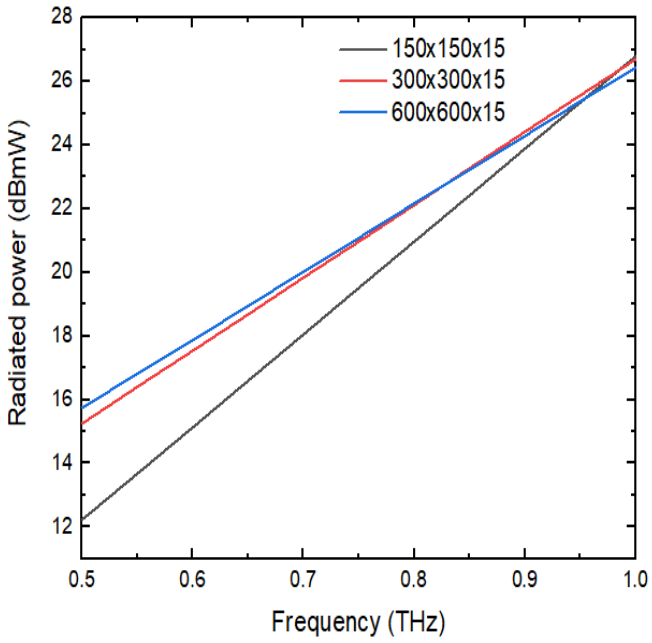

Fig. 3.7 Total radiated power when substrate thickness fixed to 75µm while the length and width are varies

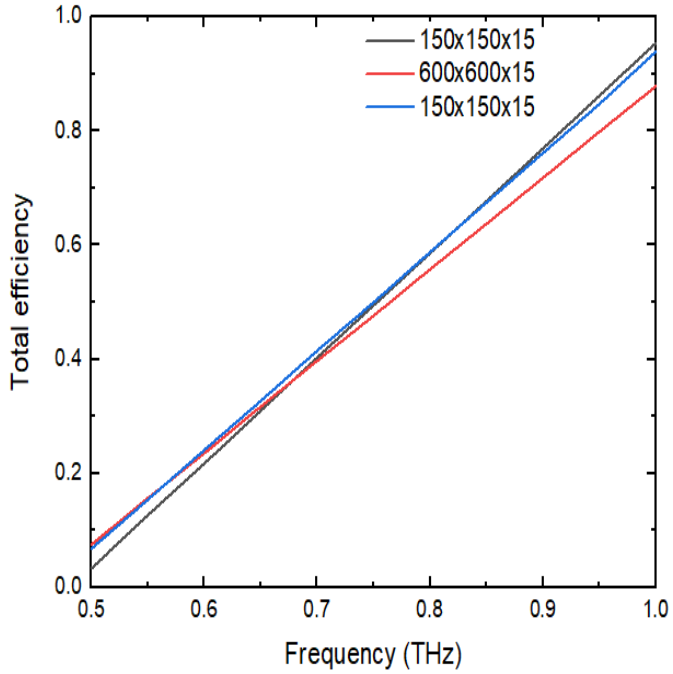

Fig. 3.8 Total efficiency when substrate thickness fixed to 75µm while the length and width are varies

3.3.2 Substrate Material

Considering all the main material properties desired for a terahertz photoconductive antenna, graphene is chosen as a semiconductor substrate in this investigation. Graphene has low permittivity ($\varepsilon_r = 5$) and high carrier mobility (15 000 $cm^2.V^{-1}.s^{-1}$) [5-7]. The dipole antenna operating at 0.5 THz – 1 THz can be modelled in CST as two electrodes separated by a small gap as in [1], driven by a discrete face port between the two electrodes. The substrate dimension used in both photoconductive antennas is set to 150 µm in length x 150 µm in width, and 150 µm in thickness as these are the parameters that showed promising results in radiated power and total efficiency as shown in previous simulations results. All simulations were done using CST Microwave Studio. The radiated power and efficiency of a graphene-based dipole antenna in [8] are compared with those of GaAs-based devices, and the results are as indicated below.

Fig. 3.9 shows that the radiated power photoconductive material with the highest mobility are higher compared to other at 0.5 THz – 0.7 THz. The power radiated by the antenna using graphene is 33% more at 0.5 THz than the antenna with the same structure but using a

GaAs substrate. Though the radiated power decreases as the frequency increases, the power increment is encouraging. Note that the carrier mobility of graphene is higher than that of GaAs; thus this generates larger photocurrent hence more radiated power. The simulation results are in good agreement with the theory in [14-16].

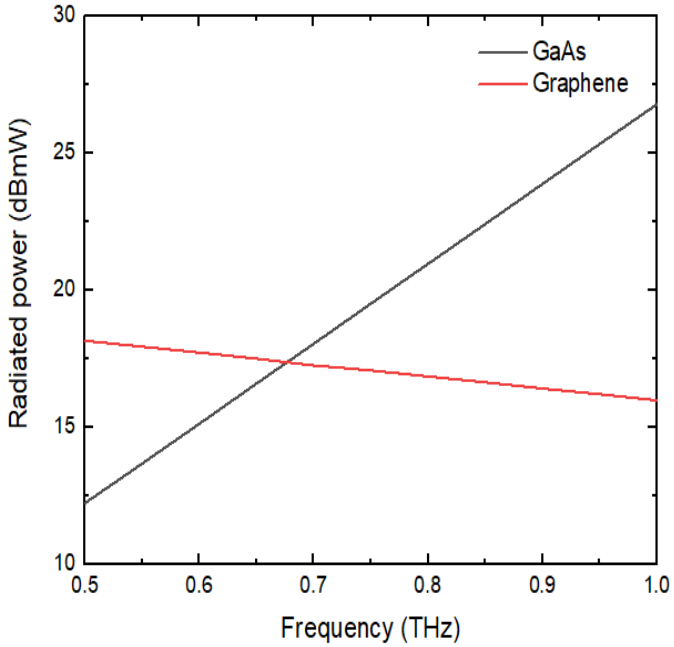

Fig. 3.9 Total radiated power for various photoconductive materials

After 0.7 THz until 1 THz, the simulation shows that the radiated power of photoconductive antenna using GaAs as a substrate supersede photoconductive antenna using Graphene as a substrate. This is might due to the fact that GaAs has a higher dielectric constant. The radiation patterns of both photoconductive antennas are shown in Fig. 3.10 and Fig. 3.11. It can be observed that the higher dielectric constant in GaAs, more energy is attracted into the substrate and the radiated to the substrate side as in [1].

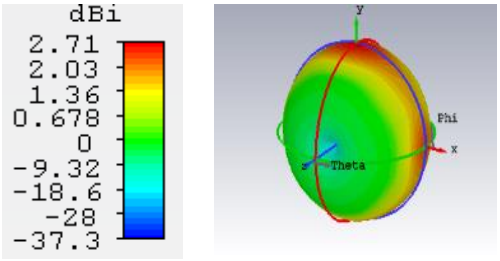

Fig. 3.10 A radiation pattern of a dipole antenna in [1] with GaAs as a substrate

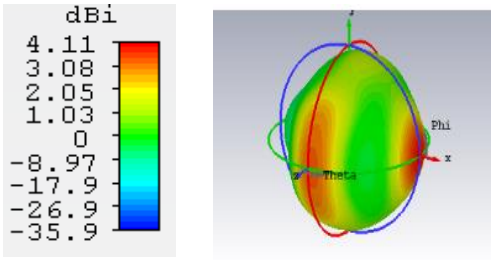

Fig. 3.11 A radiation pattern of a dipole antenna in [1] with Graphene as a substrate

Fig. 3.12 shows the efficiency of the photoconductive antenna using GaAs and graphene as the substrate material respectively. It is shown that the efficiencies are increased by 3 times at 0.5 THz – 0.55 THz. The efficiencies of a photoconductive antenna using graphene keep decreasing from 0.55 THz to 1 THz. Though the efficiencies decrease as the frequencies increase, the increment is promising. It had been stated theoretically in [14-16], that the efficiency was found to be proportional to the photoconductive material properties; hence the simulation results validated the theory.

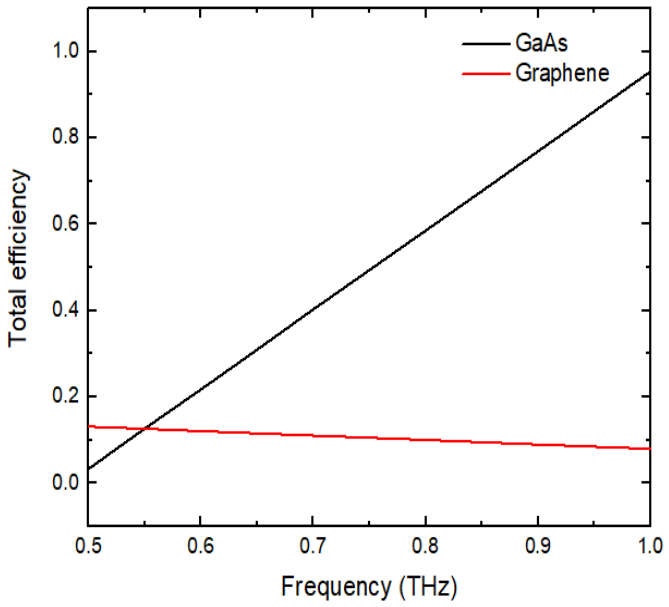

Fig. 3.12 Total efficiency for various photoconductive material

3.4 Summary

Substrate effect in THz plays an important role compared to substrate effect in microwave frequency. At 1 THz, the efficiency is 0.9543 for a substrate thickness with dimensions of 150 µm x 150 µm x 15 µm. The radiated power is higher once the thickness of the substrate is at the minimum size which is at 15 µm. Hence, the dimensions of 150 µm x 150 µm x 15 µm had been used for as substrate dimensions for any further study on a substrate material.

In the preliminary finding, it has been shown that graphene is a promising material to be used as a substrate for THz antennas. It is found that the estimated radiated power of the antenna using graphene is 33% more than the radiated power from the THz antenna using GaAs as a substrate at 0.5 THz – 0.7 THz. A new development by [17] had shown that graphene could emit ultrashort terahertz pulses. In the present experiment conducted, the electrons in graphene were excited using infrared laser light. This is indeed exciting to know that there is work done

experimentally to show that graphene can emit laser terahertz radiation. This finding, however, can be more elaborated in details.

Due to the limitations of the CST Microwave Studio software wherein the student edition, only 30 000 mesh cells can be simulated; another potential software needs to be reconsidered to prove the theory discussed more accurately. This limitation also only allows a narrow frequency range. New potential simulation software such as Comsol will provide more accurate results on the effects of a substrate material of a photoconductive antenna.

References

[1] D. Li, Y. Huang, Y. Shen, and N. Khiabani, "Effects of substrate on the performance of photoconductive THz antennas", *Proceeding of the iWAT 2010,* 2010.

[2] B. Ferguson, and X. Zhang, "Materials for Terahertz science and technology", *Nature Materials,* vol. 1, p. 26-33, 2002.

[3] J. Xu, W. Shi, L. Hou, W. Jia, K. Liu, X. Xei, and X. C. Zhang "Terahertz generation from multiple transparent dielectric coated GaAs antenna", *12th International Conference on Terahertz Electronics,* 2004.

[4] M. Martin, and E. R. Brown, "Critical Comparison of GaAs and InGaAs THz Photoconductor", *Conference 8261,* SPIE Photonics West, San Franscico, January 21-26, 2012.

[5] T. Palacios, A. Hsu, and H. Wang, "Applications of graphene devices in RF communications", *Communications Magazine,* IEEE 48.6, p. 122-128, 2010.

[6] A. K. Geim, and K. S. Novoselov, "The rise of graphene", *Nat Matter,* vol. 6, p.183-191, 2007.

[7] P. Tassin, T. Koschny, and C. M. Soukoulis, "Graphene for Terahertz applications", *Science,* vol. 341, p. 620-621, 2013.

[8] D. R. Jackson, and N. G. Alexopolous, "Microstrip dipoles on electrically thick substrates," *International Journal of Infrared and Millimetre Waves,* vol.7, No 1, 1986.

[9] N. G. Alexopoulos, P. B. Katehi, and D. B. Rutledge, "Substrate optimisation for integrated circuit antennas", *IEEE Transactions on Microwave Theory and Techniques,* vol 31, No 7, July 1983.

[10] M. Dragoman, A. A. Muller, D. Dragoman, F. Coccetti, and R. Plana, “Terahertz antenna based on graphene”, *Journal of Applied Physics*, p. 107-109, 2010.

[11] M. Tamagnone, J. S. Gomez Diaz, J. R. Mosig and J. Perruisseau-Carrier, “Analysis and design of terahertz antennas based on plasmonic resonant graphene sheets”, *Journal of Applied Physics*, p.112, 2012.

[12] J. S. Gomez-.Diaz and J. Perruisseau-Carrier “Microwave to THz properties of graphene and potential antenna applications”, *Proceeding of ISAP2012*, pp.239-242, 2012.

[13] J. Perruisseau-Carrier “Graphene for antenna applications: Opportunities and challenges from microwave to THz”, *Loughborough Antennas & Propagation Conference*, 2012.

[14] N. Khiabani, Y. Huang, Y. Shen, “Discussions on the main parameters of THz photoconductive antenna as emitters”, *Proceeding of the 5th EuCAP*, pp.462-466, April 2011.

[15] Y. Huang, N. Khiabani, Y. Shen and D. Li, “A Further Study of THz Photoconductive Antennas”, *Antennas and Propagation Society International Symposium (APSURSI)*, 2012.

[16] N. Khiabani, Y. Huang, Y. Shen, L. E. Garcia-Munoz, A. Rivera-Lavado, “A Novel THz Photomixer Antenna with Trapezoidal Electrodes”, submitted to *IEEE Transactions on Terahertz Science and Technology*, 2013.

[17] I. Gierz, J. C. Petersen, M. Mitrano, C. Cacho. E. Turcu, E. Springate, A. Stohr, A. Kohler, U. Starke and A. Cavelleri, “Non-equilibrium Dirac carrier distributions in graphene”, *Nature Materials*, 2013.

[18] Y. Lee, *Principles of terahertz science and technology*, 1st ed. New York, NY: Springer, 2008.

Chapter 4 The Effect of Electrode Design on THz Photoconductive Antenna

4.1 Introduction

A comprehensive literature survey [1-3] had summarised the main parameters that can be the solution in producing high THz output power and high optical-to-THz efficiency from the antenna. Studies had been done on the sizes of the antenna gap where sharp tip ends will produce high photo- carrier acceleration. Types of laser excitation also had been studied. The findings had been summarised in Fig. 4.1.

Nevertheless, none of the parameter studied below had been focusing on the electrode structure and electrode material that may lead to higher THz power. This chapter will focus solely on the effect of the electrode structure to the THz radiated power. This chapter also will focus on the impact of electrode material to the THz radiated power. Comparing a dipole antenna with an electrode made from noble materials with graphene and nitrides, a metamaterial will provide insight on the best electrode material for THz photoconductive antenna.

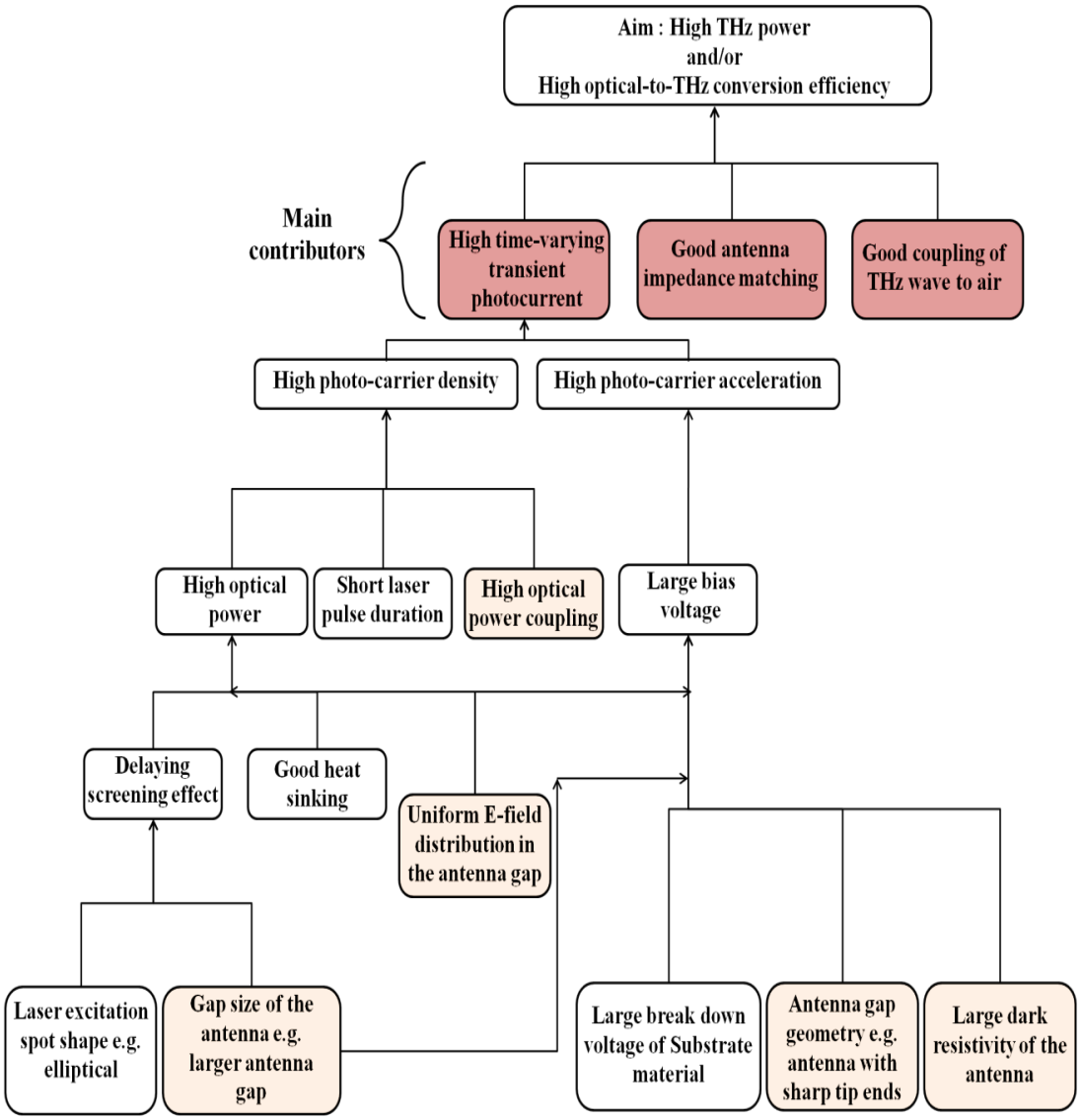

Fig. 4.1 Contribution of each parameter on THz output power and optical-to THz conversion efficiency [1-3]

4.2 The Importance of the Electrode Study

4.2.1 Electrode Structure Study

THz power can be determined by the photoconductive material characteristics and electrode geometry. Improving the effective carrier lifetime by minimising the carrier drift time can be achieved by optimising electrode design [6-7]. The longer the electrode, it had been found that the resonant frequency shifted even lower. The lower the resonant frequency, the smaller efficiency will be at higher THz frequency.

Also, by reducing the finger electrode separation, the transit time for the photogenerated carrier will be reduced, this will result in higher efficiency (photon to current conversion). Meanwhile the larger gap, the larger enhancement can be achieved. Electric field strength is also found greatest at the photoconductive gap [6-7]. Thus, the embedded electrode will generate high photo-carriers that will lead to high THz power as shown in Fig. 4.2.

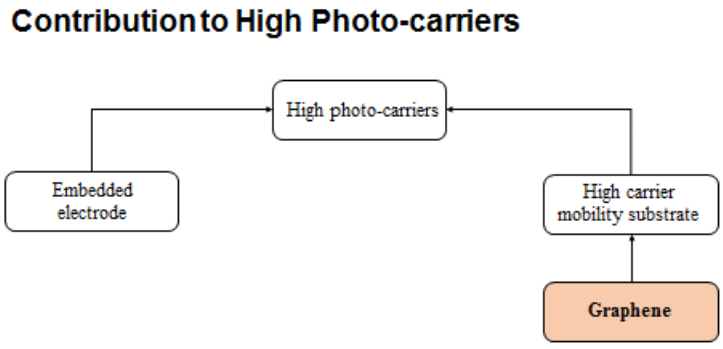

Fig. 4.2 Framework on the contributions to produce high photo-carriers.

4.2.2 Electrode Material Study

As a continuance, high optical power coupling can be achieved with the right electrode material. This will hopefully be one of the factors that will improve the conversion efficiency of a photoconductive antenna which will lead to higher THz radiated power. Fig. 4.3 is the theoretical framework that had been constructed for this study.

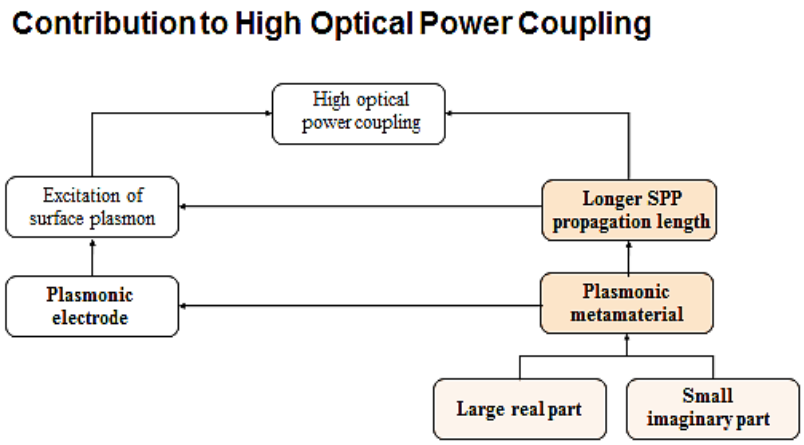

Fig. 4.3 Framework on the contributions to produce high optical power coupling

Fig. 4.4 is the summary of the theoretical framework that had been constructed for this study in order to contribute to high optical power coupling compared to the previous noble metals.

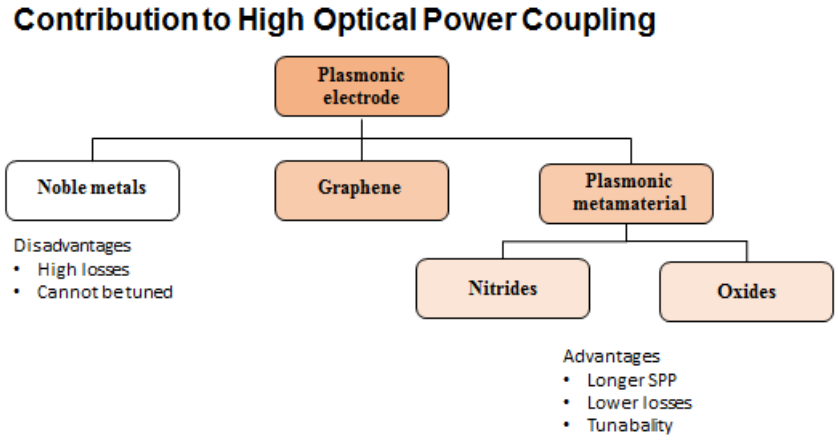

Fig. 4.4 Summary of Contribution to High Optical Power Coupling

4.3 Electrode structure study using CST

In theory, embedding the three-dimensional plasmonic contact electrode inside the substrate will drift the majority of photocarriers to the photoconductor contact electrodes, thus enhancing the optical-to-terahertz conversion efficiency of the photoconductive terahertz emitter [6].

It had been shown by [6] that 7.5 % Optical-to-Terahertz power conversion efficiency at 1.4 mW optical pump power by using three-dimensional plasmonic contact electrodes. Validated via simulation tools COMSOL, indicating the optical absorption and experimental results indicating the radiated power and photocurrent for both two-dimensional and three-dimensional, showing a significant increase in the latter.

In order to efficiently contribute to terahertz radiation, the transit time of the photocarriers to the photoconductor contact electrodes should be within a fraction of the terahertz oscillation period; thus only the photocarriers which are generated within distances of 100nm from the contact electrodes can efficiently contribute to the terahertz radiation.

4.3.1 Methodology

A dipole antenna similar to [1] in Chapter 3, was simulated using CST. The dipole antenna operating at 0.95 THz – 1 THz had been modelled in CST as two electrodes separated by a small gap, driven by a discrete face port between the two electrodes. The substrate dimension used in both photoconductive antennas is set to 150 µm in length x 150 µm in width and 150 µm in thickness. The gap is set to 10 µm. The thickness of the substrate is set to 15 µm as this is the optimum dimensions that were simulated earlier in Chapter 3. The substrate used is GaAs while the electrode used is modelled as Perfect Electric Conductor (PEC). To study the effect of the embedded electrode, the electrode is embedded 2 µm into the substrate. Fig. 4.5 shows the dipole antenna used in this electrode structure study using CST. Fig. 4.6 shows the structure of dipole antenna and their wireframe with (a) standard electrode (b) embedded electrode.

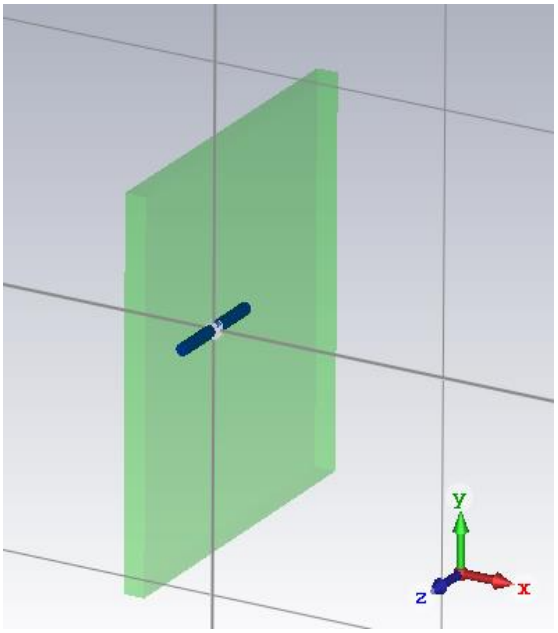

Fig. 4.5 The dipole antenna used in electrode structure study using CST.

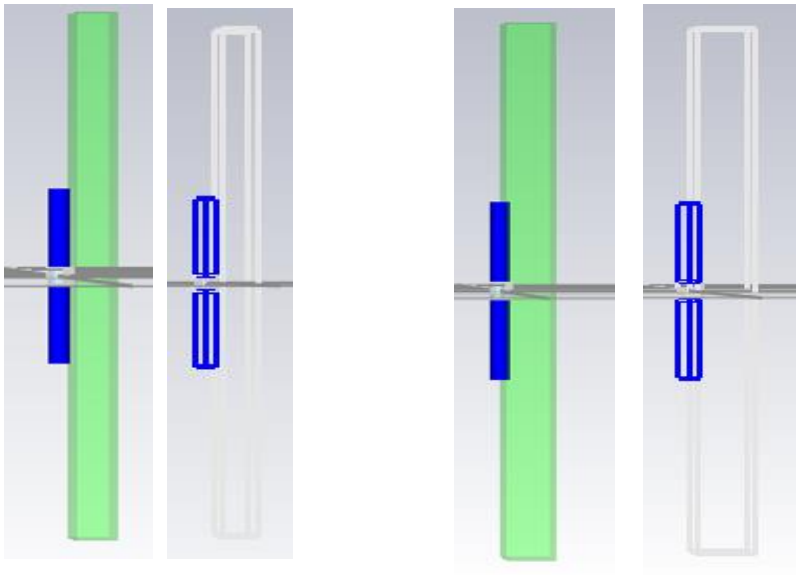

(a) (b)

Fig. 4.6 The structure of dipole antenna and their wireframe with (a) standard electrode (b) embedded electrode

4.3.2 The Simulation Results

Fig. 4.7 shows the radiated power of dipole antenna using (a) standard electrode and (b) embedded electrode, 2 µm into the substrate while Fig. 4.8 shows the efficiency of the dipole antenna using standard electrode and an embedded electrode, 2 µm into the substrate. Not so much difference in radiated power and efficiency can be observed between both structures. Less than 1% difference can be seen between both electrode structure. Hence, CST is not the best simulation tool to be used in electrode study.

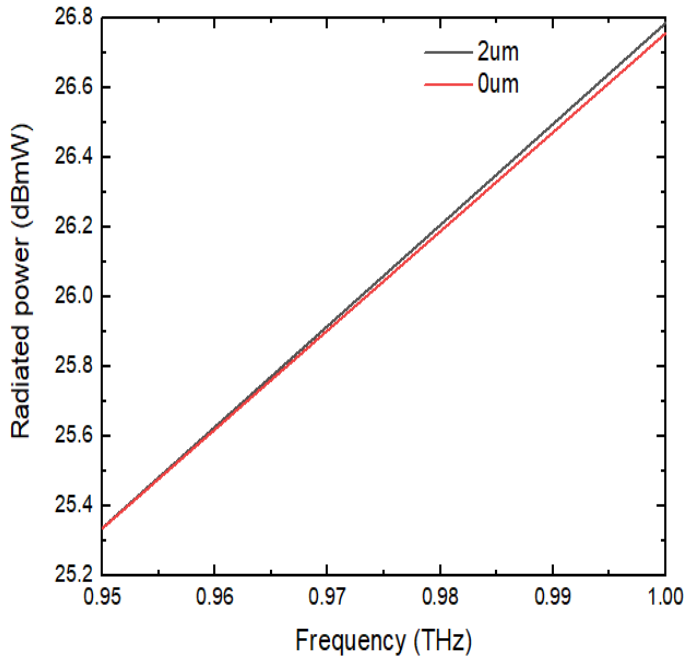

Fig. 4.7 The radiated power of dipole antenna using standard electrode and an embedded electrode, 2 µm into the substrate

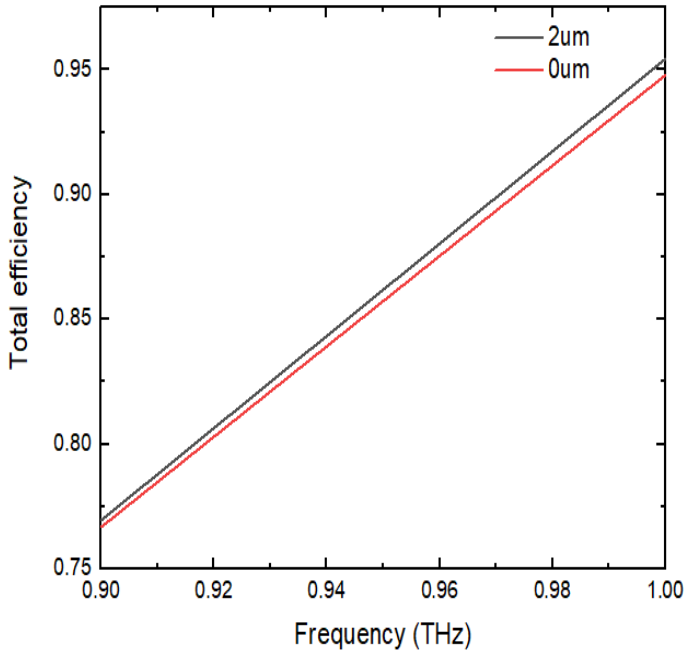

Fig. 4.8 The efficiency of the dipole antenna using standard electrode and an embedded electrode, 2 µm into the substrate

However, should the accurate simulation tools been used, the results are expected to be more accurate. This is because CST is a configurable tool uses Maxwell's Equations that describe the world of electromagnetic. These equations describe how electric and magnetic field propagate and interact. These equations also describe how the electric field and magnetic field are influenced by objects. The effects of the interactions between the semiconductor and the laser pulse had not been considered here. The physics involved in this interaction must be added to the simulation. When the substrate in the gap is illuminated with photons, the energy from the photons generates charge carriers in the substrate. If a voltage bias is applied to those traces, the generated electric field mobilises these carriers creating the current.

This behaviour of carriers over time in a substrate begins with continuity equations that account the change in carrier concentrations over time. The total change in carrier combination must equal the changes due to drift, diffusion, regeneration/combination, and other processes such as photo generation [4]. The combined effects of all carrier action must satisfy :

$$\frac{\partial n}{\partial t}\Big| = \frac{\partial n}{\partial t}\Big|_{drift} + \frac{\partial n}{\partial t}\Big|_{diffusion} + \frac{\partial n}{\partial t}\Big|_{R-G} + \frac{\partial n}{\partial t}\Big|_{other} \quad (4.1)$$

$$\frac{\partial p}{\partial t}\Big| = \frac{\partial p}{\partial t}\Big|_{drift} + \frac{\partial p}{\partial t}\Big|_{diffusion} + \frac{\partial p}{\partial t}\Big|_{R-G} + \frac{\partial p}{\partial t}\Big|_{other} \quad (4.2)$$

Where n and p are the concentrations of electrons and holes, respectively.

Defining the change in carrier concentration due to other processes as G and the change in carrier concentrations due to regeneration as R in addition to noting that

$$\frac{\partial n}{\partial t}\Big|_{drift} + \frac{\partial n}{\partial t}\Big|_{diffusion} = \frac{1}{q}\nabla . Jn \quad (4.3)$$

$$\frac{\partial n}{\partial t}\Big|_{drift} + \frac{\partial n}{\partial t}\Big|_{diffusion} = -\frac{1}{q}\nabla . Jp \quad (4.4)$$

Where q is an electric charge of an electron is the current density due to electrons, and is the current density due to holes; the continuity equations can be more written as

$$\frac{\partial n}{\partial t} = \frac{1}{q}\nabla . Jn - R\,n + G\,n \quad (4.5)$$

$$\frac{\partial p}{\partial t} = -\frac{1}{q}\nabla . Jp - R\,p + G\,p \quad (4.6)$$

Additionally, it is known that the current across the substrate is due to the drift and diffusion of the charge carriers. Therefore, the following relationships must also be satisfied:

$$Jp = q\mu_p pE - qD_p \nabla p \quad (4.7)$$

$$Jn = q\mu_n nE + qD_n \nabla n \quad (4.8)$$

Where μ and μ are the carrier mobility of the electrons and holes respectively, E is the electric field, and Dn and Dp are the carrier diffusion coefficients for the electrons and holes respectively. It is also known that the current density in steady-state conditions [21].

$$J = Jn + Jp \tag{4.9}$$

This semiconductor physics equation should be combined with Maxwell's equations in order to obtain the accurate results of the expected radiated power of the THz photoconductive antenna. Thus, the next step is to find out how these properties can be combined together by using suitable software to produce more accurate results since there is no available software that is available to do this.

4.4 Electrode material study using CST

4.4.1 The Advantages of Plasmonic Metamaterial

4.4.1.1 Surface Plasmon Excitation

The idea to excite surface plasmon waves had been introduced in [5, 8]. Excitation of surface plasmon waves allows transmission of the optical pump through the nano fingers made from gold (aurum) into the photo absorbing substrate. A surface plasmon is a travelling wave oscillation of electrons that can be excited in the surface of certain metals with the right material properties. To date, the only noble metals that can exhibit plasmonic characteristics are gold (aurum) or silver (argentum).

In [5, 8], this paper stated that in the case of the plasmonic photoconductor, the optical pump is transmitted through the nanoscale metallic grating through the coupling with surface plasmon. It is also stated that the highest optical absorption and photocarrier generation occurs in direct proximity to the metal contacts since the excited surface plasmon waves exist at the dielectric-metal interface. This is what plasmonic metamaterial is made of.

However, as a surface plasmon propagates along the surface, it loses energy to the metal due to absorption. Hence larger surface plasmon propagation is desirable to ensure that the excited surface plasmon does not lose its energy/power/intensity too early.

The propagation length of surface plasmon δ_{SPP} is defined as the distance over which the energy/power/intensity of the mode falls to 1/e of its initial value. δ_{SPP} is found from the imaginary part of the surface plasmon wavevector.

From [12], complex surface plasmon wavevector k_{SPP} is defined as

$$k_{SPP} = k'_{SPP} + ik"_{SPP} \tag{4.10}$$

From [13] k_{SPP} is defined as below where ω is the angular frequency, c is the speed of light and $\varepsilon_{m\,is}$ the and ε_d is the relative permittivity of metal and dielectric respectively.

$$k_{SPP} = \frac{\omega}{c}\sqrt{\frac{\varepsilon_m\,\varepsilon_d}{\varepsilon_m + \varepsilon_d}} \tag{4.11}$$

and k'_{SPP}, the real part of the surface plasmon wavevector

$$k'_{SPP} = k_0\sqrt{\frac{\varepsilon_d \varepsilon'_m}{\varepsilon_d + \varepsilon'_m}} \tag{4.12}$$

while $k"_{SPP}$ is the imaginary part of the surface plasmon wavevector, k_o is the light free space where $k_o = 2\pi/\lambda_0$.

Thus,

$$k"_{SPP} = k_0\,\frac{\varepsilon"_m}{2(\varepsilon'_m)^2}\left(\frac{\varepsilon_d \varepsilon'_m}{\varepsilon_d + \varepsilon'_m}\right)^{\frac{3}{2}} \tag{4.13}$$

Since surface plasmon propagation length δ_{SPP}, the distance over which the power/intensity of the mode falls to 1/e of its initial value is

$$\delta_{SPP} = 1/2k"_{SPP} \tag{4.14}$$

Given from [12], the wavelength of surface plasmon, λ_{SPP}

And λ_o is the wavelength of free space

$$\frac{\lambda_{SPP}}{\lambda_0} = \sqrt{\frac{\varepsilon_d + \varepsilon'_m}{\varepsilon_d \, \varepsilon'_m}} \tag{4.15}$$

Thus

$$\delta_{SPP} = \lambda_0 \frac{(\varepsilon'_m)^2}{2\pi(\varepsilon"_m)}\left(\frac{\varepsilon_d + \varepsilon'_m}{\varepsilon_d \, \varepsilon'_m}\right)^{\frac{3}{2}} \tag{4.16}$$

Approximate $|\varepsilon'_m| \gg |\varepsilon_d|$ that

$$\delta_{SPP} \approx \lambda_0 \frac{(\varepsilon'_m)^2}{2\pi(\varepsilon"_m)} \tag{4.17}$$

From equation (4.8), in order to have longer propagation length, a large real part of metal and small imaginary part of the metal is needed [12-13]. Thus, plasmonic metamaterial fits the criteria as it has large real part of the metal and a small imaginary part. This will ensure that the excited surface plasmon does not lose its energy too early in order for the coupling between the surface plasmon and the optical pump is transmitted through the nanoscale gratings.

A comparison is made on the dielectric function of Titanium Nitride (TiN), in contrast with conventional plasmonic materials in [14-15] as shown in Fig. 4.9 proves that the real part of these highly potential plasmonic metamaterials is more significant.

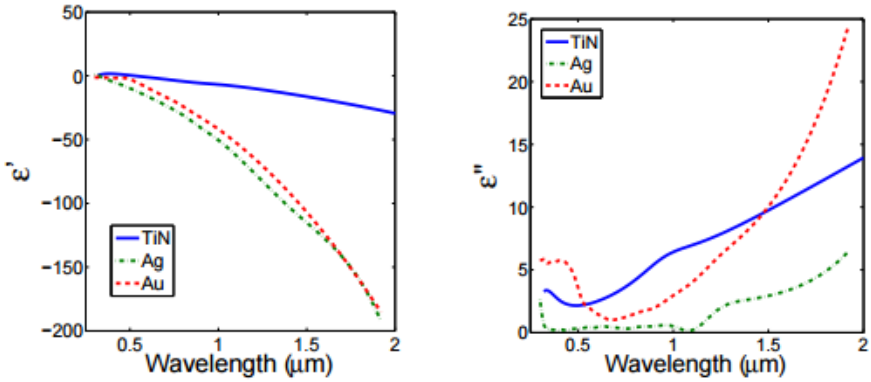

Fig. 4.9 Comparison done on the dielectric function of plasmonic metamaterial TiN with conventional metals [14-15]

The imaginary part of Titanium Nitride (TiN), is comparable to the conventional metals. Thus this proves that plasmonic metamaterial is an excellent candidate to replace conventional metals such as Gold (Aurum) or Silver (Argentum).

4.4.1.2 High Loss of Noble Metals

In [9,16], noble metals had been shown to have substantial carrier concentrations, which in turns makes their plasma frequencies very large [14]. A large plasma frequency produces a large imaginary permittivity which translates to a significant loss. Plasmonic metamaterial, however, has lower carrier concentrations hence smaller losses.

Experimentally, losses result in [9,16] of the alternatives plasmonic metamaterials of oxides and nitrides compared to Gold (Aurum) or Silver (Argentum) shown that the imaginary part of the plasmonic metamaterial of oxides (transparent conducting oxides) are found smaller compared to the noble metals.

4.4.2 Methodology

Again, a dipole antenna similar to [1] was simulated using CST. The dipole antenna operating at 0.95 THz – 1 THz had been modelled in CST as two electrodes separated by a small gap, driven by a discrete face port between the two electrodes. The substrate dimension used in both photoconductive antennas is set to 150 µm in length x 150 µm in width and 150 µm in thickness. The gap is set to 10 µm. The thickness of the substrate is also set to 15 µm as this is the optimum dimensions that were simulated earlier in Chapter 3. The substrate used is GaAs while the electrodes material used are graphene, Gold (Aurum), Silver (Argentum) and Titanium Nitride (TiN). Defined in CST's material library, Gold has an electric conductivity of 6.3012 x 10^7 S/m, while Silver has an electric conductivity of 4.561 x 10^7 S/m. These simulations were repeated for three times, and the result is shown in Fig. 4.10.

4.4.2.2 The Simulation Results

Fig. 4.10 shows the radiated power of the dipole antenna using an electrode made from noble metals and metamaterial. As expected, graphene performed better than gold and silver due to its material properties such as higher carrier mobility. Titanium nitride (TiN), performed second after Graphene. This confirms the experimental results in [10-11] that the noble metal losses found to be higher compared to metamaterial. These simulation results agree with the experimental done in [10-11]. Thus, this finding will be beneficial for design purposes. The radiation patterns of these simulations are shown in Fig. 4.11 for the graphene electrode, Fig. 4.12 for the gold electrode, Fig. 4.12 for the silver electrode and Fig. 4.13 for the TiN electrode. The radiation pattern of an electrode using noble metals becomes asymmetrical. This radiation pattern enhanced towards the substrate. Hence, this might explain the lower radiated power using noble metals as the power can be trapped in the substrate.

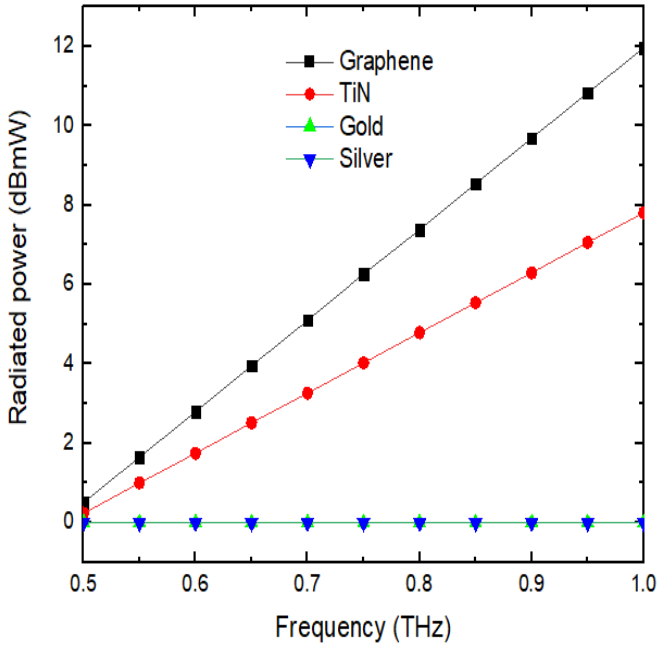

Fig. 4.10 The radiated power of dipole antenna using an electrode made from noble metals and metamaterial

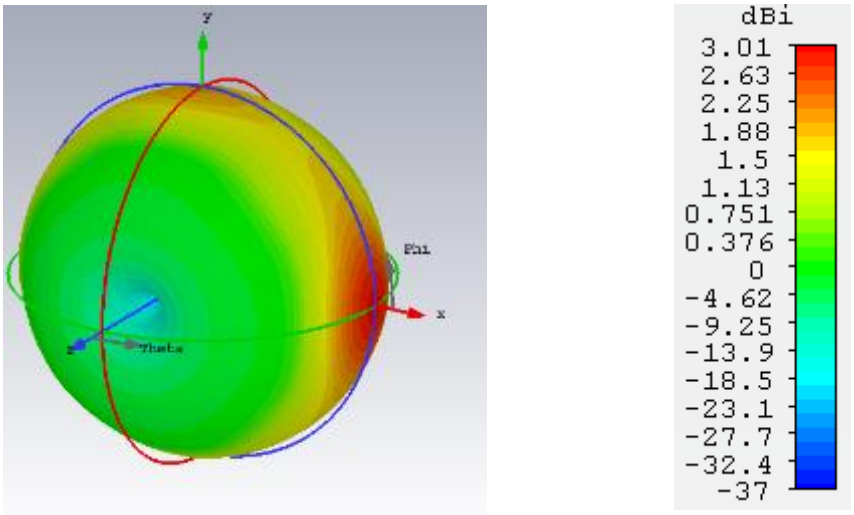

Fig. 4.11 The 3D pattern of the farfield of dipole antenna using graphene as an electrode is shown in dBi

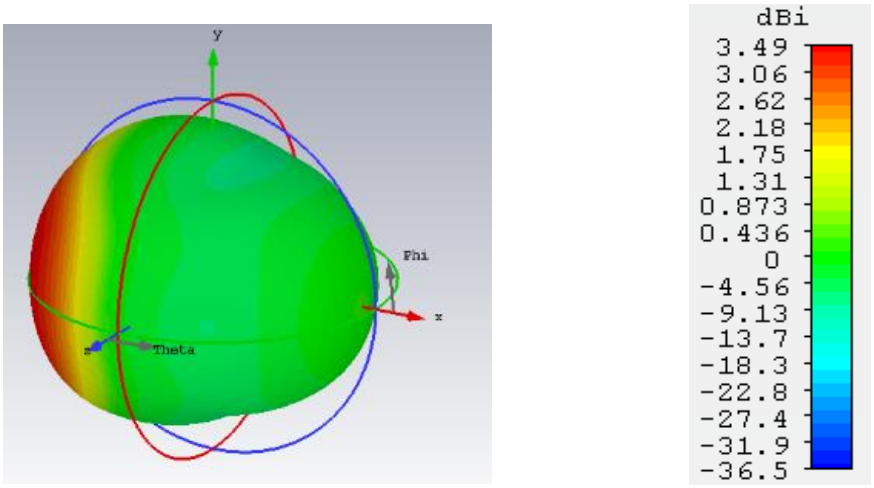

Fig. 4.12 The 3D pattern of the farfield of dipole antenna using gold as an electrode is shown in dBi

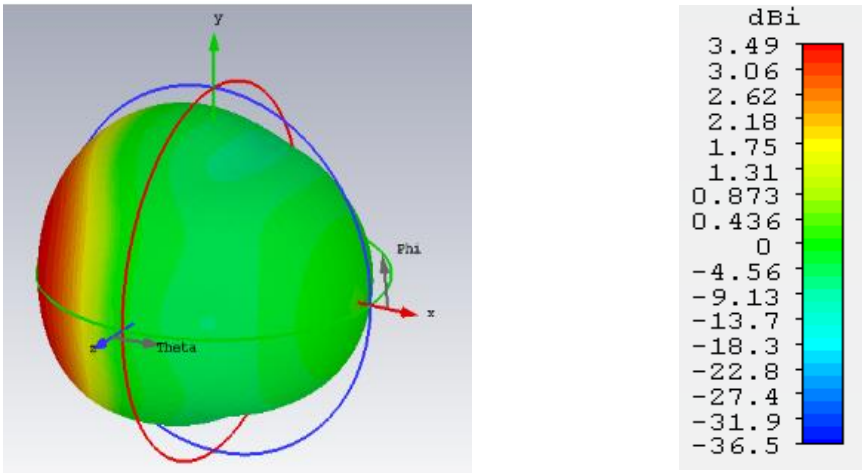

Fig. 4.13 The 3D pattern of the farfield of dipole antenna using silver as an electrode is shown in dBi

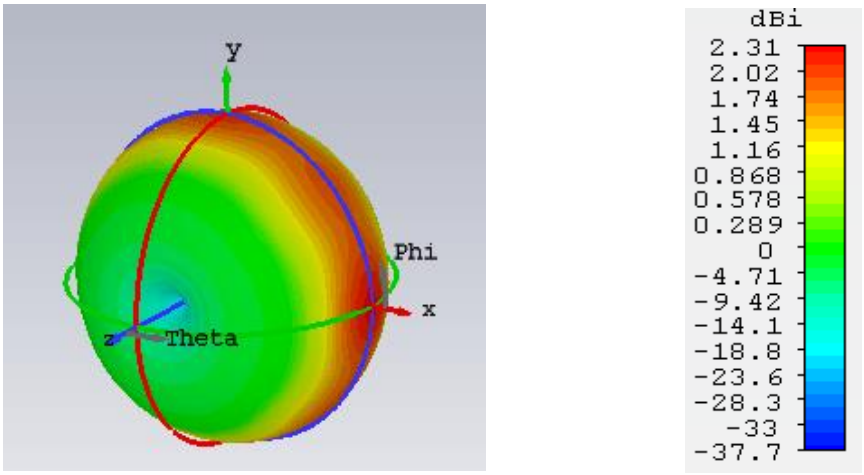

Fig. 4.14 The 3D pattern of the farfield of dipole antenna using TiN as an electrode is shown in dBi

4.6 Summary

This chapter focuses on electrode structure and electrode material study. The study of the radiated power of a dipole antenna using embedded electrode compared to the dipole antenna using standard electrode is not very encouraging. Another simulation tool needs to be used instead of CST. This semiconductor physics equation should be combined with Maxwell's equations in order to obtain the accurate results of the expected radiated power of the THz photoconductive antenna.

The study of the radiated power of a dipole antenna using noble materials such as gold (Aurum) and silver (Argentum) with graphene and Titanium Nitride (TiN) proves that graphene performed better than gold and silver due to its material properties such as higher carrier mobility as in [21]. Besides higher losses in noble materials compared to metamaterial, they also cannot be tuned. Tunability can be either static or dynamic depending. Graphene, another material that has a unique band structure and high carrier mobility had been found to enable excitation of surface plasmons [10-11, 20]. Graphene is a two-dimensional material, thus described by its surface conductivity, σ. Surface conductivity, σ can be controlled by applied bias voltage [17-18]. Thus, surface conductivity and σ can be exploited to create reconfigurable devices. However, due to the limitation of CST, this cannot be proven in the electrode material study.

References

[1] Y. Huang, N. Khiabani, Y. Shen, and D. Li, "Terahertz photoconductive antenna efficiency," *Proceeding of the iWAT 2011*, pp. 152-156, Hong Kong, 2011.

[2] Y. Huang, N. Khiabani, Y. Shen, and D. Li, "A further study of THz photoconductive antennas", *Antennas and Propagation Society International Symposium (APSURSI)*, 2012.

[3] N. Khiabani, Y. Huang, L. E Garcia-Munoz, Y. Shen, A. Rivera-Lavado, "A novel sub-THz photomixer with nano-trapezoidal electrodes," *Terahertz Science and Technology*, IEEE Transactions on, vol.4, no.4, pp.501-508, July 2014.

[4] R. F. Pierret, *Advanced semiconductor fundamentals*. Reading, Mass Addison-Wesley Pub. Co.1987.

[5] Y. Shang-Hua; M. R. Hashemi, C.W. Berry, M. Jarrahi, "7.5% Optical-to-Terahertz conversion efficiency offered by photoconductive emitters with three-dimensional plasmonic contact electrodes, "*Terahertz Science and Technology*, IEEE Transactions, vol.4, no.5, pp.575-581, Sept. 2014.

[6] H. Tanoto, J. H. Teng, Q. Y. Wu, M. Sun, Z. N. Chen, S. A. Maier, B. Wang, C. C. Chum, G. Y. Si, A. J. Danner and S. J. Chua, "Greatly enhanced continuous-wave terahertz emission by nano-electrodes in a photoconductive photomixer" *Nature Photonics*, vol. 6, pp 121-126, 2012.

[7] I. S. Gregory, C. Baker, W. R. Tribe, I.V. Bradley, M. J. Evans, E. H. Linfield, G. Davies, M. Missous, "Optimization of photomixers and antennas for continuous-wave terahertz emission," *Quantum Electronics*, IEEE Journal of, vol.41, no.5, pp.717-728, May 2005.

[8] C. W. Berry, M. R. Hashemi, M. Unlu, and M. Jarrahi, "*Significant radiation enhancement in photoconductive terahertz emitters by incorporating plasmonic contact electrodes*", Electrical Engineering and Computer Science Department, University of Michigan Ann Arbor, MI 48109, United States.

[9] A. Boltasseva, H. A. Atwater, "*Low-loss plasmonic metamaterials*", School of Electrical & Computer Engineering and Birck Nanotechnology Center, Purdue University, Indiana, West Lafayette, IN 47907, USA.

[10] G. V. Naik and A. Boltasseva, "A comparative study of semiconductor-based plasmonic metamaterials", *Metamaterials 5*, vol.1, pp. 1–7, 2011.

[11] P. R. West, S. Ishii, G.V. Naik, N. K. Emani, V. M. Shalaev and A. Boltasseva, "Searching for better plasmonic materials", *Laser & Photon*. Rev., 4: pp.795–808, 2010.

[12] H. Raether, "*Surface plasmons on smooth and rough surfaces and on gratings*", 1st ed., Berlin: Springer, 1998.

[13] W. L. Barnes, "Surface plasmon-polarition length scales: a route to sub-wavelength optics, J. *Opt. A: Pure Appl*. Opt. 8 pp.87- 93, 2006

[14] G. V. Naik, J. Kim, and A. Boltasseva, Oxides and nitrides as alternative plasmonic materials in the optical range, *Opt. Mater. Express* 1(6),pp.1090-1099, 2011.

[15] G. V. Naik, J. L. Schroeder, N. Xingjie, A. V. Kildishev, T. D. Sands, and A. Boltasseva, "Titanium nitride as a plasmonic material for visible and near-infrared wavelengths," *Opt. Mater*. Express 2, pp.478-489, 2012.

[16] G.V. Naik, J. Kim, and A. Boltasseva, "Plasmonic and metamaterials: looking beyond gold and silver," Metamaterials 2012: *The Sixth International Congress on Advanced Electromagnetic Materials in Microwaves and Optics*, 2012.

[17] M. Dragoman, A. A. Muller, D. Dragoman, F. Coccetti, and R. Plana, “Terahertz antenna based on graphene”, *Journal of Applied Physics*, pp. 107-109, 2010.

[18] J. M. Tamagnone, J. S. Gomez Diaz, J. R. Mosig, and J. Perruisseau-Carrier, “Analysis and design of terahertz antennas based on plasmonic resonant graphene sheets”, *Journal of Applied Physics*, pp.112, 2012.

[19] Sigma-Aldrich Corporation, Available: https://www.sigmaaldrich.com/

[20] P. Tassin, T. Koschny, and C. M. Soukoulis, “Graphene for Terahertz applications”, *Science*, vol. 341, pp. 620-621, 2013.

[21] A. Abu Bakar Sajak, Y. Shen, Y. Huang, and R. Alrawashdeh, “An investigation on THz antennas using graphene as a substrate”, *The 8th European Conference on Antennas and Propagation*, The Hague, The Netherlands, April, 2014.

Chapter 5 Analysis of a Photoconductive Antenna using COMSOL

5.1 Introduction

Fig. 5.1 and 5.2 show the schematic diagram of the photoconductive antenna structures and their corresponding dimensions of the conventional and the proposed photoconductive antenna, respectively. The proposed photoconductive antenna:

- Has an embedded electrode in the substrate material
- Was fed with both voltage bias and optical pump in the simulation works
- Were shown to withstand higher bias voltage than conventional photoconductive antenna hence higher THz radiation power

For simplicity, LT-GaAs was chosen as the substrate material while Gold was used as the electrode material in all simulation works. The simulated electric field values were plotted using the coordinates as defined in Figure 5.2.

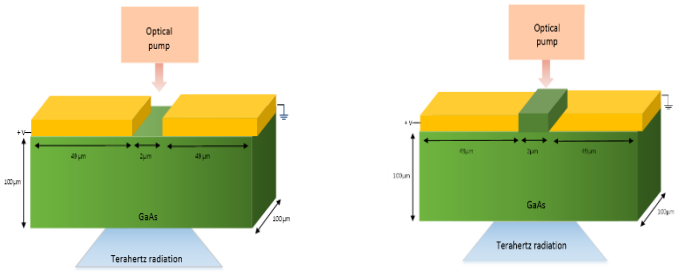

(a) (b)

Fig. 5.1 The structure of a (a) conventional model photoconductive antenna. (b) proposed model photoconductive antenna.

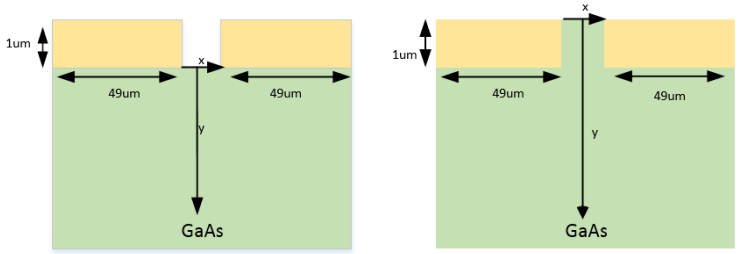

(a) (b)

Fig. 5.2 Schematic diagram of the structure of a photoconductive antenna (a) conventional model (b) proposed model and the coordinate of the simulated electric field

A commercial finite-difference time-domain (FDTD) simulation software package COMSOL version 5.2 was used in all simulation work. Unlike microwave antennas, photoconductive antennas are fed with two different sources namely the dc voltage bias and the optical pump. After defining the respective geometries as summarised in Table 5.1, the AC/DC module in the COMSOL Multiphysics was used to calculate the electric field distribution inside the photoconductive device when voltage biases were applied to the electrode. The optical pumps were modelled using the Electromagnetic Waves, Frequency Domain interface in order to calculate the density distribution of the photo-generated carriers produced by the pump laser.

Table 5.1 Parameters for Comsol Simulation

Parameter	Value
Substrate dimension (height x width x depth)	100 μm x 100 μm x 100 μm
Antenna gap	2 μm
Voltage biases	0 V - 4 V
Optical power pumps	1.4 mW - 10 mW
LT-GaAs Relative permittivity (Ɛr) [5-6]	12.9
Gold Relative permittivity (Ɛr) [5-6]	6.9
Wavelength (λ)	780 nm
Electrode thickness	0.1 μm - 1 μm

5.2 Simulation Method

Using the AC/DC module in COMSOL Multiphysics, the electric field of both the convention and the proposed antennas is simulated at the wavelength and laser power as shown in Table 5.1. Fig. 5.3a and b show the electric field map calculated at a voltage bias of 4 V for a conventional and the proposed antenna, respectively. The electric field is at the strongest at the sharp edges between the antenna gap. Note that the breakdown electric field of GaAs is 4 x 10^7 V/m while the breakdown electric field of air is 3 x 10^6 V/m; hence the chosen voltage bias of 4 V will not exceed the breakdown electric field of air in the conventional model.

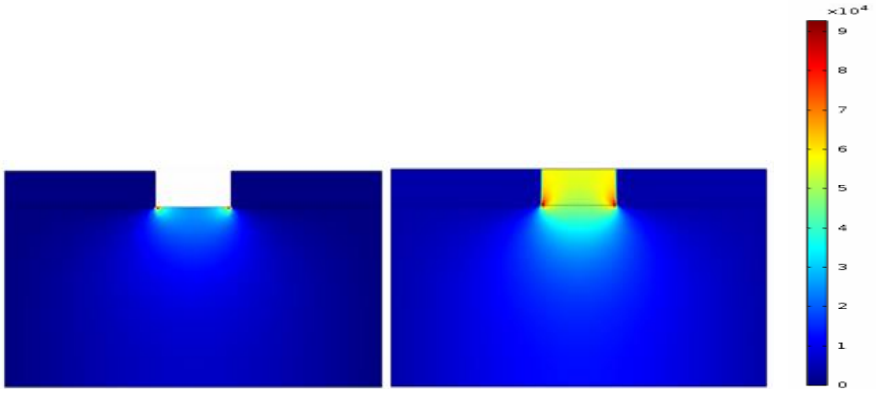

Fig. 5.3 Electric Field of (a) conventional (b) proposed THz photoconductive antenna at given voltage bias at 4 V

5.3 Simulation Results

5.3.1 Electrode Thickness

Fig. 5.4 shows the electric field distribution along the depth direction in the antenna substrate. The electric field calculated at the centre of the antenna gap of both the conventional and proposed photoconductive antenna is plotted against the depth of the substrate, starting from the substrate surface as indicated in Fig. 5.2. It is found that electrode thickness of the proposed antenna plays a role; higher electric field over larger depth is observed for a thicker electrode of the proposed antenna. In contrast, no change of the electric field can be observed when the electrode thicknesses of the conventional antenna are changed.

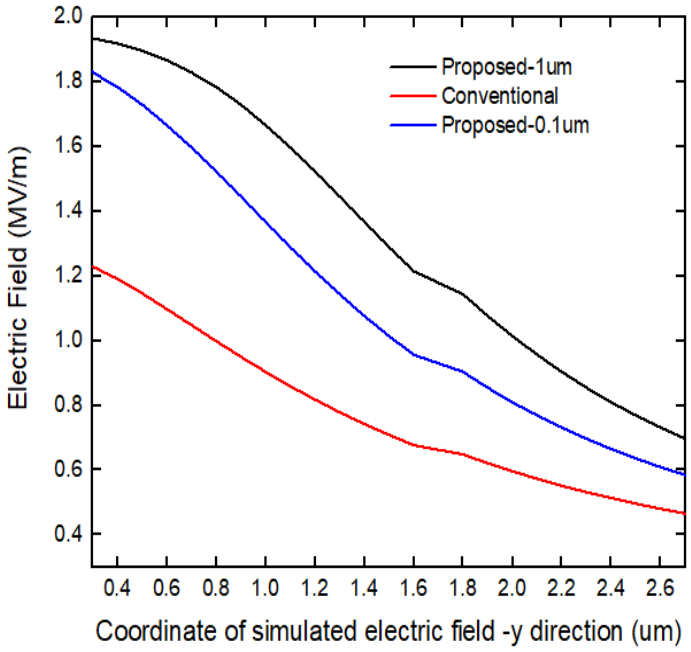

Fig. 5.4 Electric Field of the proposed photoconductor and the conventional photoconductor at 4V voltage bias

Fig. 5.5 shows the electric field across the gap of the proposed photoconductive antenna at the surface of the electrode and at a depth of 1 μm electrode where the electric field of the proposed model are at the highest. The electric field of a conventional photoconductive antenna is also shown in Fig. 5.4. As expected, the electric field near the two electrodes is largest; suggesting that the largest THz power could be expected when focusing pump laser near the edge of the electrodes.

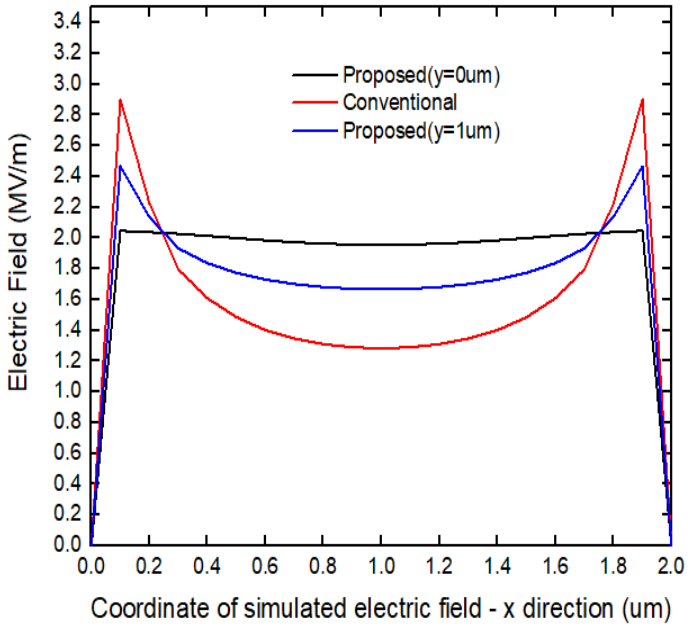

Fig. 5.5 Electric Field of the proposed photoconductor of 1 μm electrode thickness and the conventional photoconductor at 4 V voltage bias

The simulated electric field can be converted to the electric energy density which is given by,

$$E_1 = 0.5\,|E|^2\,\varepsilon_0 \tag{5.1}$$

Where E = electric field, ε_0 = constant dielectric permittivity.

As the electric field is higher in the proposed photoconductive antenna as compared to the conventional photoconductive antenna, the electric energy density should be higher too. This stored static electric power could be potentially converted into THz radiation power when the antenna device is excited with, for example, short laser pulses from a femtosecond laser.

Not all stored electric power could be converted in to THz radiation power since most of the photo-generated carriers are near the surface of the LT-GaAs. Fig. 5.3a and Fig 5.3b show the electric field of the proposed model simulated in COMSOL at voltage bias of 4 V and laser pump of 10 mW, respectively. The total *effective* energy stored in the conventional and

proposed antenna can then be calculated in COMSOL Multiphysics using the following equation:

$$\iiint (0.5\ |E_1|^2\ \varepsilon_0)\ x\ \ |E_2|^2\ dv \tag{5.2}$$

Where E_1 = electric field from Fig. 5.6a, E_2 = electric field from Fig. 5.6b and ε_0 = constant dielectric permittivity. Note that $|E_2|^2$ is proportional to the density of the photo-generated carriers. As shown in Fig. 5.7, the total effective energy conserved in the proposed antenna was found to be almost double than that of the conventional model. The equation is inspired by the fact that the total electric current (**I**) can be related to the current density (**J**) by integrating the current density over the area where a charge is flowing**,** which in this case is the proposed model. Also, the current density can be related to the electric field with its electric conductivity. Since LT-GaAs has non-zero conductivity, this electric field will produce a current. Experimental results of this proposed antenna can prove these equations.

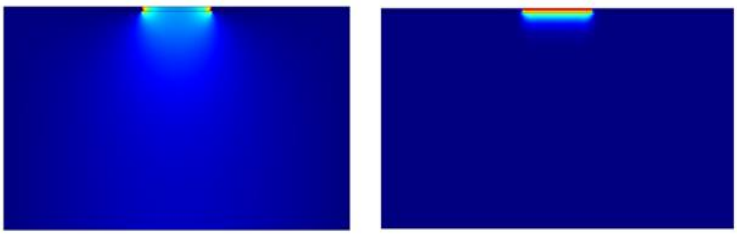

(a) (b)

Fig. 5.6 Electric field of proposed THz photoconductive antenna with 0.1 um electrode thickness from (a) electric current module (b) electromagnetic module simulated in COMSOL Multiphysics

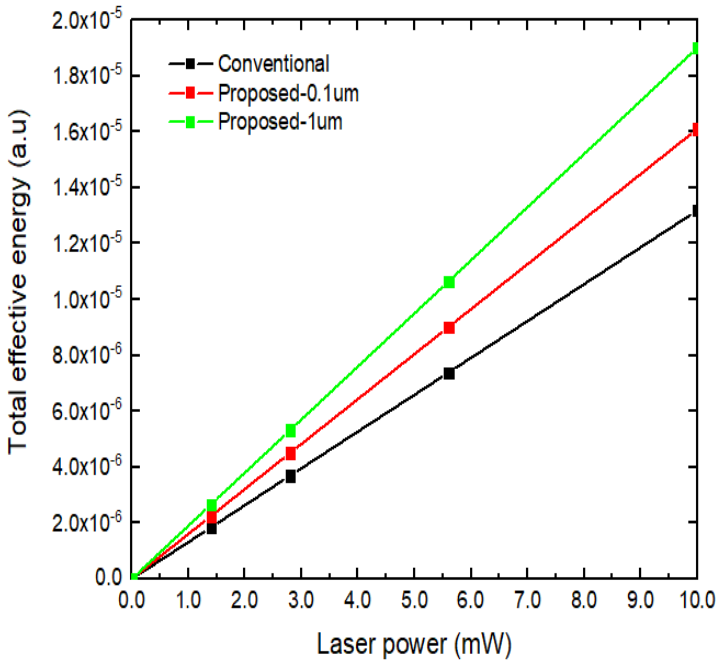

Fig. 5.7 Total effective energy of the conventional photoconductor vs proposed photoconductor at 4V voltage bias and various laser power

5.3.2 Substrate Mobility

Fig. 5.8 shows the simulated current across the gap of the proposed photoconductive antenna at the surface of the electrode until the depth of 0.5 μm where the voltage biases are varying from 1 V to 10 V. The optical pump is given at 1 nW. The substrate used is LT-GaAs that has the hole mobility of 400 cm^2/Vs and electron mobility of 8500 cm^2/Vs. The bandgap of LT-GaAs is 1.424 V. The current is proportional to the voltages. The linear relationship is expected and theoretically proven.

Fig. 5.8 also shows the simulated current across the gap of the proposed photoconductive antenna at the surface of the electrode until the depth of 0.5μm where the voltage biases are varying from 1 V to 10 V. The optical pump is also given at 1 nW. The substrate used is LT-GaAs that has the hole mobility of 200 cm^2/Vs and electron mobility of 4500 cm^2/Vs. The bandgap of LT-GaAs is fixed at 1.424 V. The value of the current is still proportional to the voltages, but it is now reduced.

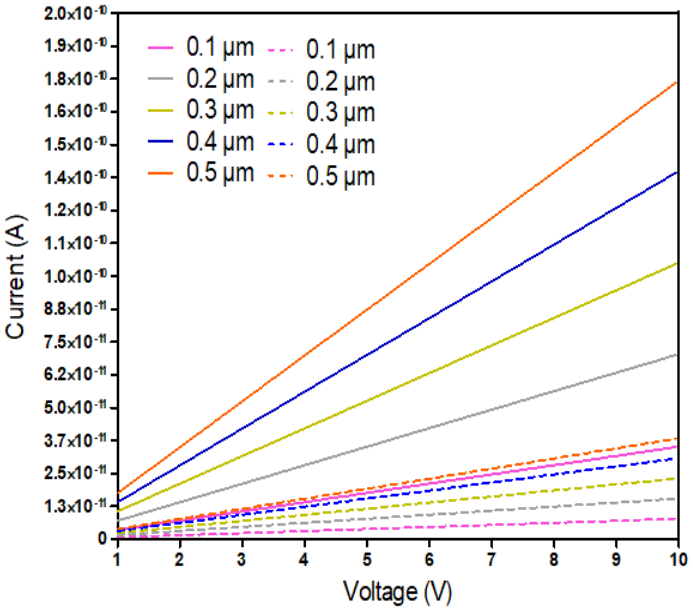

Fig. 5.8 Current density of the proposed model at different depth using GaAs as the substrate using its actual carrier mobility of 8500 cm^2/Vs – straight line and half of the carrier mobility of 4500 cm^2/Vs - dashed line

Fig. 5.9a and b show the total current density plot of the proposed model at 1 µm depth using LT-GaAs as the substrate using at half of its carrier mobility of 4500 cm^2/Vs and LT-GaAs actual carrier mobility of 8500 cm^2/Vs. Due to the limitation of COMSOL Multiphysics, the electrode thickness which is made of gold (Aurum) is modelled as a straight line and assigned as a conductor. The voltage bias given is 4V. The optical pump given is at 1nW. The bandgap of LT-GaAs is fixed at 1.424 V. The current density plot of a photoconductive antenna using LT-GaAs as a substrate at its actual carrier mobility at 8500 cm^2/Vs has higher value based on the colour scale plot indication.

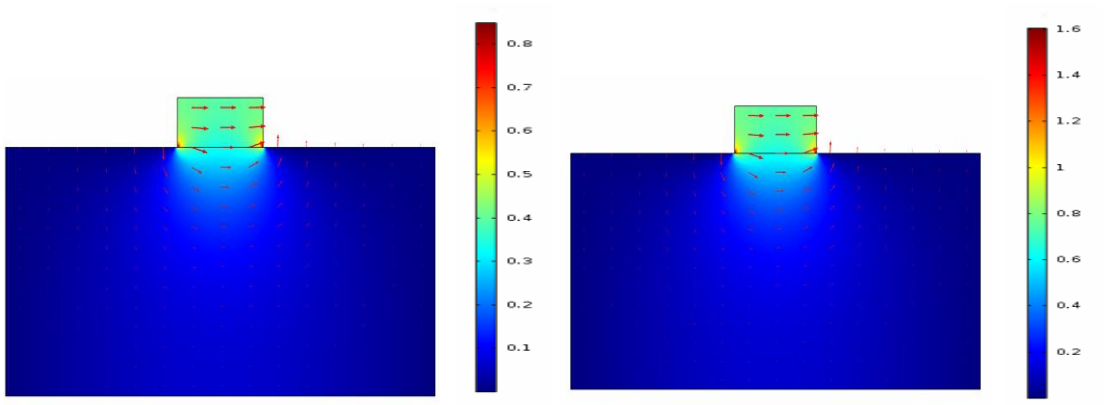

(a) (b)

Fig. 5.9 Total current density plot of the proposed model at 1 µm depth using GaAs as the substrate using (a) half of its carrier mobility of 4500 cm^2/Vs and (b) actual carrier mobility of 8500 cm^2/Vs at 4V.

Fig. 5.10 shows the comparison of the simulated current across the gap of the proposed photoconductive antenna at different mobility.

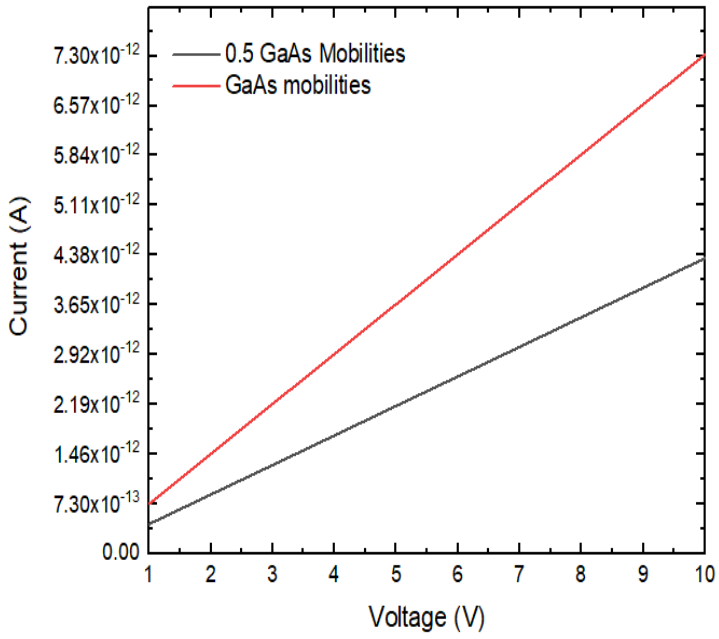

Fig. 5.10 The integration of the current density across the cross-sectional area of the proposed model simulated at different carrier mobilities

The sum of the current in the proposed model at lower mobility is half of the sum of the current at the actual mobility of LT-GaAs. This proves that the mobility of a substrate material plays a crucial role in determining the current generated by the photoconductive antenna. The results agree with the findings previously in [1-3].

5.3.3 Antenna Gap

Fig. 5.11 shows the electric field distribution along the depth direction in the antenna substrate. Again, the electric field calculated at the centre of the antenna gap of both the conventional and proposed photoconductive antenna is plotted against the depth of the substrate, starting from the substrate surface as indicated in Fig. 5.2. However, the antenna gap is now changed to 2 µm and 4 µm. Theoretically, the electric field is indirectly proportional to the gap of the antenna. It is found that the proposed antenna with larger antenna gap has lower electric field compared to the proposed antenna with 2 µm antenna gap. Hence, the results agree with the theory.

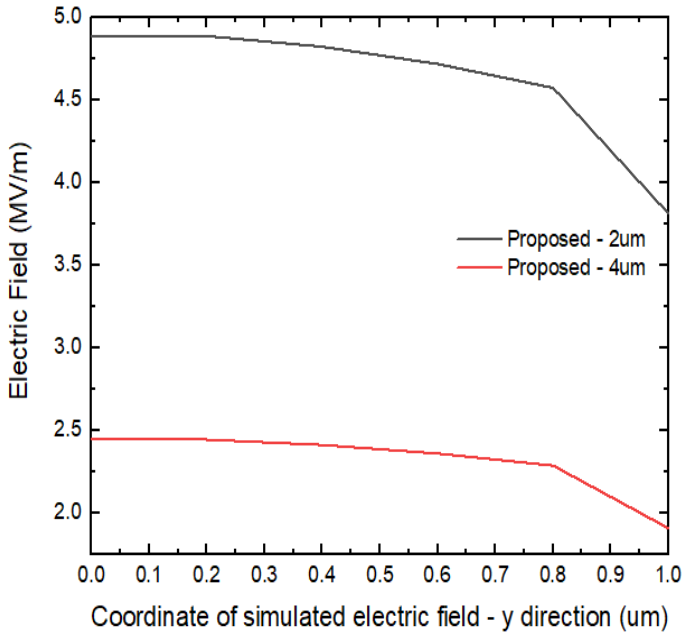

Fig. 5.11 Electric Field of the proposed photoconductor with 4 µm and 2 µm antenna gap at 4 V voltage bias

5.3.4 Substrate Thickness

Fig. 5.12 shows the electric field calculated at the centre of the antenna gap of the proposed photoconductive antenna is plotted against the depth of the substrate, starting from the substrate surface as indicated in Fig. 5.2. The substrate thicknesses of the proposed antenna are changing from 100 µm, 90 µm and 80 µm. No change of the electric field can be observed when the substrate thicknesses of the proposed antenna are changed. These simulations results are expected as most of the photo-generated carriers are near the surface hence the substrate thicknesses does not contribute to any changes in the number of photo-carriers.

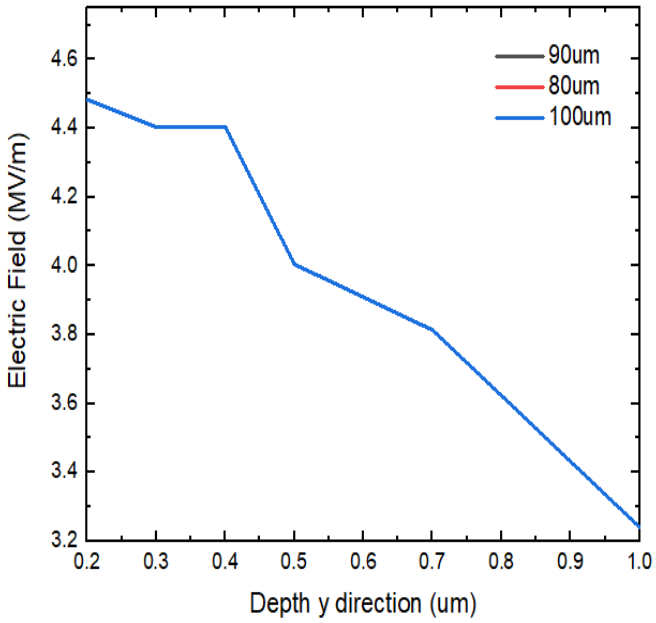

Fig. 5.12 Electric Field of the proposed photoconductor with 100 µm, 90 µm and 80 µm substrate thickness at 4V voltage bias

5.3.5 Material Comparison

Indium Phosphide (InP) is a semiconductor that has a direct bandgap [4] which is similar to Gallium Arsenide (GaAs). Hence, InP is chosen to be as a substrate replacing GaAs for the proposed model. Fig. 5.13 shows the simulated current across the gap of the proposed photoconductive antenna at the surface of the electrode until the depth of 0.5 µm where the voltage biases are varied from 1 V to 10 V. The substrate used is InP that has the hole mobility of 200 cm^2/Vs and electron mobility of 5400 cm^2/Vs. The bandgap of InP is 1.344 V. At these

thicknesses, the current simulated in the proposed model using InP as a substrate material is almost four times higher more value than the proposed model using GaAs as a substrate material in Fig. 5.8.

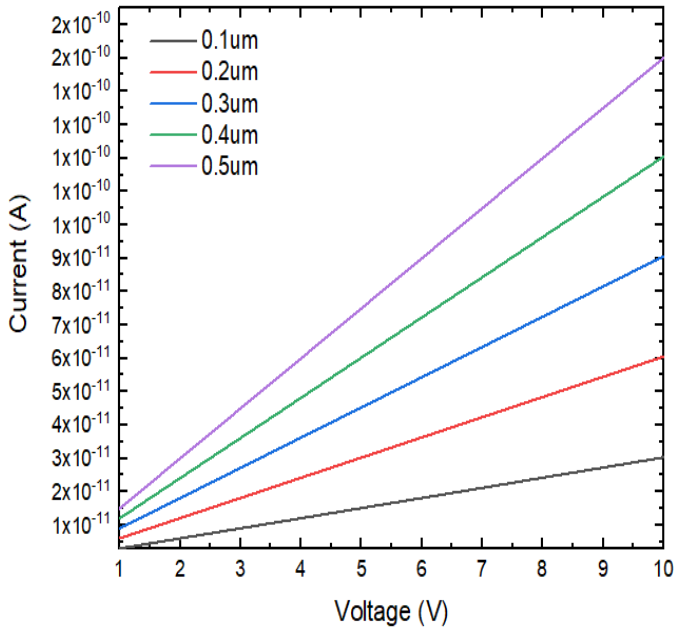

Fig. 5.13 Current density of the proposed model at different depth using InP as the substrate

Fig. 5.14 shows the comparison of the total simulated current across the gap of the proposed photoconductive antenna at different materials. The sum of the current in the proposed model using InP as a substrate material is almost four more times higher than the sum of the current in the proposed model using LT-GaAs as a substrate material. This proves that both the mobility of a substrate and the bandgap are amongst the factor in determining the potential current of the proposed antenna.

Fig. 5.15a and b show the total current density plot of the proposed model at 1 µm depth using LT-GaAs and InP. Due to the limitation of COMSOL Multiphysics, the electrode thickness which is made of gold (Aurum) is modelled as a straight line and assigned as a conductor. The voltage bias given is 4V. The optical pump given is at 1nW. The bandgap of LT-GaAs is fixed

at 1.424 V, and the bandgap of InP is 1.344 V. The current density plot of a photoconductive antenna using InP as a substrate has higher value based on the colour scale plot indication.

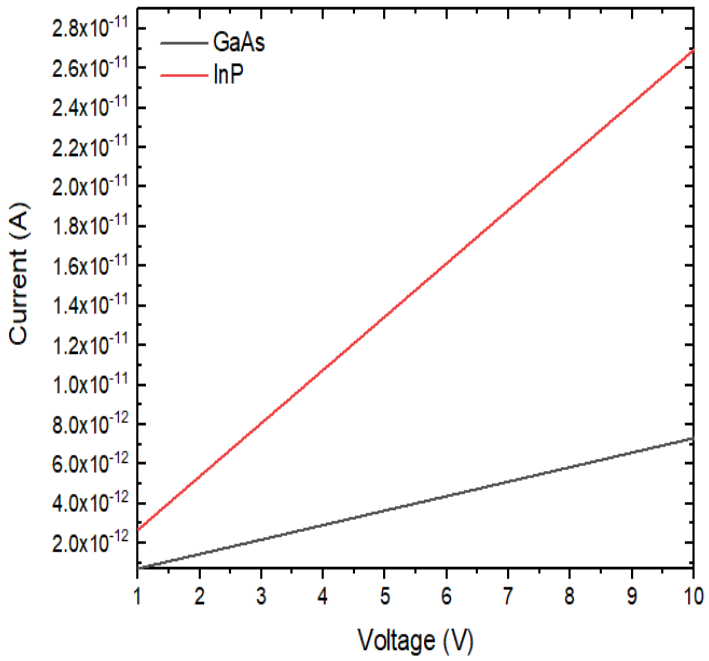

Fig. 5.14 Comparison of the integration of the current density across the cross-sectional area of the proposed model simulated at different materials

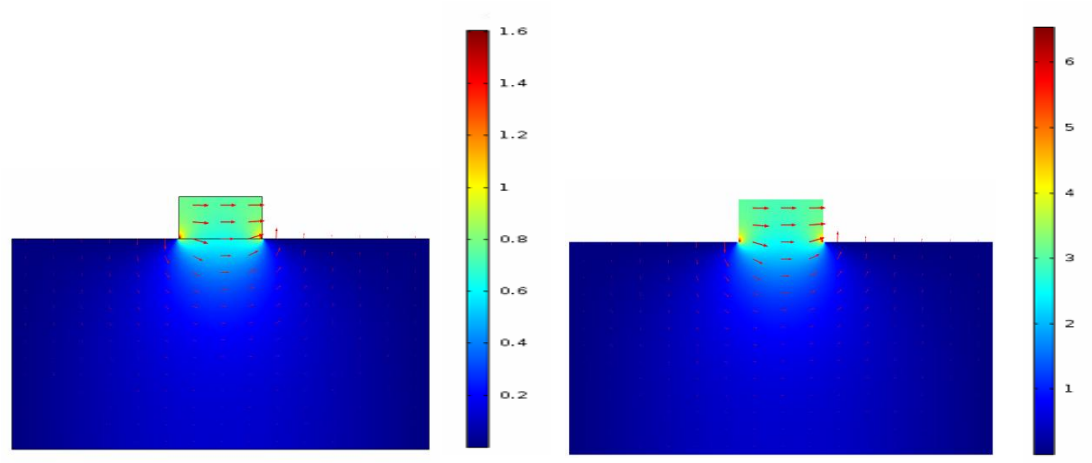

(a) (b)

Fig. 5.15 Total current density plot of the proposed model at 1 µm using (a) GaAs as the substrate (b) InP as a substrate at 4V.

5.4 Summary

Numerical simulations using COMSOL Multiphysics indicate that the proposed THz antenna structure can store two times more effective electric energy than the conventional model. This suggests that by using this embedded model, the expected THz power could also potentially be doubled. Furthermore, in the conventional photoconductive devices, the highest electric field is at the surface of GaAs thus the highest bias voltage that could be applied will be determined by the breakdown electric field of air which is 2×10^6 V/m. In the proposed device, the highest electric field is found to be within the GaAs substrate which has a much high breakdown electric field of is 4×10^7 V/m. Therefore, for the same gap width of the electrodes, the proposed device would withstand a higher bias voltage than the conventional ones. This would lead to even higher THz radiation power for the proposed device as the radiated THz power is expected to increase with the applied bias voltage. This is the achievement of this thesis, where the proposed model had been proven numerically to be better than the conventional model. In Chapter 4, using CST, a dipole antenna embedded in GaAs as substrate material had been simulated and compared with a conventional dipole antenna. The results, however, are not encouraging. Using COMSOL Multiphysics, by focusing on the electric field of the proposed model, the advantage of the proposed model had been proven.

Carrier mobility of material had also been identified as a factor that can increase the current in the proposed antenna. Based on the simulation results, the current with double carrier mobility produces twice the sum of current compared to the proposed model with half of the carrier mobility. This high photo carrier density results to high time-varying transient photocurrent that can lead to high THz power.

Substrate thicknesses do not have any impact on the electric field of the proposed antenna simulated. Antenna gap, however, does have an impact on the electric field computed hence proposed antenna with a smaller gap is advisable to achieve higher THz current as smaller antenna gap is proven to compute higher current. In the previous work in Chapter 3, however, substrate thickness had been proven to have an impact on the radiated power and the efficiency

of THz photoconductive antenna. The antenna was fed with a discrete port, due to the limitation of CST. Hence, the results might not be accurate. In COMSOL, the fed of a THz photoconductive antenna is emulated with both voltage bias and optical pump.

To achieve the wavelength of 780nm, the bandgap of the material chosen as substrate material should be in the range of 1.3 V-1.4 V. As bandgap energy of a material is fixed, Indium Phosphide (InP) is chosen as an alternative substrate material to LT-GaAs in order to investigate the current's result once the proposed model substrate material is changed to LT-GaAs. The bandgap energy of InP is lower than LT-GaAs bandgap energy [5-7]. The photocurrent simulated is found to be almost four times higher than the original proposed model using LT-GaAs. Hence, as a conclusion, the electrode thickness and material mobility are among the most crucial factor in determining the current of the proposed model.

References

[1] A. Abu Bakar Sajak, Y. Shen, Y. Huang, and R. Alrawashdeh, "A Comparison of the Effect of Substrate on the Performance of THz Antenna", *Proceeding of the ICE2T*, Malaysia, August 2014.

[2] A. Abu Bakar Sajak, Y. Shen, Y. Huang, and R. Alrawashdeh, "An Investigation on THz Antennas Using Graphene as a Substrate", *The 8th European Conference on Antennas and Propagation*, The Hague, The Netherlands, April 2014.

[3] N. Khiabani, "Modelling, design and characterisation of Terahertz photoconductive antenna". PhD thesis, University of Liverpool, 2013.

[4] A. Abu Bakar Sajak, Y. Shen and Y. Huang "Analysis of a Photoconductive Antenna using COMSOL", *10th UK-Europe-China Workshop on Milimetre Waves and Terahertz Technologies (UCMMT)*, Liverpool, UK, September 2017.

[5] R. L. David, *Handbook of Chemistry and Physics*, 87th ed., CRC Press, pp. 4–61,.1998

[6] S. Adachi, *Physical properties of III-V semiconductor compounds InP, InAs, GaAs, GaP, InGaAs and InGaAsP*, Wiley, New York, 1992

[7] G. Carpintero, et al., *Semiconductor Terahertz Technology: Devices and Systems at Room Temperature Operation*, John Wiley & Sons, Incorporated, 2015.

Chapter 6 Conclusions and Future Work

6.1 Conclusions

THz photoconductive antenna consists of two metal usually gold electrodes on a photoconductive substrate. Substrate effect in THz plays an important role compared to substrate effect in microwave frequency. Chapter 3 investigated the impact of substrate dimensions and substrate material on the performance of THz photoconductive antenna. The investigations were done using CST simulation. At 1 THz, the efficiency and the radiated power are the highest for a substrate thickness with the minimum size which is at 15 µm. Hence, the dimensions of 150 µm x 150 µm x 15 µm had been used for as substrate dimensions for any further study on a substrate material. Graphene, a promising material to be used as a substrate for THz antennas had been found to radiate 33% more power than the THz antenna using GaAs as a substrate at 0.5 THz – 0.7 THz.

In Chapter 4, the investigation centres on electrode structure and electrode material study. The study of the radiated power of a dipole antenna using embedded electrode compared to the dipole antenna using standard electrode is not very encouraging. Due to the limitations of the CST Microwave Studio software wherein the student edition, only 30 000 mesh cells can be simulated; another potential software needs to be reconsidered to prove the theory discussed more accurately. This limitation also only allows a narrow frequency range. This semiconductor physics equation should be combined with Maxwell's equations in order to obtain the accurate results of the expected radiated power of the THz photoconductive antenna. Also, the study of the radiated power of a dipole antenna using noble materials such as gold (Aurum) and silver

(Argentum) with graphene and Titanium Nitride (TiN) proves that graphene performed better than gold and silver due to its material properties such as higher carrier mobility.

In chapter 5, a novel photoconductive antenna with an embedded electrode structure, rather than the conventional planner electrode structures had been introduced. Electric field simulated using COMSOL Multiphysics proves that the proposed model performs better than the conventional model. The electric field calculated at the centre of the gap between two electrodes for both the conventional and the proposed photoconductive antenna is plotted against the depth of the substrate, starting from the substrate surface. A higher electric field over larger depth is observed for a thicker electrode of the proposed antenna. In contrast, no change of the electric field can be observed when the electrode thicknesses of the conventional antenna are changed. The new findings in Chapter 5, disputes the conclusions of Chapter 3, where in Chapter 3 substrate thickness had been proven to have an impact on the radiated power and the efficiency of THz photoconductive antenna. Due to the limitation of CST, the antenna was fed with a discrete port. Hence, the results earlier might not be accurate.

The simulated electric field can be converted to the electric energy density. This stored static electric power represents the maximum electric power that could potentially be converted into THz radiation when the antenna device is excited with, for example, short laser pulses from a femtosecond laser. The total *effective* energy stored in the conventional and proposed antenna had then be calculated in COMSOL Multiphysics using the novel equation and the total effective energy stored in the proposed antenna was found to be almost double than that in the conventional antenna. The equation is inspired by the fact that the total electric current (**I**) can be related to the current density (**J**) by integrating the current density over the area where a charge is flowing, which in this case is the proposed model. Also, the current density can be related to the electric field with its electric conductivity. Since LT-GaAs has non-zero conductivity this electric field with produce a current. Experimental results of this proposed antenna can prove these equations.

Besides the electrode thickness, substrate mobilities and antenna gap are among the related parameters that had been identified and proven in this research to produce more photocurrent hence possibility of higher radiated THz power. The integration of the current density across the cross-sectional area in the proposed model at lower mobility is half of the integration of the current density across the cross-sectional area in the proposed model at the actual mobility of LT-GaAs. This proves that the mobility of a substrate material plays a crucial role in determining the current generated by the photoconductive antenna.

In conclusion, the proposed THz photoconductive antenna had been proven numerically to improve THz photocurrent compared to the conventional photoconductive.

6.2 Future Work

Photoconductive antennas (PCAs) are among the most popular devices used in THz radiation emission and detection of THz radiation. Compare to other THz emitter and detector, photoconductive antennas are compact, able to work in room temperature and they can work both as an emitter and detector. However, due to their low optical-to-THz conversion efficiencies, applications of these devices are limited. Extensive research had been done to understand and identify the improvement that can be done in order to rectify the low optical-to-THz conversion.

Using nanoplasmonic structures is very effective in improving the quantum efficiency of photoconductive THz devices. The reason for this fact originates from the unique capability of nanoplasmonic structures to enhance the absorption of incident laser pulses. Fabrication of such structures, however, is difficult and costly. Hence, the equation proposed in this research together with the simulation tool that combines both optoelectronic and electromagnetic simulations is the approach which should be adopted for THz antenna analysis in order to a predict the results of THz photocurrent and avoid any costly and unsuccessful experiment.

Though photoconductive antenna is basically consisting of simple electrode geometry such as bow tie and dipole, with the proof of concept of an embedded electrode using both the equation and simulation software, more robust and more complicated design can now be implemented and simulated before proceeding with the experimental work. Table 6.1 shows the suggested substrate dimensions, for THz Photoconductive Antenna based on the simulation done throughout the thesis. The findings on Chapter 5, disputes the conclusions of Chapter 3, where in Chapter 3 substrate thickness had been proven to have an impact on the radiated power and the efficiency of THz photoconductive antenna.

Semiconductor as the substrate material of terahertz photoconductive antenna is one of the main contributions of the THz radiation where high electron mobility is needed to obtain strong THz signals, high intrinsic resistivity and high breakdown voltage in order to support

applying high bias voltages. Many recent developments had been done on improving the characteristics of the substrate material. Though graphene had been shown to be a superior substrate material and electrode material using CST, the investigation in COMSOL focuses both on Gallium Arsenide (GaAs) and Indium Phosphide (InP) as potential substrate materials since graphene had been a challenge to be constructed into a structurally useful form on a three-dimensional level. Based on the simulation done throughout the thesis, Table 6.1 also shows the suggested substrate material for THz Photoconductive Antenna with antenna gap of 2 µm.

Table 6.1 Suggested parameters for THz Photoconductive Antenna

Substrate Material	Substrate Parameter (Length x Width x Thickness)	Electrode Structure
GaAs	100 µm x 100 µm x 100 µm	Embedded Electrode
InP	100 µm x 100 µm x 100 µm	Embedded Electrode

Appendix A E-field of THz Small and Large Gap Antennas

A.1. Small Gap THz Antennas

Hertzian dipole is an antenna with infinitesimal length *dl* (*dl*<<λ). Since the antenna length is very small, the current of the Hertzian antenna can be assumed to have a constant amplitude of I_{pc} with a constant phase; hence antenna is equivalent to a constant current source of $I_{pc}dl$. It is good to state that $I_{pc}dl=J_{pc}dV$, where J_{pc} is the current density and dV is the source volume. The Hertzian dipole antenna geometry is illustrated in Fig. A.1.

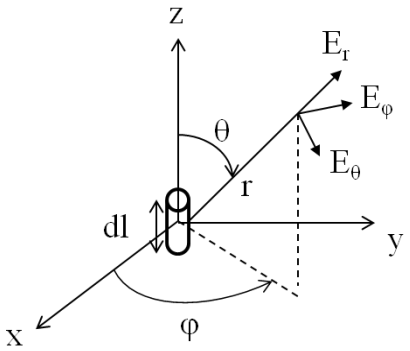

Fig. A.1 Geometry of a Hertzian dipole with its associated electric field components in the spherical coordinate

To derive the radiated electromagnetic fields using Maxwell's equations, first, the vector potential, A_z, needs to be calculated through equation (A.1) and then it is transformed to spherical coordinate as shown in equation (A.2) [1].

$$A_z = \frac{\mu I_{pc} dl}{4\pi r} e^{-jkr} \tag{A.1}$$

$$A_\theta = -A_z \sin\theta = -\frac{\mu I_{pc} dl}{4\pi r} e^{-jkr} \sin\theta \tag{A.2a}$$

$$A_r = A_z \cos\theta = \frac{\mu I_{pc} dl}{4\pi r} e^{-jkr} \cos\theta \tag{A.2b}$$

$$A_\varphi = 0 \tag{A.2c}$$

here μ is the permeability, $k = \frac{2\pi}{\lambda}$ is the wave number and r is the observation distance.

Considering the relations of electric and magnetic fields with the vector potential according to equation (A.3),

$$\vec{H} = \frac{1}{\mu} \nabla \times A \tag{A.3a}$$

$$\nabla \times \vec{E} = -j\omega\mu\vec{H} \tag{A.3b}$$

Electric, E, and magnetic, H, fields can be calculated as presented in (A.4):

$$H_\varphi = \frac{kI_{pc}dl}{4\pi r} \sin\theta \left[j + \frac{1}{kr} \right] e^{-jkr} \tag{A.4a}$$

$$E_\theta = \eta \frac{kI_{pc}dl}{4\pi r} \sin\theta \left[j + \frac{1}{kr} - \frac{j}{(kr)^2} \right] e^{-jkr} \tag{A.4b}$$

$$E_r = \eta \frac{kI_{pc}dl}{2\pi r^2} \cos\theta \left[1 + \frac{1}{jkr} \right] e^{-jkr} \tag{A.4c}$$

$$H_r = 0 \, , H_\theta = 0 \, , E_\varphi = 0 \tag{A.4d}$$

where $\eta = \sqrt{\frac{\mu}{\varepsilon}}$ are the intrinsic impedance and ε is the permittivity.

In THz photoconductive antennas, time domain behaviour of fields is used. Therefore, by multiplying field components of equation (A.4) with $e^{j\omega t}$, getting the real part of fields and considering the time difference between the observation point and source point as $t_d = t - \frac{r}{c}$ (c is the light velocity), time domain equations of the fields of equation (A.4) can be obtained by (A.5).

$$\tilde{H}_\varphi = \frac{I_{pc}dl}{4\pi} \sin\theta \left[\frac{-\omega \sin\omega t_d}{rc} + \frac{\cos\omega t_d}{r^2} \right] \tag{A.5a}$$

$$\tilde{E}_\theta = \frac{I_{pc}dl}{4\pi\varepsilon} \sin\theta \left[\frac{-\omega \sin\omega t_d}{rc^2} + \frac{\cos\omega t_d}{r^2 c} + \frac{\sin\omega t_d}{\omega r^3} \right] \tag{A.5b}$$

$$\tilde{E}_r = \frac{I_{pc}dl}{2\pi\varepsilon} \cos\theta \left[\frac{\cos\omega t_d}{r^2 c} + \frac{\sin\omega t_d}{\omega r^3} \right] \tag{A.5c}$$

From equation (A.5) it can be interpreted that $\tilde{E}_\theta$ and $\tilde{H}_\varphi$ are radiative components in the far field ($kr>>1$) since they have the factor of $1/r$. Assuming that $I_{pc}(t_d) = I_{pc}\cos\omega t_d$ and considering the relation between charge and current $I_{pc}(t) = \frac{\partial q}{\partial t}$, equations (A.5a) and (A.5b) can be rewritten as (A.6a) and (A.6b) respectively:

$$\tilde{H}_\varphi = \frac{dl}{4\pi rc}\sin\theta\frac{\partial I_{pc}(t_d)}{\partial t_d} + \frac{dl}{4\pi r^2}\sin\theta I_{pc}(t_d) \tag{A.6a}$$

$$\tilde{E}_\theta = \frac{dl}{4\pi\varepsilon rc^2}\sin\theta\frac{\partial I_{pc}(t_d)}{\partial t_d} + \frac{dl}{4\pi\varepsilon r^2 c}\sin\theta I_{pc}(t_d) + \frac{dl}{4\pi\varepsilon r^3}\sin\theta\frac{\partial q}{\partial t_d} \tag{A.6b}$$

Thus, the radiated electric field is proportional to the time derivative of the current (or equivalently it is proportional to the current density).

It is good to mention that in previous work in the literature, the relation of radiated THz power to the current was explained through Hertz vector potential of a time-varying dipole moment [34, 68] which is a popular method in areas like quantum electronics and solid-state physics. However, here this relation was explained through the usage of vector potential and considering the time-varying behaviour of the Hertzian dipole as an antenna.

A.2. Large-Aperture THz Antennas

The geometry of a large-aperture THz antenna is shown in Fig. A.2. Spectral and temporal format of emission of THz radiation from this antenna according to Maxwell's equations can be written as [84]:

$$\vec{E}_{THz} = -j\omega\vec{A} \tag{A.7a}$$

$$\vec{E}_{THz}(r,t) = -\frac{\mu}{4\pi}\int\frac{\partial\vec{J}_s(t)}{\partial t}\frac{dS}{r} = -\frac{\mu S}{4\pi z}\frac{d\vec{J}_s(t)}{dt} \tag{A.7b}$$

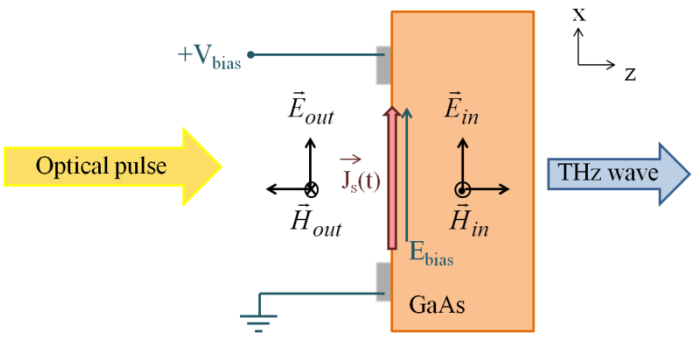

Fig. A.2 Geometry of a large-aperture THz antenna

As mentioned earlier, the size of the excitation area by the laser on the photoconductive gap is greater than the wavelength of the emitted THz wave. Therefore, the fields from this type of antenna can be assumed as plane waves and be modelled by considering boundary conditions [75]. Thus, according to Fig. A.2 and based on the basics of electromagnetic fields, the boundary conditions for electric and magnetic fields at the air-substrate interface can be written as:

$$\vec{E}_{in}(t) = \vec{E}_{out}(t) \tag{A.8a}$$

$$\vec{H}_{in}(t) - \vec{H}_{out}(t) = \vec{J}_s(t) \tag{A.8b}$$

The relation of E-field to H-field in two regions of air and substrate are:

$$\vec{H}_{in}(t) = -\frac{\sqrt{\varepsilon_r}}{\eta_0}\vec{E}_{in}(t) \tag{A.9a}$$

$$\vec{H}_{out}(t) = \frac{1}{\eta_0}\vec{E}_{out}(t) \tag{A.9b}$$

Where η_0 is the intrinsic impedance of air and ε_r is the relative permittivity of the substrate. Thus, using equations (A.8) and (A.9) and considering Ohm's law that surface current density can be expressed as $\vec{J}_s(t) = \sigma_s(t)(\vec{E}_{in}(t) + \vec{E}_{bias}(t))$, and the surface current in a large-aperture antenna is derived as:

$$\vec{J}_s(t) = \frac{\sigma_s(t)\vec{E}_{bias}(t)}{\frac{\sigma_s(t)\eta_0}{1+\sqrt{\varepsilon_r}} + 1} \tag{A.10}$$

Appendix B Calculation of efficiencies

The average photocurrent I_{avp} and approximate photoconductive resistance R_{app} are considered as equations (B.1) and (B.2) respectively:

$$I_{avp} = \frac{e\mu_e \tau_c V_{bias} P_{av}}{hfL^2} \tag{B.1}$$

$$R_{app} = \frac{3hfL^2}{2e\mu_e P_{av} t_{rep}} \tag{B.2}$$

where V_{bias} is the bias voltage, L is the antenna gap length, and P_{av} is the average optical power. Then, the optical-to-electrical efficiency can be estimated as:

$$\eta_{1p} = \frac{R_{app} I_{avp}^2}{P_{av}} = \frac{3e\mu_e \tau_c^2 V_{bias}^2}{2t_{rep} hfL^2} \tag{B.3}$$

Considering some typical values as

μ_e = 1000 $cm^2.V^{-1}.s^{-1}$

τ_c = 0.5 ps

V_{bias} = 30 V

P_{av} = 50 mW

L = 5 μm

t_{rep} = 1/80 μs

h = 6.626 x 10^{-34} J.s

e = 3 x 10^{-8} ms^{-1}

c = 1.6 x 10^{-19} C

f = 375 THz

in equation (B.3), $\eta_{1p} = 7.2 \times 10^{-5}$.

The matching efficiency can be calculated according to equation (B.4) for a half-wavelength dipole antenna on a substrate with ε_r = 12.9. Assuming the antenna resistance in free space, Z_{free}, is 73 Ω and

by using the above values in equation (B.2) R_{app} is 0.89 Ω, then the matching efficiency will be η_{2p} = 0.16.

$$\eta_{2p} = 1 - \left| \frac{Z_{free} / \sqrt{\varepsilon_r} - R_{app}}{Z_{free} / \sqrt{\varepsilon_r} + R_{app}} \right|^2 \quad \text{(B.4)}$$

Assuming also that a radiation efficiency η_{3p} of can be relatively high, typically over 80%, the total antenna efficiency for this sample, which is a multiplication of efficiencies from three described processes, is calculated as 5.7×10^{-6}.